

**INVESTIGATION OF TUNNEL BORING MACHINE-  
LANDSLIDE RELATION IN A TUNNEL EXCAVATING  
IN A COMPLEX GEOLOGICAL CONDITION: BAHÇE-  
NURDAĞ TUNNEL**

**KARMAŞIK JEOLJİK KOŞULLARDA AÇILAN BİR  
TÜNELDE TÜNEL DELME MAKİNESİ-HEYELAN  
İLİŞKİSİNİN ARAŞTIRILMASI: BAHÇE-NURDAĞ  
TÜNELİ**

**MÜGE PINAR KÖMÜ**

**Prof. Dr. CANDAN GÖKÇEOĞLU**

**Supervisor**

Submitted to

Graduate School of Science and Engineering of Hacettepe University

as a Partial Fulfillment to Requirements

for the Award of Degree of Master of Science

in Geological Engineering.

2019

This work titled “**Investigation of Tunnel Boring Machine-Landslide Relation in a Tunnel Excavating in a Complex Geological Condition: Bahçe-Nurdağ Tunnel**” by **MÜGE PINAR KÖMÜ** has been approved as a thesis for the Degree of **Master of Science in Geological Engineering** by the Examining Committee Members mentioned below.

Prof. Dr. Ahmet TÜRER

Head



Prof. Dr. Candan GÖKÇEOĞLU

Supervisor



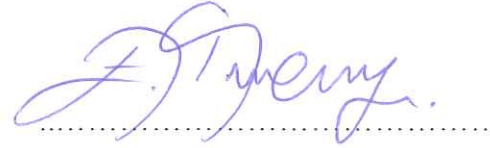
Prof. Dr. Bahtiyar ÜNVER

Member



Prof. Dr. Ergün TUNCAY

Member



Doç. Dr. Hakan A. NEFESLİOĞLU

Member



This thesis has been approved as thesis for the Degree of **Master of Science in Geological Engineering** by Board of Directors of the Institute of Graduate School of Science and Engineering on ..... / ..... /.....

Prof. Dr. Menemşe GÜMÜŞDERELİOĞLU

Director of the Institute of

Graduate School of Science and Engineering

*TO MY BELOVED PARENTS*

## ETHICS

In this thesis study, prepared in accordance with the spelling rules of Institute of Graduate School of Science and Engineering of Hacettepe University,

I declare that,

All the information and documents have been obtained in the base of the academic rules

All audio-visual and written information and results have been presented according to the rules of scientific ethics

In case of using others works, related studies have been cited in accordance with the scientific standards

All cited studies have been fully referenced

I did not do any distortion in the data set

And any part of this thesis has not been presented as another thesis study at this or any other university.



14/06/2019

**Müge Pınar KÖMÜ**

## YAYIMLAMA VE FİKRİ MÜLKİYET HAKLARI BEYANI

Enstitü tarafından onaylanan lisansüstü tezimin/raporumun tamamını veya herhangi bir kısmını, basılı (kağıt) ve elektronik formatta arşivleme ve aşağıda verilen koşullarla kullanıma açma iznini Hacettepe üniversitesine verdiğimi bildiririm. Bu izinle Üniversiteye verilen kullanım hakları dışındaki tüm fikri mülkiyet haklarım bende kalacak, tezimin tamamının ya da bir bölümünün gelecekteki çalışmalarda (makale, kitap, lisans ve patent vb.) kullanım hakları bana ait olacaktır.

Tezin kendi orijinal çalışmam olduğunu, başkalarının haklarını ihlal etmediğimi ve tezimin tek yetkili sahibi olduğumu beyan ve taahhüt ederim. Tezimde yer alan telif hakkı bulunan ve sahiplerinden yazılı izin alınarak kullanılması zorunlu metinlerin yazılı izin alarak kullandığımı ve istenildiğinde suretlerini Üniversiteye teslim etmeyi taahhüt ederim.

Yükseköğretim Kurulu tarafından yayınlanan "*Lisansüstü Tezlerin Elektronik Ortamda Toplanması, Düzenlenmesi ve Erişime Açılmasına İlişkin Yönerge*" kapsamında tezim aşağıda belirtilen koşullar haricince YÖK Ulusal Tez Merkezi / H.Ü. Kütüphaneleri Açık Erişim Sisteminde erişime açılır.

Enstitü / Fakülte yönetim kurulu kararı ile tezimin erişime açılması mezuniyet tarihimden itibaren 2 yıl ertelenmiştir.

Enstitü / Fakülte yönetim kurulu gerekçeli kararı ile tezimin erişime açılması mezuniyet tarihimden itibaren.....ay ertelenmiştir.

Tezim ile ilgili gizlilik kararı verilmiştir.



14/06/2019

Müge Pınar KÖMÜ

## **ABSTRACT**

# **INVESTIGATION OF TUNNEL BORING MACHINE- LANDSLIDE RELATION IN A TUNNEL EXCAVATING IN A COMPLEX GEOLOGICAL CONDITION: BAHÇE-NURDAĞ TUNNEL**

**Müge Pınar KÖMÜ**

**Master of Science, Department of Geological Engineering**

**Supervisor: Prof. Dr. Candan GÖKÇEOĞLU**

**June 2019, 124 pages**

In recent years, Tunnel Boring Machine (TBM) has become increasingly more popular for long tunnel operations in terms of its characteristic of features of rapid and having low vibration. Twin-tubes railway tunnels are opened in between Bahçe (Osmaniye)-Nurdağ (Gaziantep) are also the longest railway tunnels in Turkey as the length of approximately 10 km. They started to be excavated from Nurdağ with using tunnel boring machines (TBM). Tunnels will be completed in intense slope debris and landslide which is caused by intense debris on Bahçe portal part. Therefore, geological environment of the study is one of the rare examples in terms of its complex engineering problems in the World. The construction of tunnel without subjecting to critical failure impacts depends on realistic geological and geotechnical characterization. For this reason, engineering parameters are determined by examining boreholes data in order to define geology of the study area. Consequently, the purpose of the thesis is investigation of the interaction effects landslide-TBM during construction on twin tubes tunnelling by performing 3D finite element analyses. MIDAS GTS NX software was used in stages of 3D numerical analyses. According to prepared 3D deformation results, TBM has negative effects on debris and landslide. Thus, inactivation of TBM tunnelling excavation for last 600 meters

is vital with respect to safety and preventing economical loses. By taking into consideration its aims and goals, this thesis contributes the worldwide engineering geology and tunnel literature.

**Key words:** 3D numerical analysis, TBM, Bahçe - Nurdağ, Debris, Landslide

## ÖZET

# KARMAŞIK JEOLJİK KOŞULLARDA AÇILAN BİR TÜNELDE TÜNEL DELME MAKİNESİ-HEYELAN İLİŞKİSİNİN ARAŞTIRILMASI: BAHÇE-NURDAĞ TÜNELİ

**Müge Pınar KÖMÜ**

**Tez Danışmanı: Prof. Dr. Candan GÖKÇEOĞLU**

**Yüksek Lisans Tezi, Jeoloji Mühendisliği Bölümü,  
Haziran 2019, 124 sayfa**

Son yıllarda özellikle uzun tünel imalatları, tünel delme makinelerinin hızlı ve düşük titreşime sahip olması bakımından tünel delme makineleri ile gerçekleştirilmektedir. Bahçe (Osmaniye)–Nurdağ (Gaziantep) arasında açılmakta olan çift tüp demiryolu tünelleri yaklaşık 10 km’lik uzunluğu ile Ülkemizin en uzun demiryolu tünelleri olma özelliğine sahiptir. Çift tüp olarak projelendirilen tüneller, tünel delme makineleri kullanılarak Nurdağ’dan başlayarak açılmaya başlanmıştır. Tüneller, Bahçe çıkışında yoğun yamaç molozları ve bu molozlar içinde gerçekleşmiş heyelan bölgesinde sonuçlanacaktır. Bu nedenle çalışmaya konu olan jeolojik-ortam sahip olduğu mühendislik sorunları açısından Dünyada ender karşılaşılabilecek örneklerden biridir. Tünelin ciddi bir yenilmeye maruz bırakılmadan tamamlanması jeolojik-jeoteknik ortamın mümkün olduğu kadar doğruya yakın biçimde karakterize edilmesine bağlıdır. Bu nedenle inceleme alanındaki jeolojik ortamın tanımlanması amacıyla sondaj verileri incelenerek mühendislik parametreleri tayin edilmiştir. Elde edilen veriler kullanılarak üç boyutlu sonlu elemanlar analizleri gerçekleştirilmiş, özellikle metamorfik birimler ile



yamaç molozu sınırında oluşacak deformasyonlar, tünel delme makinesinin moloz ve heyelan üzerindeki etkisi araştırılmıştır. Nümerik analiz aşamalarında MIDAS GTS NX yazılımı kullanılmıştır. Elde edilen üç boyutlu analiz sonuçlarına göre; tünel delme makineleri, moloz ve heyelan üzerinde olumsuz etkisi yaratmaktadır. Bu sebeple tünelin son 600 metrelik kısmında TBM tünel kazısının durdurulması, güvenlik ve ekonomik kayıp yaşanmaması açısından önemlidir. Bu tez çalışması, amaç ve hedefleri göz önünde bulundurulduğunda Dünya mühendislik jeolojisi ve tünel literatürüne katkı koyabilecek niteliktedir.

**Anahtar Kelimeler:** 3D Nümerik Analiz, TBM, Bahçe - Nurdağ, Moloz, Heyelan

## ACKNOWLEDGEMENTS

First of all, I would like to sincerely thank my supervisor Prof. Dr. Candan GÖKÇEOĞLU to give me an opportunity to work under his guidance. I am grateful to his remarkable theoretical support, precious guidance, comments, trust and encouragements at all stages of this research.

I wish to thank my examining jury members. Their comments and recommendations have been very useful for bettering the final version of the thesis.

Special thanks to General Directorate of Turkish State Railways for having provided part of TBM data, geological/geotechnical information and data, and their continuous support.

I would also like to deepest thanks to Zehra KAYA, Ümit GÜNEY and Nurgül GÜLTEKİN for their supports and advices.

Finally, I also express my gratefulness to my mother (Şengül KÖMÜ) and father (Yusuf KÖMÜ), who have provided me continuously emotional support and love in all my life. They encouraged me to obtain high achievements in all time of the my life. This thesis would not have been completed without endless support of my parents.

## TABLE OF CONTENTS

ABSTRACT.....	i
ÖZET .....	iii
ACKNOWLEDGEMENTS .....	v
TABLE OF CONTENTS.....	vi
LIST OF TABLES.....	viii
LIST OF FIGURES .....	ix
SYMBOLS AND ABBREVIATIONS.....	xii
1. INTRODUCTION .....	1
2. PREVIOUS STUDIES.....	4
3. DESCRIPTION OF STUDY AREA .....	9
3.1. Location .....	9
3.2. Topography .....	10
3.2.1. Altitude.....	11
3.2.2. Slope.....	12
3.2.3. Aspect.....	13
3.3. Climate and Vegetation .....	14
3.4. Geology .....	17
3.4.1. Stratigraphy .....	17
3.4.1.1. Zabuk Formation (Ez).....	18
3.4.1.2. Çaltepe, Formation (Eç).....	18
3.4.1.3. Seydişehir Formation (EOs).....	18
3.4.1.4. Kardere Formation (Ok) .....	18
3.4.1.5. Dedeler Formation (Sd) .....	19
3.4.1.6. Hasanbeyli Formation (Dch).....	19
3.4.1.7. Amanos Group (aTRJK).....	19
3.4.1.7.1. Olucak Formation (aTRO) .....	19
3.4.1.7.2. Nurdağı Formation (aTRn).....	19
3.4.1.7.3. İslahiye Formation (aJKi) .....	19
3.4.1.7.4. Beyoğlu Formation (KTbe).....	19
3.4.2. Lithological Characteristics of Study Area .....	22

3.5. Hydrogeology.....	25
3.6. Landslide.....	26
4. SEISMICITY OF THE STUDY AREA .....	28
5. GEOTECHNICAL SITE CHARACTERIZATION.....	36
5.1. Laboratory Test.....	36
5.2. Rock Mass Rating (RMR) Classification .....	42
5.3. Geological Strength Index (GSI) .....	43
5.4. Geotechnical Parameters .....	45
6. TUNNELLING EXCAVATION METHOD .....	49
7. MODEL DEVELOPMENT AND CALIBRATION.....	51
7.1. Numerical Model.....	51
7.1.1. Finite Element Method (FEM) .....	51
7.2. Midas Software .....	52
7.3. Modelling of Bahçe - Nurdağ Tunnel .....	52
7.3.1. Definition of Terrain and Tunnel Geometry .....	54
7.3.2. Geotechnical Parameters .....	58
7.3.3. Construction of Model .....	63
7.3.4. Modelling Scenarios .....	64
8. DISCUSSION.....	103
9. CONCLUSION .....	104
10. REFERENCES .....	105
APPENDICES.....	112
Appendix 1- Boreholes Information .....	112
Appendix 2- Test Standard.....	121
Appendix 3- Permission Form.....	122
Appendix 4- Thesis Originality Report.....	123
CURRICULUM VITAE.....	124

## LIST OF TABLES

Table 3.1.	Extreme maximum, minimum and average temperatures measure in the period of 1987-2018 in Osmaniye (Turkish State Meteorological Service, 2018). .....	15
Table 3.2.	Extreme maximum, minimum and average temperatures measure in the period of 1940-2018 in Gaziantep (Turkish State Meteorological Service, 2018). .....	16
Table 3.3.	Boreholes information for between KM: 3+510 and 4+400 (TCDD, 2014). .....	23
Table 3.4.	Groundwater levels measured in the boreholes by TCDD. ....	25
Table 4.1.	Distribution of the ground movements having a magnitude of $M \geq 4.0$ occurred between 1915-2019 in the study area and its immediate surrounding. ....	30
Table 4.2.	The probabilities of occurrence of the specific earthquake magnitudes and the average return periods in the study area and its surrounding calculated for 1, 10, 50, 75 and 100 years. ....	34
Table 4.3.	The peak ground acceleration values that will be effective in the study area in case of realization of the highest moment magnitudes evaluated in the study area and its surrounding. ....	35
Table 5.1.	Laboratory test results (TCDD, 2014). ....	37
Table 5.2.	RMR parameters for heavily jointed metasandstone-metamudstone and metasandstone-metamudstone. ....	42
Table 7.1.	Model parameters. ....	58
Table 7.2.	Maximum and minimum displacement values for Km: 3+810 – 4+110. ....	65
Table 7.3.	Maximum and minimum stress values for Km: 3+810 – 4+110. ....	67
Table 7.4.	Maximum and minimum tunnel section displacement values for Km: 3+810 – 4+110. ....	71
Table 7.5.	Maximum and minimum displacement values for Km: 3+710 – 3+810. ....	74
Table 7.6.	Maximum and minimum stress values for Km: 3+710 – 3+810. ....	77
Table 7.7.	Maximum and minimum tunnel section displacement values for Km: 3+710 – 3+810. ....	80
Table 7.8.	Maximum and minimum displacement values for Km: 3+660 – 3+710. ....	84
Table 7.9.	Maximum and minimum stress values for Km: 3+660 – 3+710. ....	86
Table 7.10.	Maximum and minimum tunnel section displacement values for Km: 3+660 – 3+710. ....	90
Table 7.11.	Maximum and minimum displacement values for Km: 3+510 – 3+660. ....	93
Table 7.12.	Maximum and minimum stress values for Km: 3+510 – 3+660. ....	96
Table 7.13.	Maximum and minimum tunnel section displacement values for Km: 3+510 – 3+660. ....	99

## LIST OF FIGURES

Figure 1.1.	Flow chart of the study. ....	3
Figure 3.1.	The location map of the study area has been presented as WGS 1984. ....	10
Figure 3.2.	Altitude map of the study area. ....	11
Figure 3.3.	Slope map of the study area. ....	12
Figure 3.4.	The aspect map of the study area. ....	13
Figure 3.5.	Graph showing monthly total precipitation and average temperature of Osmaniye meteorological station for the period of 1987-2018. ....	15
Figure 3.6.	Graph showing monthly total precipitation and average temperature of Gaziantep meteorological station for period of 1940-2018. ....	16
Figure 3.7.	Bahçe Nappe stratigraphy (Reproduced after MTA, 2018). ....	17
Figure 3.8.	Geological map of tunnel route (Modified after MTA, 2018). ....	20
Figure 3.9.	Geological map of study area. ....	21
Figure 3.10.	Engineering geological cross section of the tunnel route (Reproduced after TCDD, 2018). ....	24
Figure 3.11.	Landslide inventory map of study area (Modified after MTA, 2019). ...	27
Figure 4.1.	Location map of EAFZ (Bulut et al., 2012) ....	28
Figure 4.2.	Stress accumulation on EAFZ (Nalbant et al., 2002). ....	29
Figure 4.3.	Active faults observed in the study area and it surrounding and distribution of the ground movements having a magnitude of $M \geq 4$ occurred between 1915-2019. ....	32
Figure 4.4.	Frequency distribution relating to the strong ground movements occurred in the study area and its surrounding between the years 1915-2019 (distribution is given for $M \geq 4.0$ ). ....	32
Figure 4.5.	Average earthquake magnitude relating to the strong ground movements occurred in the study area and it's surrounding between the years 1915- 2019 and $\log(\Sigma N/t)$ relationships. ....	33
Figure 5.1.	Unit weight test results graph (TCDD, 2014). ....	39
Figure 5.2.	UCS test graph Km: 3+510 and 4+110 (TCDD, 2014). ....	39
Figure 5.3.	Point load strength graph Km: 3+510 and 4+110 (TCDD, 2014). ....	40
Figure 5.4.	Brazillian test graph for Km: 3+510 and 4+110 (TCDD, 2014). ....	40
Figure 5.5.	Elasticity modulus graph for Km: 3+510 and 4+110 (TCDD, 2014). ....	41
Figure 5.6.	The modified GSI classification suggested by Sönmez and Ulusay (2002) for metasandstone-metamudstone and heavily jointed metasandstone- metamudstone. ....	44
Figure 5.7.	Results of Roclab for heavily jointed metasandstone-metamudstone when $D=0$ ....	47
Figure 5.8.	Results of Roclab for heavily jointed metasandstone-metamudstone when $D=0.5$ . ....	47
Figure 5.9.	Results of Roclab for metasandstone-metamudstone when $D=0$ ....	48

Figure 5.10.	Results of Roclab for metasandstone-metamudstone when D=0.5.....	48
Figure 7.1.	Flow chart of the model construction.....	53
Figure 7.2.	Terrain geometry in AUTOCAD. ....	55
Figure 7.3.	Tunnel geometry in AUTOCAD.....	55
Figure 7.4.	Stage of creating terrain topography in MIDAS GTS NX. ....	56
Figure 7.5.	Stage of creating tunnel geometry in MIDAS GTS NX.....	56
Figure 7.6.	Tunnel geometry in MIDAS GTS NX. ....	57
Figure 7.7.	Conceptual 3D model of the Bahçe portal in MIDAS GTS NX.....	57
Figure 7.8.	Assigning the parameters for debris.....	60
Figure 7.9.	Assigning the parameters for heavily jointed metasandstone- metamudstone. ....	61
Figure 7.10.	Assigning the parameters for metasandstone-metamudstone.....	62
Figure 7.11.	Construction stages analyses. ....	63
Figure 7.12.	Meshed model for Km: 3+810 – 4+110. ....	64
Figure 7.13.	Total displacement model for Km: 3+810 – 4+110.....	65
Figure 7.14.	Horizontal displacement model for Km: 3+810 – 4+110.....	66
Figure 7.15.	Displacement model along Y axis for Km: 3+810 – 4+110.....	66
Figure 7.16.	Vertical displacement model for Km: 3+810 – 4+110.....	67
Figure 7.17.	Total stress model for Km: 3+810 – 4+110.....	68
Figure 7.18.	XX stress model for Km: 3+810 – 4+110. ....	68
Figure 7.19.	YY stress model for Km: 3+810 – 4+110. ....	69
Figure 7.20.	ZZ stress model for Km: 3+810 – 4+110. ....	69
Figure 7.21.	Mean effective stress model for Km: 3+810 – 4+110.....	70
Figure 7.22.	Material status model for Km: 3+810 – 4+110.....	70
Figure 7.23.	Tunnel section of total displacement model for Km: 3+810 – 4+110. ....	71
Figure 7.24.	Tunnel section of X displacement model for Km: 3+810 – 4+110. ....	72
Figure 7.25.	Tunnel section of Y displacement model for Km: 3+810 – 4+110. ....	72
Figure 7.26.	Tunnel section of Z displacement model for Km: 3+810 – 4+110.....	73
Figure 7.27.	Tunnel section of material status model for Km: 3+810 – 4+110. ....	73
Figure 7.28.	Meshed model for Km: 3+710 – 3+810. ....	74
Figure 7.29.	Total displacement model for Km: 3+710 – 3+810. ....	75
Figure 7.30.	Horizontal displacement model for Km: 3+710 – 3+810.....	75
Figure 7.31.	Displacement model along the Y-axis for Km: 3+710 – 3+810.....	76
Figure 7.32.	Vertical displacement model for Km: 3+710 – 3+810.....	76
Figure 7.33.	Total stress model for Km: 3+710 – 3+810.....	77
Figure 7.34.	XX stress model for Km: 3+710 – 3+810. ....	78
Figure 7.35.	YY stress model for Km: 3+710 – 3+810. ....	78
Figure 7.36.	ZZ stress model for Km: 3+710 – 3+810. ....	79
Figure 7.37.	Mean effective stress model for Km: 3+710 – 3+810.....	79
Figure 7.38.	Material status model for Km: 3+710 – 3+810.....	80
Figure 7.39.	Tunnel section of total displacement model for Km: 3+710 – 3+810. .....	81
Figure 7.40.	Tunnel section of X displacement model for Km: 3+710 – 3+810....	81
Figure 7.41.	Tunnel section of Y displacement model for Km: 3+710 – 3+810....	82

Figure 7.42.	Tunnel section of Z displacement model for Km: 3+710 – 3+810. .....	82
Figure 7.43.	Tunnel section of material status model for Km: 3+710 – 3+810.	83
Figure 7.44.	Meshed model for Km: 3+660 – 3+710. ....	83
Figure 7.45.	Total displacement model for Km: 3+660 – 3+710. ....	84
Figure 7.46.	Horizontal displacement model for Km: 3+660 – 3+710. ....	85
Figure 7.47.	Displacement model along the Y-axis for Km: 3+660 – 3+710. ...	85
Figure 7.48.	Vertical displacement model for Km: 3+660 – 3+710. ....	86
Figure 7.49.	Total stress model for Km: 3+660 – 3+710. ....	87
Figure 7.50.	XX stress model for Km: 3+660 – 3+710. ....	87
Figure 7.51.	YY stress model for Km: 3+660 – 3+710. ....	88
Figure 7.52.	ZZ stress model for Km: 3+660 – 3+710. ....	88
Figure 7.53.	Mean effective stress model for Km: 3+660 – 3+710. ....	89
Figure 7.54.	Material status model for Km: 3+660 – 3+710. ....	89
Figure 7.55.	Tunnel section of total displacement model for Km: 3+660 – 3+710. ....	90
Figure 7.56.	Tunnel section of X displacement model for Km: 3+660 – 3+710.	91
Figure 7.57.	Tunnel section of Y displacement model for Km: 3+660 – 3+710.	91
Figure 7.58.	Tunnel section of Z displacement model for Km: 3+660 – 3+710.	92
Figure 7.59.	Tunnel section of material status model for Km: 3+660 – 3+710.	92
Figure 7.60.	Meshed model for Km: 3+510 – 3+660. ....	93
Figure 7.61.	Total displacement model for Km: 3+510 – 3+660. ....	94
Figure 7.62.	Horizontal displacement model for Km: 3+510 – 3+660. ....	94
Figure 7.63.	Displacement model along the Y-axis for Km: 3+510 – 3+660. ...	95
Figure 7.64.	Vertical displacement model for Km: 3+510 – 3+660. ....	95
Figure 7.65.	Total stress model for Km: 3+510 – 3+660. ....	96
Figure 7.66.	XX stress model for Km: 3+510 – 3+660. ....	97
Figure 7.67.	YY stress model for Km: 3+510 – 3+660. ....	97
Figure 7.68.	ZZ stress model for Km: 3+510 – 3+660. ....	98
Figure 7.69.	Mean effective stress model for Km: 3+510 – 3+660. ....	98
Figure 7.70.	Material status model for Km: 3+510 – 3+660. ....	99
Figure 7.71.	Tunnel section of total displacement model for Km: 3+510 – 3+660. ....	100
Figure 7.72.	Tunnel section of X displacement model for Km: 3+510 – 3+660. .....	100
Figure 7.73.	Tunnel section of Y displacement model for Km: 3+510 – 3+660. .....	101
Figure 7.74.	Tunnel section of Z displacement model for Km: 3+510 – 3+660. .....	101
Figure 7.75.	Tunnel section of material status model for Km: 3+510 – 3+660. .....	102



## SYMBOLS AND ABBREVIATIONS

### Symbols

$^{\circ}\text{C}$	Centigrade
$c$	Cohesion
$D$	Disturbance factor
$E_i$	Elasticity modulus
$E_m$	Deformation modulus
$J_v$	Volumetric rating
$K_o$	Coefficient of earth pressure
$m_i$	Intact rock parameter
$M$	Earthquake magnitude
$M_w$	Moment magnitude
$P_n(t)$	Probability of number of $n$ earthquakes
$R_e$	Distance to epicentre
$R_f$	Infilling rating
$R_w$	Weathering rating
$R_r$	Roughness rating
$S_{A, B}$	Site conditions
$\Phi$	Internal friction angle
$\sigma_c$	Compressive strength
$\sigma_t$	Tensile strength
$\nu$	Poisson's ratio
$\bar{\nu}$	Number of the average occurrence of earthquakes
$\gamma$	Unit weight

### Abbreviations

AFAD	Republic of Turkey Prime Ministry Disaster & Emergency Management
EAFZ	East Anatolian Fault Zone

EPB	Earth Pressure Balance
BDM	Boundary Difference Method
DEM	Digital Elevation of Model
FDM	Finite Difference Method
FEM	Finite Element Method
GSI	Geological Strength Index
MTA	General Directorate of Mineral Research and Exploration
PGA	Peak Ground Acceleration
RMR	Rock Mass Rating
RMS	Rock Mass Strength
RQD	Rock Quality Designation
SCR	Surface Condition Rating
SR	Structure Rating
SRF	Stress Reduction Factor
SRTM	Shuttle Radar Topography Mission
TBM	Tunnel Boring Machine
TCDD	General Directorate of Turkish State Railways
UCS	Uniaxial Compressive Strength
3D	Three Dimensions

# 1. INTRODUCTION

Due to increasing of population, transportation needs engineering studies which aim to decrease the transportation time and to improve transportation alternatives. Time is important notion for every people since people want to use their time efficiently. Therefore, they do not want to lose long time for transportation. When transportation can be preferred the possible shortest way between the two stations, it is beneficial for people and comfortable transportation in terms of economy. Tunnel is one of the transportation alternatives which try to be cut the way. Although tunnels have many advantages, construction of tunnels may have difficulties because of many reasons. Thus, detailed engineering studies which contain geological and geotechnical investigations are necessary to construct safe and economical construction and service. These details are also significant to be decided to tunnel excavation methods. Nowadays tunnel boring machine (TBM) tunnelling projects are increasingly as an preferred alternative for long tunnel operations because of its extreme rate and low vibration in comparison to drilling and blasting method; however, the applicability of TBM for long tunnelling needs attentive considerations. One of the rail transit projects, known as Bahçe-Nurdağ tunnels, is considered in this thesis because geological and geotechnical conditions of the tunnel route are highly complex.

Twin-tubes railway tunnels are being constructed between Bahçe (Osmaniye)-Nurdağ (Gaziantep). Tunnels are the longest railway tunnels of Turkey with respect their lengths as about 10 km. Tunnel construction with TBM has started to be open from Nurdağ Region. Tunnels will be completed in Bahçe. Tunnel route is passing through East Anatolian Fault Zone and under the Taurus Mountains. Folding of the limestone, metasandstone, metamudstone and quartzite have high grade of rocks can be observable in tunnel route. Debris and landslide are examined in Bahçe Region so it has also high landslide risk in debris. Taking into account of certain these criteria, railway tunnel route has very complex. This study aims to investigate the relationship between TBM and landslide by using comprehensive 3D numerical analyses for Bahçe portal in order to decide whether tunnels are completed with TBM or not. It is important because TBMs used in this construction are more suitable for high strength rock environment. Thus,

analysis of debris and TBM relationships have a significant role in this study. Considering possible risks of the project; geology, engineering geology and geotechnical conditions are examined employing the borehole data provided by General Directorate of Turkish State Railways (TCDD) for this thesis. Required experiments results which are obtained from the existing boreholes information were inspected to determine the engineering parameters. It should be known that if geological and lithological units can be defined more close to in-situ conditions, successful numerical analysis can be obtained. These data were evaluated 3D finite element method (FEM) in the MIDAS GTS NX software to obtain the deformations on metamorphic rocks and debris, and effects of TBM on debris and landslide. This study is also crucial in terms of two reasons. The first reason is that these results are guide for other future long TBM tunnel projects in order to be safely completed the tunnel. The second reason is that software –which is MIDAS GTS NX – is efficiently used to work on numerical analysis in tunnel by using finite elements methods in complex geological conditions. Considering these information, it can be stated that investigation of TBM tunnel – landslides relationship with 3D numerical analyses for Bahçe region contributes literature.

The thesis is composed of nine separate chapters. First, introduction chapter aimed to give brief information about research topics and their objectives. The second chapter concentrates on previous works which are related to this study. Essential information associated to numerical analyses are arranged with reviewing of literature. Third chapter describes the general characteristics of the study area. Additionally, chapter four explains the seismicity of the study area because the study area locates in the vicinity of East Anatolian Fault Zone. Fifth chapter is geotechnical site characterization which includes data analysis for study area. Analyses are necessary to create 3D finite model in 3D software of MIDAS. Furthermore, chapter six is necessary for having background of excavation method of TBM in order to evaluate this option for the study area. Seventh chapter presents of model development, while it also gives information about numerical analyses, Midas software, preparation stages of modelling and modelling results within the scope of this thesis. In addition, all results acquired from models are laid out in chapter eight which is discussion. Finally, conclusion chapter is concerned with research summary, research contributions and future recommendations. In order to provide better understand, a flow chart of summarizing the study is also presented in Figure 1.1.

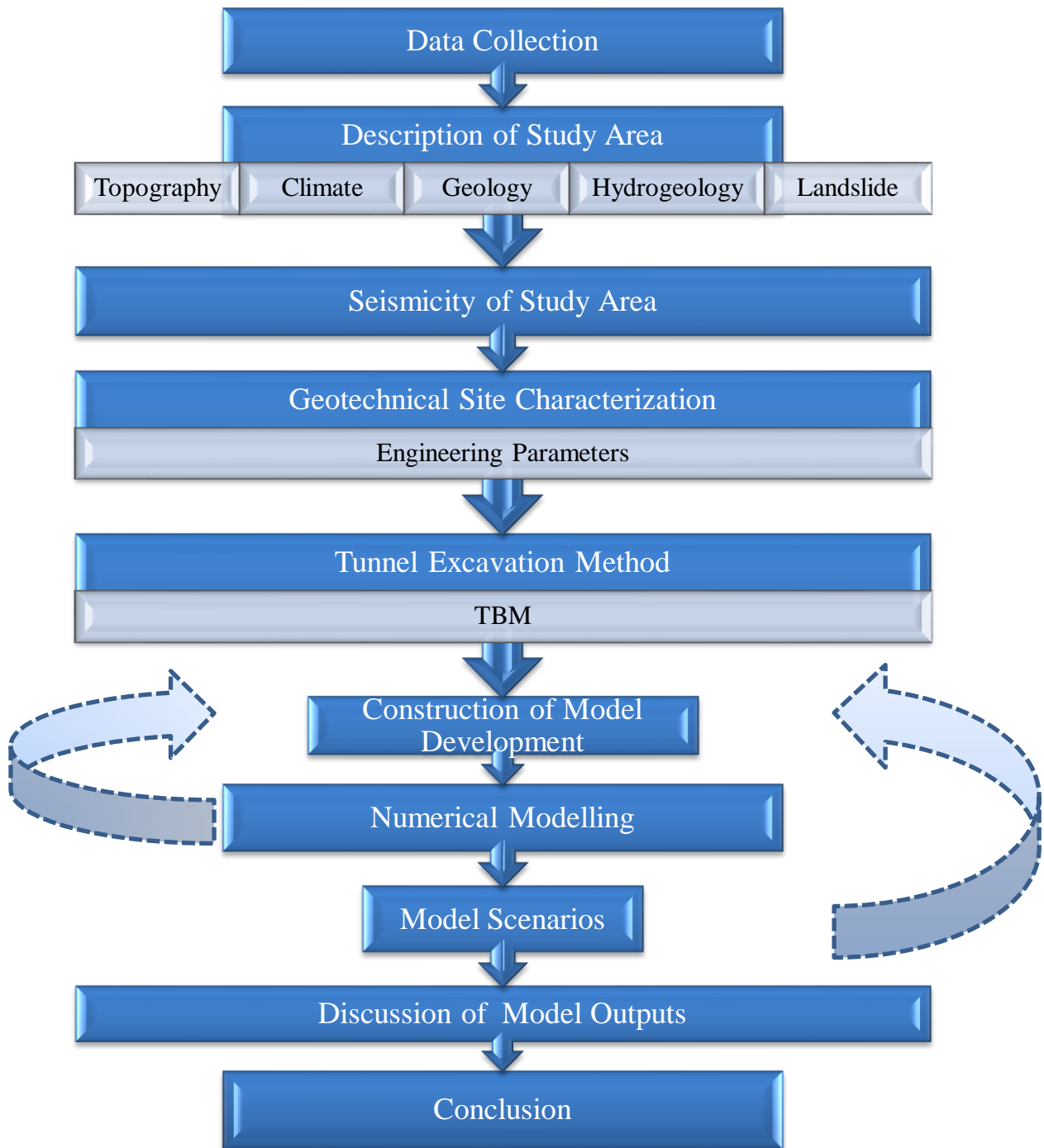


Figure 1.1. Flow chart of the study.

## 2. PREVIOUS STUDIES

Literature on tunnelling has huge number of publications. For the purpose of the study, only TBM tunnelling and 3D FEM analyses are considered and the studies encountered were summarized as follows:

Ulusay and Aydan (1997) worked on advantages and disadvantages of tunnel boring machine (TBM) in tunnel excavation. They pointed out that when the failure occurs, it is very difficult to interference in very short time in fault zone. The shield of TBM is piled up materials. Therefore, it is very important to estimate the deformations when tunnel is opening.

Barla and Pelizza (2000) emphasised that when the type of TBM is chosen, geological, economic and environmental factors should be considered in complex geological characteristics of the regions. Otherwise, the optimization of the problem will be very difficult. Relationships between TBM and instability of excavation walls, instability of excavation face, fault zones and squeezing were investigated in their study.

Abdel-Meguid et al. (2002) suggested that 3D FEM results are realistic to analyse the effects of the surface excavation for York-Mills Centre on the Toronto Transit Commission tunnels. They also compared 3D and 2D FEM models results site data. While compressive stress affect in bottom of fibers of lining, in the top of fibers of lining is impacted by tensile stresses during the excavation.

Berilgen et al. (2007) pointed out that PLAXIS 3D numerical analysis software enables the modelling of grouting pressure and TBM compressive force. Furthermore, the observed ground behaviour is very close to actual model with using PLAXIS 3D during the tunnel excavations. They criticized numerical analyses results of lateral and angular deformations for their study of Esenler-Bağcılar Metro Tunnel.

Doğruoğlu (2009) investigated soil displacements and surface settlements considering field and laboratory experiment results for Otogar-Bağcılar metro project. PLAXIS finite element tool was used to calculate displacements. He also pointed out that it is critical to choose proper parameters which are cohesion, internal friction angle, elasticity modulus and thickness for construction of modelling. He obtained that displacements on the ground surface was not influenced by TBM vibration.

Dragojević (2012) predicted ground settlement caused by tunnel construction with 2D and 3D finite element methods. She thought that 3D finite element methods is better than 2D finite element methods because deformation, changing in stress and damages can be more easily apprehend by using 3D finite element methods along tunnel route.

Lee et al. (2012) noticed analysis on the behaviour of tunnel excavated by TBM under high overburden stress using the numerical analysis method of FEM. Tunnel behaviours were evaluated through the analysis on strength factor, maximum displacement, differential stresses and safety factor of tunnel support systems.

Ochmanski and Bzowka (2012) studied on Fovam Square station of 4<sup>th</sup> metro line in Budapest. Midas GTS software was applied for their tunnel study area because it could enable to solve complex engineering geology problems and give good technical supports. They noticed that fault zone has significant influence on behaviour of structure and occurrence of specific stresses, which acting on the structure and generate undesirable displacements. Fault zone was modelled as an interface in order to model stress- strain behaviour in this study. However, they emphasized that mesh performance which are applied in fault zone regions may have some problems. Therefore, when analyses are studied, special attention is mandatory.

Allahverdi and Nasri (2013) examined their study area where tunnel were excavated with TBM. Midas-GTS software which has been concerned with geotechnical studies was used to evaluate the effects of the ground behaviour and adjacent structures in three dimension.

Haghi et al. (2013) analysed the ground settlements for EPB-TBM using numerical analysis “PLAXIS 3D Tunnel” were used to determine anticipated ground deformation at different loads and approximate the ground settlement and to checked displacements in Esfahan Subway Project.

Ota et al. (2013) evaluated landslide and deformation risks which have occurrence possibility in tunnel route by using the method of numerical analysis. They emphasised that three dimensional modelling give the best results in interpreting landslide and ground relationships in tunnel route. On ground stresses, displacement of the ground surface and deformations are criticized with numerical analyses.

Salimi et al. (2013) studied on surface subsidence caused by tunnel which was opened with TBM by using PLAXIS software with numerical analysis. Geometry of the tunnel and engineering geological properties of rock conditions were described in order to examine lining material, characteristics of the settlement and stress-deformation relationships in software program of PLAXIS.

Cho et al. (2014) reported that if jointed zone behaviours are examined, TBM and complex ground interactions should be considered. They preferred to utilize MIDAS-GTS NX software for FEM in order to understand the ground surface settlements, displacement and stability of the segments during the tunnel excavation. They compared fractured zone orientation and width with utilizing finite element methods to compute vertical displacement results when Earth Pressure Balance (EPB)-TBM excavates the tunnel.

Paltrinieri (2015) concentrated on TBM performance in highly jointed rock masses and fault zones. He emphasised that suitable TBM selection is critical for the achievement of the study. Thus, TBM performance parameters, property of tunnel, geological and engineering geology parameters should be analysed carefully.



Salam et al. (2015) claimed that rock, soil, ground and TBM's properties can be easily evaluated with 3D FEM in Greater Cairo Metro Line 3. Ground surface settlements due to construction of tunnels by slurry shield tunnel boring machine are predicted by MIDAS GTX NX software program which is crucial role in achieving effective results.

Ninic et al. (2016) characterized the geotechnical model, the alignment, the TBM and the lining shell, including various operational parameters. Large number parameters which represent the existing infrastructure are generally used in 3D numerical modelling of a tunnelling project for characterization of complex geotechnical condition.

The study region of Vassallo et al. (2016) has possible risk of landslide when railroad tunnel is excavated. Therefore, they focused on three dimensional modelling by using finite element methods in order to examine deformations. They emphasised that suitable software which can enable to evaluate engineering geological data sets with 3D numerical analysis are important to comprehend the landslide and tunnel relationships.

Yang et al. (2016) focused on numerical analysis of ground deformation stimulated by TBM in sand. FEM was applied by using PLAXIS 3D in order to capture the stress dilatancy behaviour of sand. They deduced that FEM simulation enables more assertive predictions of ground movements and flourish information about the risks.

Heama et al. (2017) utilized PLAXIS 3D software and FEM in their study. They analysed the effect of adjacent pile under loading on the existing tunnel by 3D FEM. On ground of structures, ground characteristics, tunnel depth, structural elements were also considered in undrained conditions to examine calculate deformations.

Vineetha et al. (2017) benefited from 3D numeric analyses in their study. Ground deformations and pore water pressures were evaluated for their critical parts by using 3D numerical analyses. During the TBM operation, TBM excavation stages and ground relations were successfully evaluated.

Sun et al. (2018) performed a study on TBMs dynamic behaviour. Load prediction of TBMs is vital in order to design safe operation for complicated engineering systems. TBMs dynamic behaviour has a significant impact on the load. Dynamic load prediction can be predicted by integration of heterogeneous in situ data which contain three steps. First, the geological data are extended to match the scale of the operation data using an interpolation method. Secondly, data which are categorical and numerical are combined with a 8picentre88 encoding method. Finally, the geological data are merged with the operation data according to the location of each operation datum.

The present study aims to examine the relationship between TBM and landslide by using 3D numerical analysis in complex Bahçe Region. The literature review showed that a TBM tunnel – landslides relationship investigated with 3D numerical analyses has not been encountered. During the present study, MIDAS software assists to develop FEM 3D model.

### **3. DESCRIPTION OF STUDY AREA**

This chapter is concerned with identifying the study area in terms of location, topography, climate and vegetation, geology, hydrogeology and landslide. ArcGIS software was used for data acquisition, preparation, and presentation of maps in this chapter.

#### **3.1. Location**

Twin tubes of Bahçe-Nurdağ railway tunnel route locates in about south-east Turkey between Km: 3+510-13+452 (Figure 3.1). Cities of Osmaniye and Gaziantep are connected with Bahçe-Nurdağ railway tunnel project. While tunnel coordinates from the Northern Hemisphere  $37^{\circ} 11'$  north latitude and  $36^{\circ} 35'$  east longitude for Bahçe portal, coordinates of Nurdağ portal are  $37^{\circ} 10'$  north latitude  $36^{\circ} 42'$  east longitude. Yanıktepe et al. (2011) described that Osmaniye is located in eastern the region of Mediterranean. It is also surrounded by the cities of Gaziantep, Hatay, Adana and Kahramanmaraş. While city of Gaziantep can be observable the east part of the Osmaniye, Adana has borders in west part of the Osmaniye. Moreover, Kahramanmaraş can be visible in north part of Osmaniye. Hatay also locates in south part of the Osmaniye.

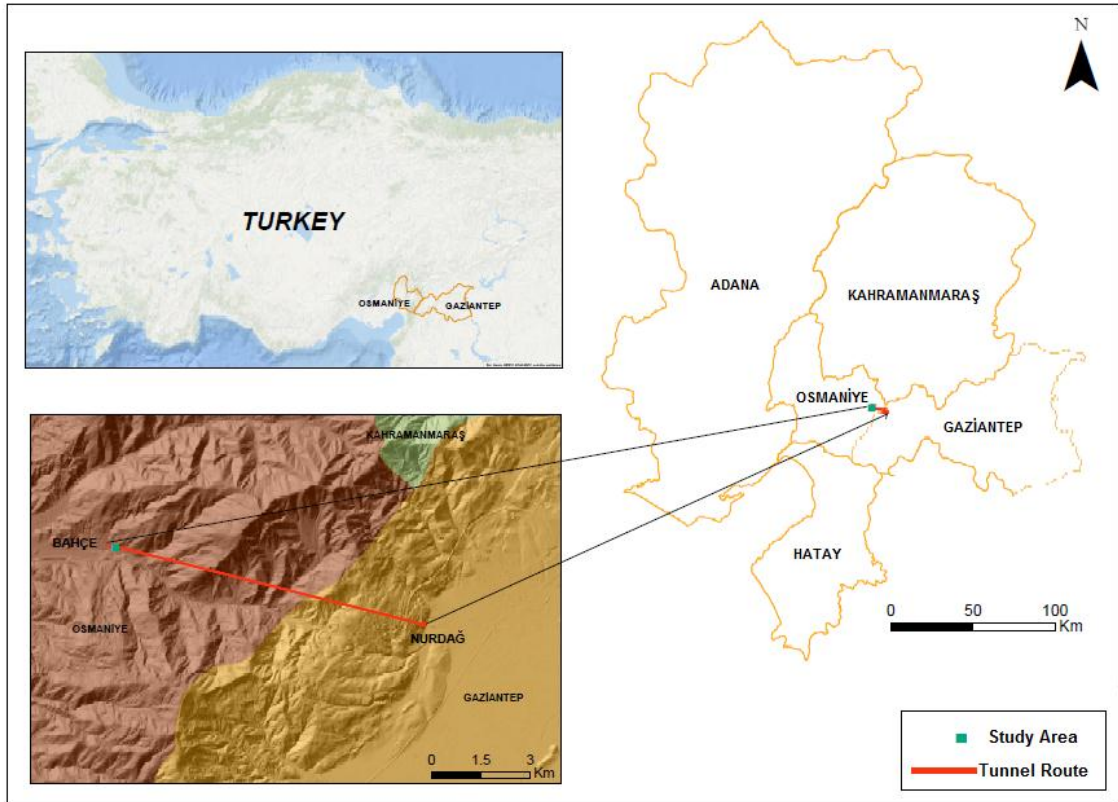


Figure 3.1. The location map of the study area has been presented as WGS 1984.

### 3.2. Topography

Interpretation of topographic maps have an important role in understanding of the morphology and geology of the surface and geological structures. Topography is also helpful to create geological maps and produce cross sections to be needed. Moreover, terrain is quantitatively representable by preparing DEM (Digital Elevation of Model). Using DEM obtained by SRTM (Shuttle Radar Topography Mission), various topographical analyses of an area in terms of altitude, slope and aspect maps can be performed.

### 3.2.1. Altitude

Republic of Turkey Ministry of Environment and Urbanization-Directory of Osmaniye Province (2017) stated that Amanos Mountain, Taurus Mountain, Dumanlı Mountain, Düldül Mountain and Tırtıl Mountain are significant mountains around the study region. Altitude map enables to analyse the categorized maximum and minimum of height of terrain (Yalcın et al., 2011). Altitude map is also critical for this study in order to analyse the tunnel route. Figure 3.2 demonstrates that the altitude varies between 400 and 1700 meters. Altitude was sorted into five classes (in units of meters): 400–600, 600–800, 800–1000, 1000–1300 and 1300–1700. The overburden of tunnel varies drastically as can be seen from the altitude map (Figure 3.2).

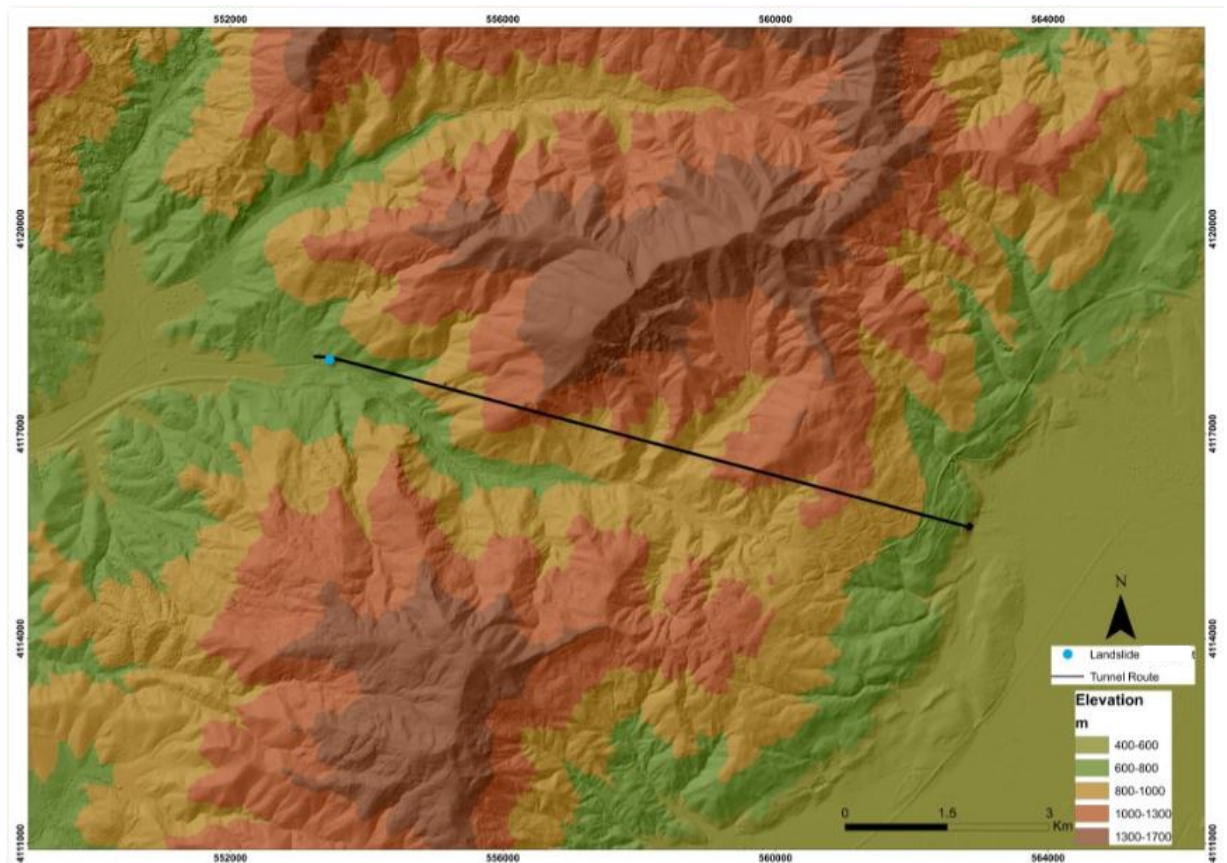


Figure 3.2. Altitude map of the study area.

### 3.2.2. Slope

Kanungo et al. (2006) pointed out that slope has a significant role in inducing slope instability. The slope map can be distinguished five classes which are  $0^{\circ}$ - $5^{\circ}$ ,  $5^{\circ}$ - $15^{\circ}$ ,  $15^{\circ}$ - $30^{\circ}$ ,  $30^{\circ}$ - $45^{\circ}$  and  $45^{\circ}$ - $85^{\circ}$ . The slope values vary between 0 to 85 degrees in the study area (Figure 3.3). In tunnel route has high slope degree some points because of high altitude points. As can be seen Figure 3.3, the Bahçe portal has high slope degree and tunnel at this part is shallow. Additionally, valley effect on the tunnel can be expected at near of the Bahçe portal.

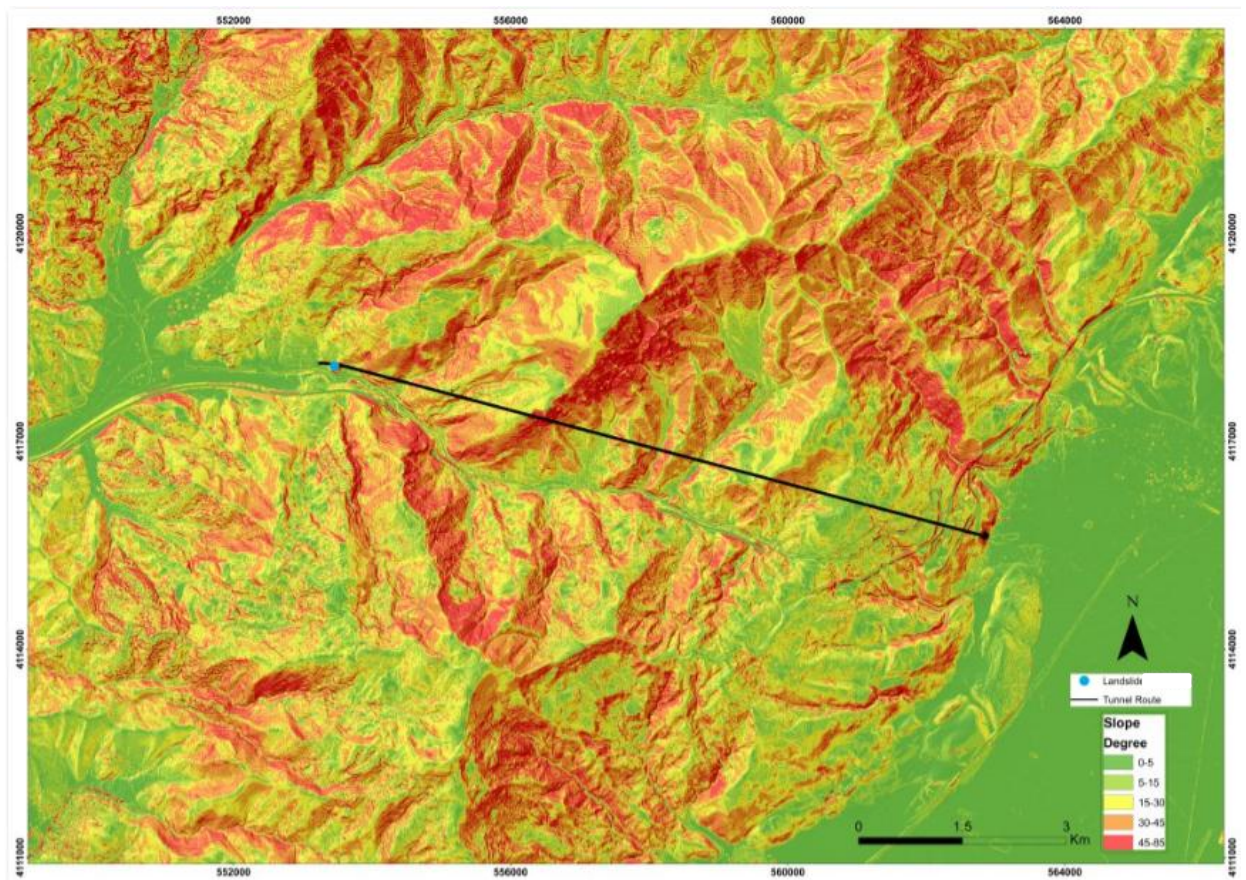


Figure 3.3. Slope map of the study area.

### 3.2.3. Aspect

Slope map and aspect map have close relationships to figure out the terrain. For instance, if terrain is flat, aspect map cannot be prepared due to not observable of slope. Quantities of sunshine and precipitation direction have effects on creating aspect map. Aspect values of the area change ranging from  $-1^\circ$  to  $360^\circ$ , where  $-1^\circ$  shows to flat areas. The aspect data layers were classified into nine classes; flat ( $-1^\circ$ ), north ( $0^\circ-22.5^\circ$ ), north-east ( $22.5^\circ-67.5^\circ$ ), east ( $67.5^\circ-112.5^\circ$ ), south-east ( $112.5^\circ-157.5^\circ$ ), south ( $157.5^\circ-202.5^\circ$ ), south-west ( $202.5^\circ-247.5^\circ$ ), west ( $247.5^\circ-292.5^\circ$ ), north-west ( $292.5^\circ-337.5^\circ$ ) and north ( $337.5^\circ-360^\circ$ ) (Figure 3.4). The general physiographic trend of area is approximately parallel to tunnel route (Figure 3.4).

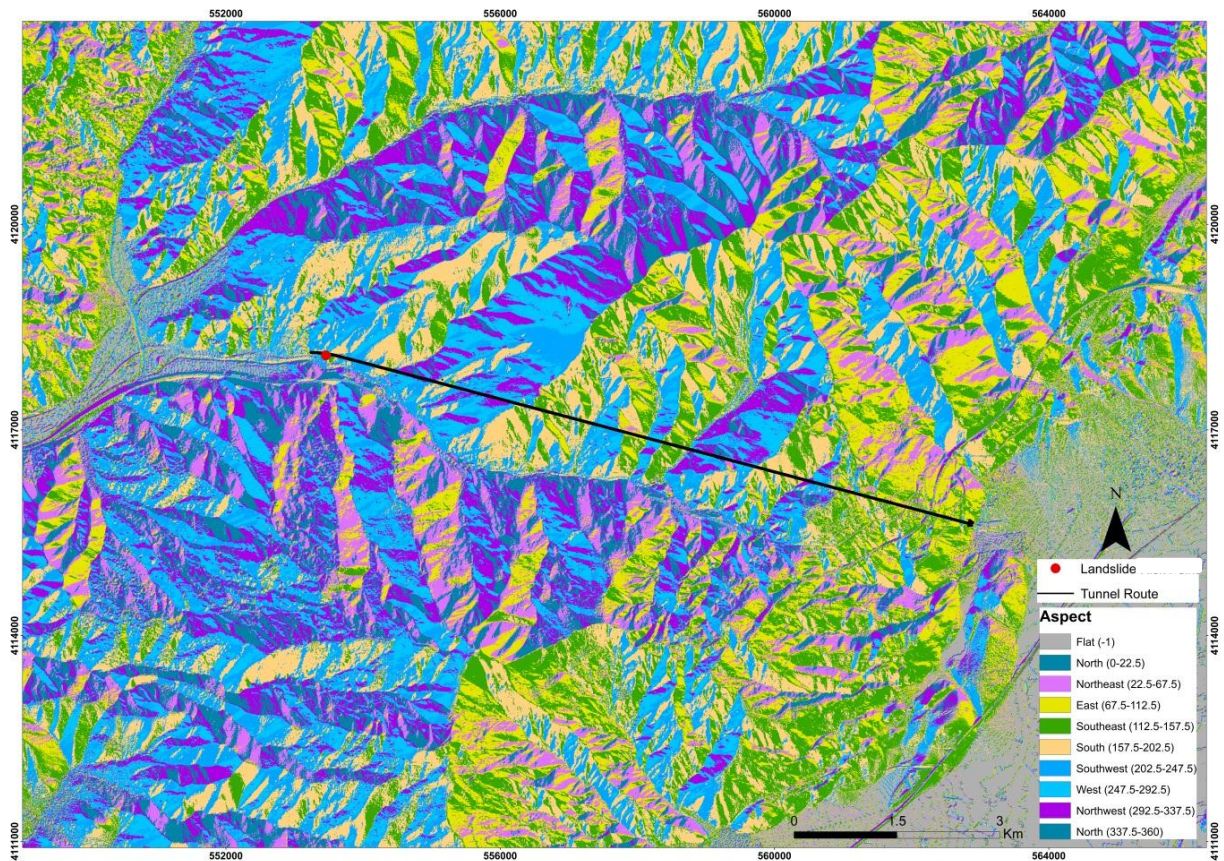


Figure 3.4. The aspect map of the study area.

### 3.3. Climate and Vegetation

In this part, Osmaniye's and Gaziantep's climate and vegetation were discussed because of tunnel route which is located in between Bahçe (Osmaniye) and Nurdağ (Gaziantep). Republic of Turkey Ministry of Environment and Urbanization-Directory of Osmaniye Province (2017) declared that vegetation covers pinus brutia, 14picen pine, black pine, oak and cypress etc. in the Osmaniye.

Tunnel route climate has a transition between Mediterranean and Eastern Anatolian Climate. However, Mediterranean climate is dominated in this region. Moreover, both cities climates are evaluated "Csa" according to Koppen climate classification (Turkish State Meteorological Service, 2016). "Csa" represents that while summer is dry and hot, climate is warm in winter. Detailed evaluations of climates for both cities are in below:

First, Table 3.1 which reveals the data taken from Turkish State Meteorological Service represents the extreme maximum, minimum and average temperatures between the period of in 1987 and 2018. When the average temperatures are examined with respect to month, the coldest month is January about 8.6 °C in Osmaniye. The hottest month is August about 28.5°C. Moreover, average of annually total precipitation is 827.6 mm in Osmaniye. Figure 3.5 is graphical monitoring annotation of Table 3.1.

Second, Gaziantep extreme maximum, minimum and average temperatures between the period of in 1940 and 2018 can be summarized in Table 3.2 which was prepared employing data taken from Turkish State Meteorological Service. Although the coldest month is January about 3 °C, the hottest month is July about 27.7 °C in Gaziantep. Furthermore, the value of 552.8 mm indicates the average of annually total precipitation in Gaziantep. Table 3.2 is used when producing Figure 3.6. However, the tunnel route locates in mountainous area and hence, the climate is perhaps different from all points of the route.



Table 3.1. Extreme maximum, minimum and average temperatures measure in the period of 1987-2018 in Osmaniye (Turkish State Meteorological Service, 2018).

	Average Temperature (°C)	Average Maximum Temperature (°C)	Average Minimum Temperature (°C)	Average of Monthly Total Precipitation (mm)	Maximum Temperature (°C)	Minimum Temperature (°C)
<b>January</b>	8.6	14.5	3.5	101.3	23.7	-8.5
<b>February</b>	10	16.1	4.6	102.2	28	-6.8
<b>March</b>	12.9	19.1	7.2	120.5	32	-4
<b>April</b>	17	23.5	10.9	82.6	36.5	0.1
<b>May</b>	21.1	27.7	14.9	75.2	41.7	4.6
<b>June</b>	25.2	31.3	18.9	36.2	42.6	11.5
<b>July</b>	27.9	33.5	22.5	10.3	42.8	15
<b>August</b>	28.5	34.3	23.1	5.7	43.6	15
<b>September</b>	25.5	32.1	19.3	29	41.2	7.8
<b>October</b>	20.6	28	14.2	73.8	38.3	4.1
<b>November</b>	14	21.5	8.2	94.7	31	-4.5
<b>December</b>	9.9	16	4.9	96.1	29	-5.4
<b>Annually</b>	18.4	24.8	12.7	827.6	43.6	-8.5

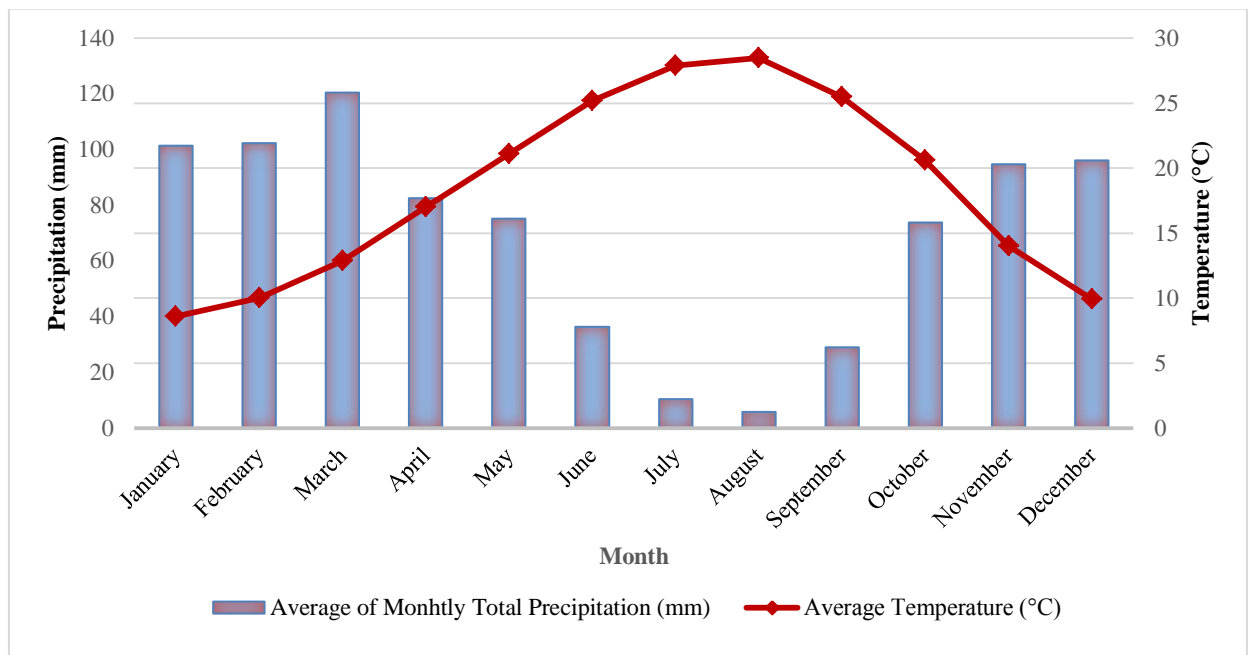


Figure 3.5. Graph showing monthly total precipitation and average temperature of Osmaniye meteorological station for the period of 1987-2018.

Table 3.2. Extreme maximum, minimum and average temperatures measure in the period of 1940-2018 in Gaziantep (Turkish State Meteorological Service, 2018).

	Average Temperature (°C)	Average Maximum Temperature (°C)	Average Minimum Temperature (°C)	Average of Monthly Total Precipitation (mm)	Maximum Temperature (°C)	Minimum Temperature (°C)
January	3	7.5	-0.7	102.1	19	-17.5
February	4.3	9.4	0.1	82.6	24.3	-15.6
March	8	13.9	3	71.3	28.1	-11
April	13.2	19.7	7.3	52.6	34	-4.3
May	18.6	25.4	11.9	31.3	37.8	0.4
June	24	31.2	17.1	6.9	39.6	4.5
July	27.7	35.1	21.1	2.7	44	9
August	27.4	35.1	20.9	1.8	42.8	10.8
September	22.8	31.1	16.2	5.7	40.8	3.4
October	16.1	24.1	10	36.4	36.4	-3.9
November	9.4	16.2	4.5	61.8	27.3	-9.7
December	4.8	9.7	1	97.6	24.4	-15
Annually	14.9	21.5	9.4	552.8	44	-17.5

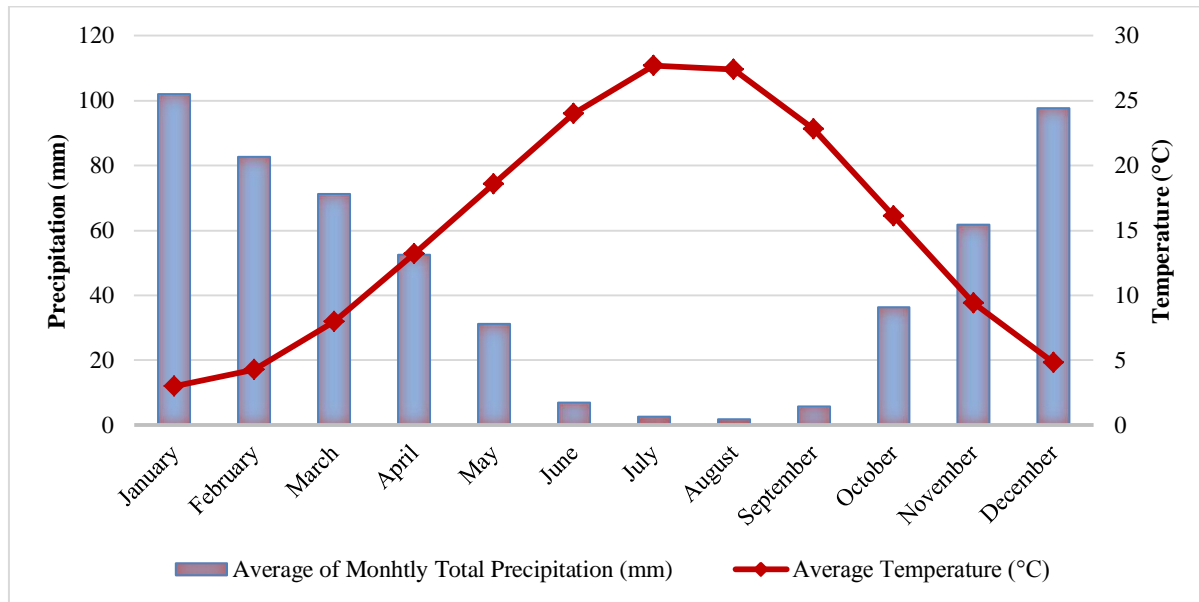


Figure 3.6. Graph showing monthly total precipitation and average temperature of Gaziantep meteorological station for period of 1940-2018.

### 3.4. Geology

In order to identify the geology of study area, this part of thesis is composed of two parts: stratigraphy and lithological characteristics of study area.

#### 3.4.1. Stratigraphy

The general geological characteristics of the study area and its surroundings are summarized from Usta (2018) which is publication of MTA Earthsciences. Formations which are Beyoğlu, İslahiye, Nurdağı, Olucak, Hasanbeyli, Dedeler, Kardere, Seydişehir, Çaltepe and Zabuk are observed around the tunnel route (Figure 3.7). Figure 3.7 is vital to comprehend the Bahçe Nappe stratigraphy. Furthermore, Figure 3.8 manifests the geological map of the tunnel route.

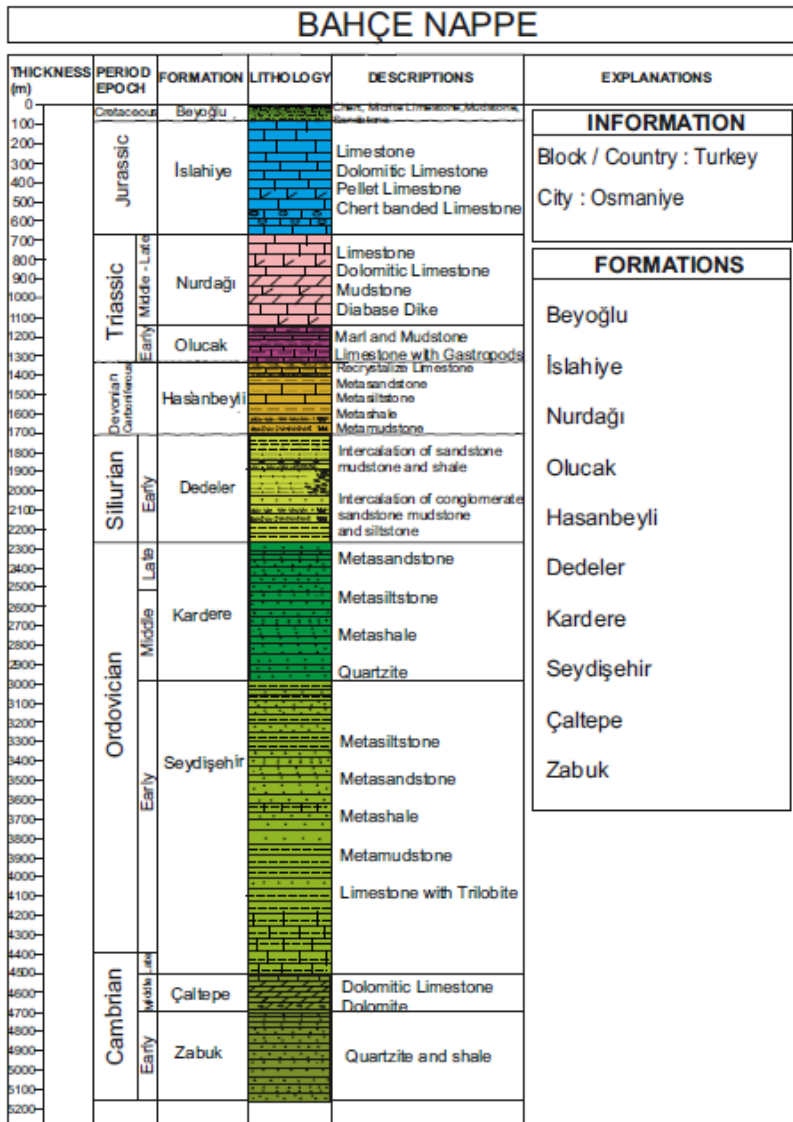


Figure 3.7. Bahçe Nappe stratigraphy (Reproduced after Usta, 2018).

#### **3.4.1.1. Zabuk Formation (Ez)**

The formation was named by Schmidt (1964). Usta (2018) express that white, yellowish-beige, pink, green colour quartzite and shale is dominated in this formation. Zabuk formation is conformably overlaid by Çaltepe formation. Zabuk formation does not have specific fossils. It was deposited in shallow shelf environment. Thickness of formation is approximately 450-500 meters (Usta, 2018).

#### **3.4.1.2. Çaltepe, Formation (Eç)**

Çaltepe formation which was named Dean and Monod (1970) is characterized with dolomite and dolomitic limestone. It includes intercalation of gray, dark colour gray, black and brown dolomite, dolomitic limestone and oolitic dolomite. It is conformable with Zabuk and Seydişehir formations. Contrary to Zabuk and Seydişehir formations, it is unconformable with İslahiye formation. Thickness of Çaltepe formation is 175 m (Usta, 2018).

#### **3.4.1.3. Seydişehir Formation (EOs)**

Formation consists of intercalation of limestone, metasiltstone, metasandstone, metashale, metamudstone (Blumenthal, 1947; Dean and Monod, 1970). This formation was named as Sosink formation in Amanos, Kızlaç formation in Villages of Kızlaç, Bahçe formation in Bahçe. It was also deposited in shallow shelf environment. Formation is conformably located above of Çaltepe and settled unconformably below of Kardere. Traces of trilobites are also observable in limestone (Usta, 2018).

#### **3.4.1.4. Kardere Formation (Ok)**

Kardere formation contains the lithology of metasandstone, metashale and quartzite. It was named by Yalçın (1979). However, this formation was examined as Bahçe Formation by Lahner (1972). In addition, this formation was named as Seydişehir formation which is divided as Kardere and Kızlaç by Yılmaz et al. (1984). Formations can be representable as gray, light gray, light pink, brownish and purple quartzite, shale and intercalation of metasandstone and metasiltstone (Usta, 2018). It is conformable with Seydişehir and Dedeler formations. It was deposited in shallow marine environment (Usta, 2018).

#### **3.4.1.5. Dedeler Formation (Sd)**

Formation is composed of intercalation of metaconglomerate, metasandstone, metamudstone, metasilstone, metashale (Lahner 1972).

#### **3.4.1.6. Hasanbeyli Formation (Dch)**

Formation consists of metashale, metasandstone, kalkschist, metasilstone, quartzite, dolomite and recrystallized limestone (Usta, 2018).

#### **3.4.1.7. Amanos Group (Atrjk)**

##### **3.4.1.7.1. Olucak Formation (Atro)**

Limestone, dolomite, intercalation of mudstone and marl and quartzite are main units to define the Olucak formation. It unconformably overlies Hasanbeyli formation, Kardere formation and Seydişehir formation (Usta, 2018).

##### **3.4.1.7.2. Nurdağı Formation (aTRn)**

Nurdağı formation includes dolomite, limestone and dolomitic limestone. Nurdağ formation conformably overlies Olucak formation. It is also conformably overlaid by İslahiye formation. Unlike İslahiye formation, it is unconformable with Hasanbeyli, Kardere and Seydişehir formations. This formation is defined in shallow marine environment in terms of containing shallow marine carbonates. Nevertheless, it is also represented by terrestrial environment with respect to including mudstone (Usta, 2018).

##### **3.4.1.7.3. İslahiye Formation (aJKi)**

İslahiye formation consists of limestone, dolomite and dolomitic limestone and limestone with chert. While it is conformable with Nurdağı formation, it is cut by Beyoğlu formation. The formation was formed in shallow marine environment (Usta, 2018).

##### **3.4.1.7.4. Beyoğlu Formation (Ktbe)**

It consists of mudstone, sandstone, micritic limestone, chert and shale. Beyoğlu formation was named by Usta (2015). The formation was formed in deep marine environment (Usta, 2018).

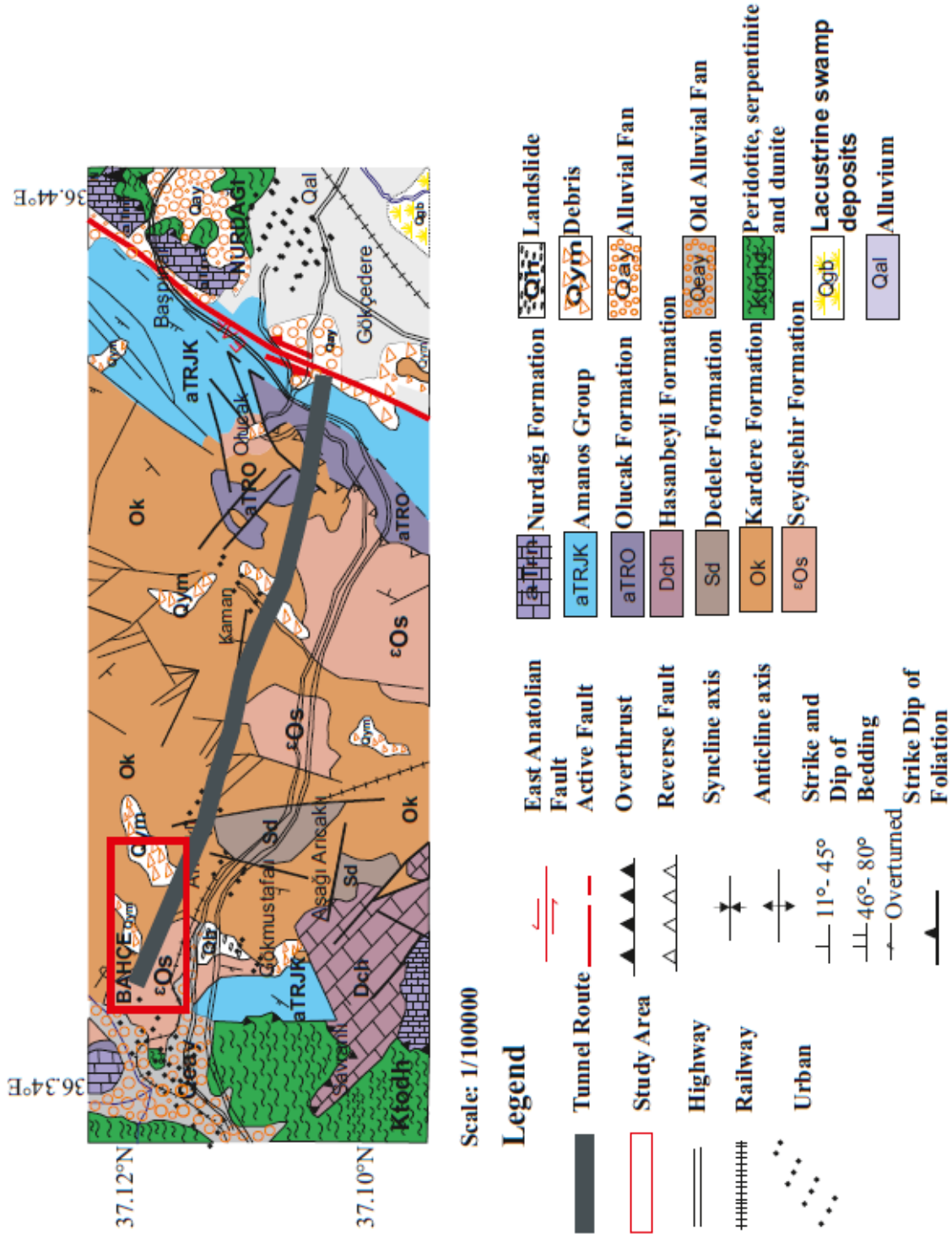


Figure 3.8. Geological map of tunnel route (Modified after Usta, 2018).

In addition, Figure 3.9 is important to understand the geology of the study area. It enables to see formations, drillholes and tunnel route around the study area. According to Figure 3.9, Seydişehir and Kardere formations are critical for Bahçe portal.

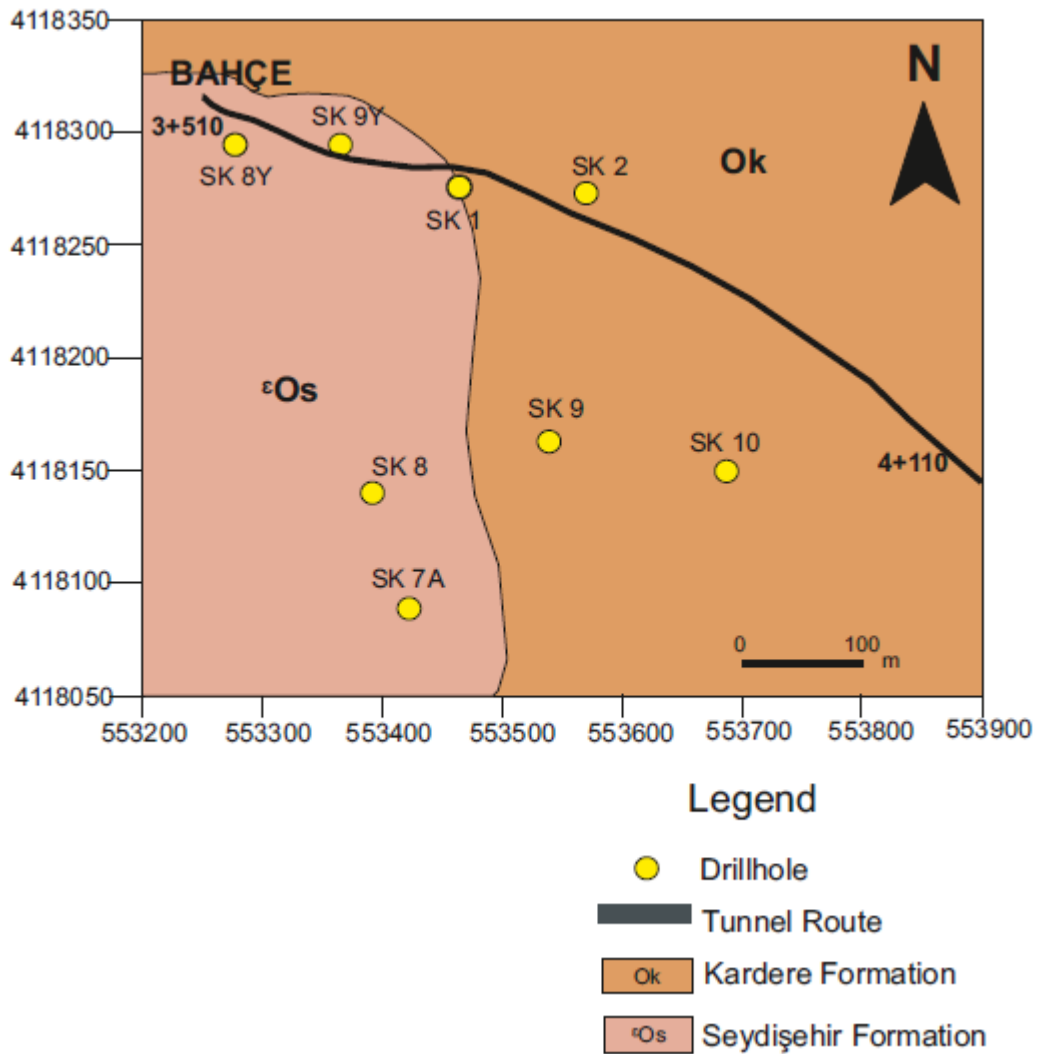


Figure 3.9. Geological map of study area.

### **3.4.2. Lithological Characteristics of Study Area**

General stratigraphy of the project area was expounded in previous section under title of Geology. Description of the geological characteristics of the study area has a critical role in suggesting convenient solution some problems such as landslide.

Main units which are observable in tunnel route are debris, metamudstone, metasandstone, quartzite and limestone (Usta, 2018). While debris materials which are dark brownish and red colour are conglomerate with clay, metamudstone and metasandstone are brownish-gray colour, fractured and fragmented. Usta (2018) described that quartzite are purple, green, white, yellow colour, parallel and cross laminated and middle to thick layered. In addition, he stated that dolomitic limestone and recrystallized limestone is observable in this study area. While dolomitic limestone is brownish gray colour, thick layered and oolitic, recrystallized limestone is brownish-gray colour and middle to thick layered.

This thesis especially focuses on Km: 3+510 and Km: 4+110 of the route. General geology of project area consists of three major units which are metamudstone, metasandstone and debris for Km: 3+510 and 4+110. In order to identify the geology in detail, cross section was drawn denoted as (Figure 3.10). Necessary information and data which are SK1, SK2, SK7A, SK8, SK8Y, SK9, SK9Y, SK10 and SK11 provided by TCDD were combined together to characterize the geological area (Table 3.3). Reproduced borehole information were also given in Appendix. Engineering geological cross section allows to monitor the geology of the area (Figure 3.10). According to Figure 3.10, there are metasandstone-metamudstone bedrock at the bottom, heavily jointed metasandstone-metamudstone above it and finally debris as the cover. This section displays the general characteristics of the subsurface.



Table 3.3. Boreholes information for between KM: 3+510 and 4+400 (TCDD, 2014).

<b>Borehole</b>	<b>Coordinates</b>	<b>Lithology</b>
SK1	X: 553486.445	0-75.00 m:
	Y: 4118276.627	Metasandstone-Metamudstone
	Z: 674.144	
SK2	X: 553582.824	0-76.00 m:
	Y: 4118278.827	Metasandstone-Metamudstone
	Z: 673.999	
SK7A	X: 553448.802	0-17.40 m: Debris
	Y: 4118083.800	17.40-41.00 m:
	Z: 627.407	Metasandstone-Metamudstone
SK8	X: 553414.789	0-13.50 m: Debris
	Y: 4118139.799	13.50-40.00 m:
	Z: 629.850	Metasandstone-Metamudstone
SK8Y	X: 553302.3337	0-12.00 m: Debris
	Y: 4118294.786	12.00-40.00 m:
	Z: 634.8622	Metasandstone-Metamudstone
SK9	X: 553544.349	0-1.00 m: Debris
	Y: 4118154.948	1.00-50.00 m:
	Z: 639	Metasandstone –Metamudstone
SK9Y	X: 553382.91	0-10.50 m: Debris
	Y: 4118295.532	10.50-50.00 m:
	Z: 644.3197	Metasandstone-Metamudstone
SK10	X: 553701.371	0-15.50 m: Debris
	Y: 4118151.093	15.50-50.00 m:
	Z: 642.300	Metasandstone-Metamudstone
SK11	X: 554035.719	0-18.90 m: Debris
	Y: 4118164.758	18.90-92.50 m:
	Z: 685	Metasandstone-Metamudstone

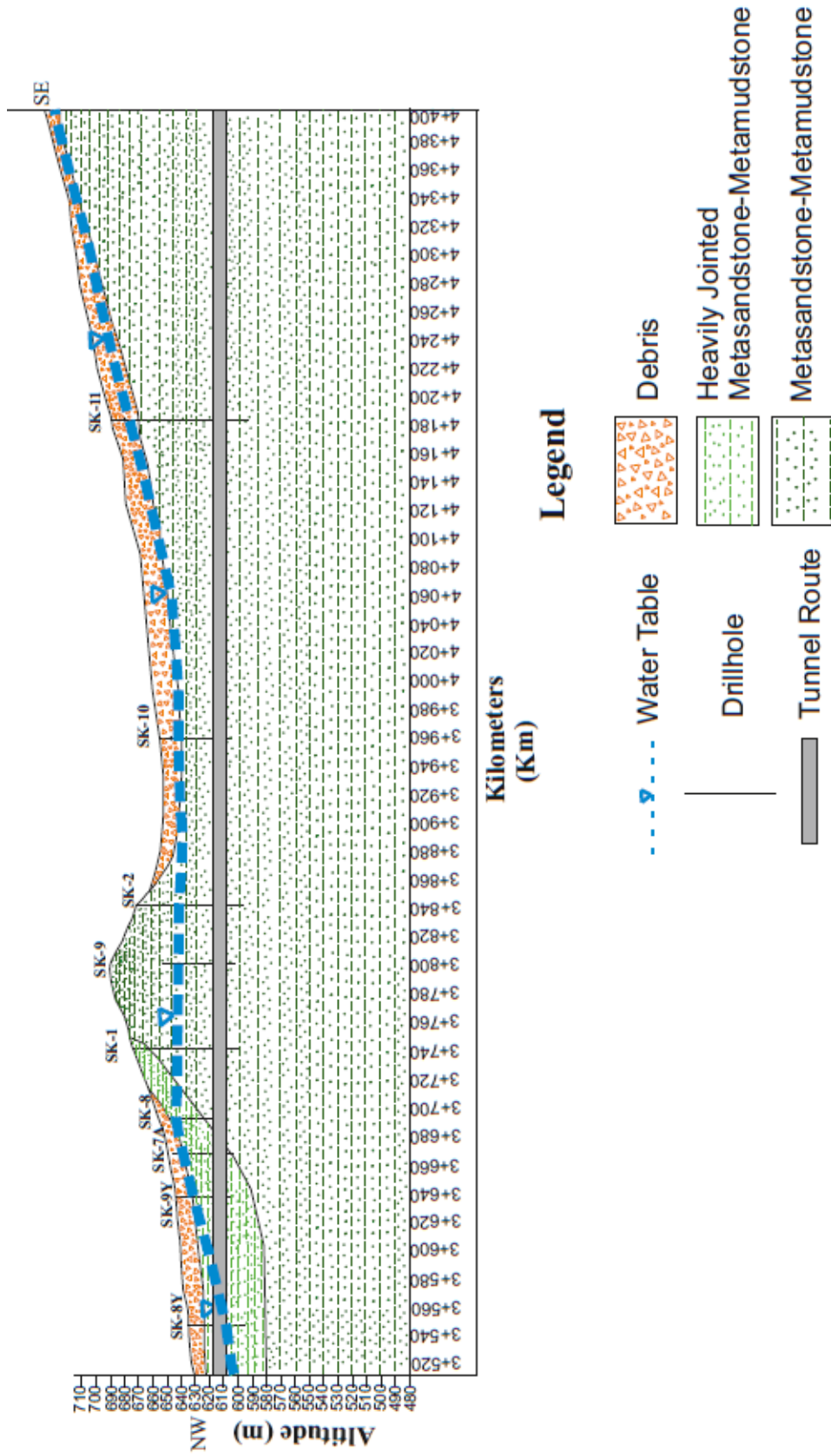


Figure 3.10. Engineering geological cross section of the tunnel route (Reproduced after TCDD, 2018).

### 3.5. Hydrogeology

Republic of Turkey Ministry of Environment and Urbanization-Directory of Osmaniye Province (2017) remarked that Ceyhan River, Kalecik River, Karaçay, Kesiş Creek, Horu Creek, Karaçay River, Savrun Creek, Kesiksuyu River, Sabunsuyu Creek and Yarbuz Creek can be observable with respect to hydrologic features around the study area. They also pointed out that groundwater flows east to west.

Hydrogeological characterization is very important issue to develop an understanding the hydrogeological setting by maximizing the benefit of the data at hand. Data are used to explain subsurface. Adequate amounts of lithologic and hydrologic data are available which are obtained from boreholes to create a complete characterization of the hydrogeology. According to information obtained from boreholes, while metamudstone is impermeable stratum, metasandstone and quartzite has secondary porosity. Groundwater levels are manifested in Table 3.4. According TCDD (2014) data sets, SK7A, SK8, SK9, SK10, SK11 groundwater levels were taken at the period of between July, 2013 to January, 2014. SK1 and SK2 groundwater levels were also measured on April, 2017. Groundwater levels can also be observed from Figure 3.10 shows engineering geological cross section of the tunnel route. Groundwater level decreases toward tunnel portal. Depending on this cross section and obtained data, it is comprehensible that the prevalent direction of groundwater flow in the tunnel route is toward the west.

Table 3.4. Groundwater levels measured in the boreholes by TCDD.

<b>BH ID</b>	<b>SK-1</b>	<b>SK-2</b>	<b>SK-7A</b>	<b>SK-8</b>	<b>SK-9</b>	<b>SK-10</b>	<b>SK-11</b>
<b>Groundwater Level (m)</b>	639.14	639.99	627.43	625.35	635.65	639.35	680.00

### **3.6. Landslide**

Cruden (1991) defined that landslide is the movement of rock mass, soil, and debris near the earth's surface under the effect of gravity. Not only natural activities cause landslide but human activities also trigger landslides in the environment (USGS, 2008). While natural conditioning and triggering factors are slope, aspect, geology, hydrologic properties, seismicity and volcanic activity, human impacts are urbanization, decreasing of forests, unconscious land use and constructions.

The landslide problem is a common hazard throughout the World. In Turkey, the second most widespread geological hazards are landslides (AFAD, 2018). Some region in Turkey has a high landslide hazard. One of the high landslide regions is Bahçe Region. When construction project such as tunnel work can be applied by considering landslide, landslide related damages can be eliminated. Thuro et al. (2011) expressed that tunnel excavation cause landslide in landslide-prone areas. Bahçe-Nurdağ railway tunnel route is located in vicinity of landslide. When tunnel construction alternative is chosen, Bahçe region should be evaluated in terms of landslide activity. Active and old landslides on the route can also be examined from landslide inventory map (Duman et al., 2011), which is presented in Figure 3.11. It was obtained from Earthsciences Portal of MTA. It manifests that tunnel route area has high potential landslide. In addition, landslide occurred in the between Km: 3+215 and 3+580 during construction of Gaziantep-Osmaniye highway. This area is very close to Bahçe-Nurdağ railway tunnel portal part of Bahçe which is located in between Km: 3+510 and 4+110. Thus, landslide effect should not be neglected during tunnel construction. Moreover, tunnel is very long to be completed with TBM in this study. If tunnels are finalized with TBM, TBM may trigger landslide. Therefore, ground surrounding, the tunnel will be modelled to clarify TBM and landslide relationships in Chapter 7.

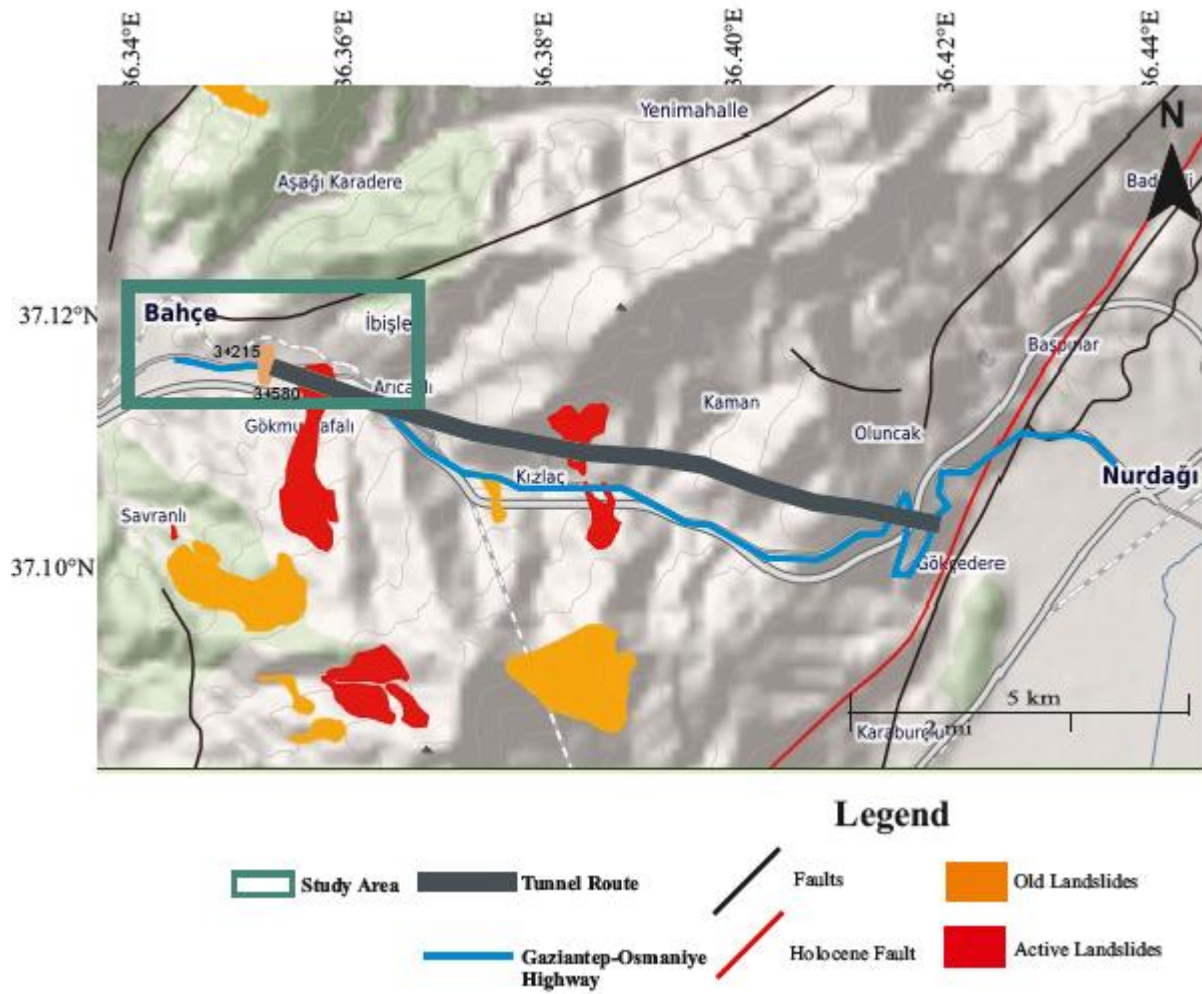


Figure 3.11. Landslide inventory map of study area (Modified after Duman et al., 2011).

#### 4. SEISMICITY OF THE STUDY AREA

Within the scope of the study, seismic analyses of the study area and its immediate surrounding were performed in this chapter. There are five important steps to evaluate the seismicity of the particular region. First, it should be indicated that seismic hazard analysis especially focuses on Bahçe in the Osmaniye Province. Bahçe which is district of Osmaniye has high the earthquake risk according to Earthquake Hazard Maps of Turkey (AFAD, 2018). Secondly, active faults characteristics should be determined to identify the seismicity of the study area. For this study area, EAFZ observed as an active fault. EAFZ is one of the major fault zone is still active and left lateral strike slip fault in Turkey (Figure 4.1). East Anatolian Fault Zone is elongated about 580 km between Karlıova and Antakya (Arpat et al., 1972; McKenzie, 1972; Seymen, 1972; Arpat et al., 1975; Ambrasseys, 1989; Doruk, 1991; Herece et al., 1992; Şaroğlu et al., 1992a; Şaroğlu et al., 1992b; İmamoğlu and Çetin, 2007). As is known that the other main fault zone is North Anatolian Fault Zone. Intersection of EAFZ and NAFZ represents the beginning of the EAFZ which continue to valley of Göynük with fault throw of 17 km. Although in Bingöl Region the fault zone is not seen clearly, it can be visible in between Palu and Pötürge regions (Şaroğlu et al., 1987; Herece et al., 1992). EAFZ is divaricated in the south region of Kahramanmaraş. One is contributed to occurring of Amanos Fault. The other continues to North of Osmaniye-Bahçe. When it passes Osmaniye, it reaches Karataş (İmamoğlu and Çetin, 2007).

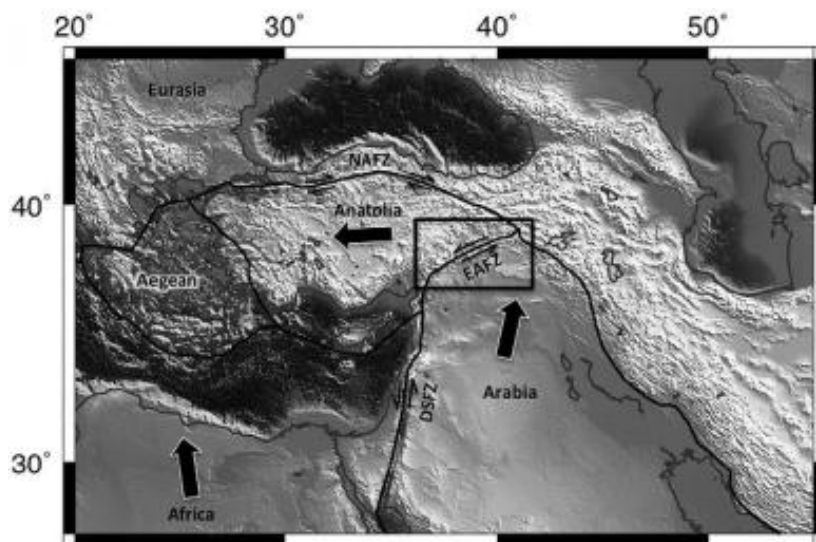


Figure 4.1. Location map of EAFZ (Bulut et al., 2012)

Additionally, Nalbant et al. (2002) studied about EAFZ stress evolution since 1822 in order to investigate high stresses accumulations for Kahramanmaraş (KM) region (Figure 4.2). In spite of limited information about KM seismic activity, they also pointed that earthquake may occur magnitude of 7.3 in case of 29picentre29 segments broken. Historical records show that an earthquake occurred in 1114; in fact, its magnitude has been estimated to be equal or greater than 7.8 (Nalbant et al., 2002). In addition, another earthquake occurred whose magnitude is predicted about 7.4 in 1513. Not only Mısır was affected from this earthquake but it also caused severe damages in Tarsus and Malatya (Gökçeoğlu, 2018). Considering these information about this fault segment, an earthquake is expected to be  $\geq 7.3$ .

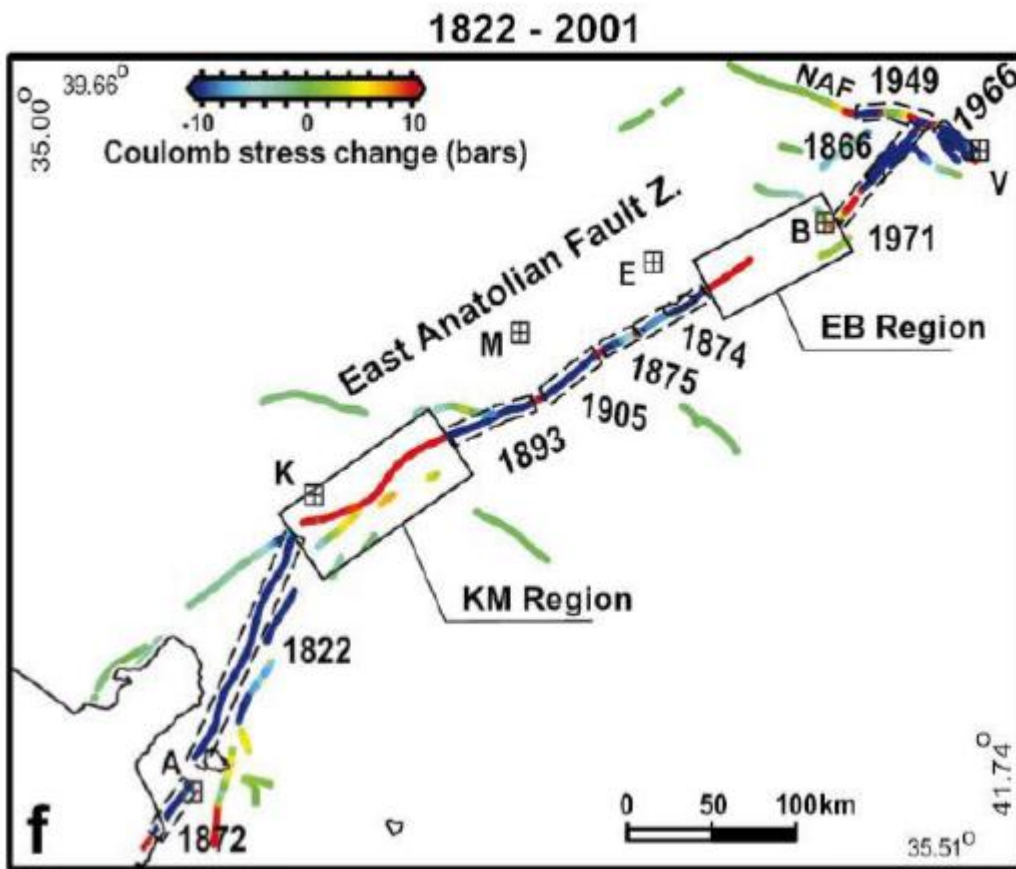


Figure 4.2. Stress accumulation on EAFZ (Nalbant et al., 2002).

Third step is to analyse the study area in terms of seismicity, earthquake data have to be prepared for determined magnitude through years to today. When study area is accepted as the center, distributions of earthquake 30picentre records are analysed. In this study, distribution of the earthquakes having a magnitude of  $M=4$  and above occurred between years of 1915-2019 were considered. Table 4.1 represents that between the periods of 1915-2019 earthquake data having magnitudes of  $M \geq 4$  were provided from Boğaziçi University, Kandilli Observatory and Earthquake Research Institute National Earthquake Monitoring Center. Distribution of magnitude of  $M \geq 4$  in the study area and main active faults are also indicated in Figure 4.3. According to Figure 4.3, the study area can be defined as intense in terms of the seismic activity.

Table 4.1. Distribution of the ground movements having a magnitude of  $M \geq 4.0$  occurred between 1915-2019 in the study area and its immediate surrounding.

<b>Region</b>	<b>Date</b>	<b>Magnitude</b>	<b>Type</b>	<b>Latitude</b>	<b>Longitude</b>
Belen/ Hatay	25.12.1915	5.4	Xm,Mw	36.47	36.14
Ceyhan/Adana	20.03.1945	6.0	Xm,Mw	37.11	35.70
İskenderun/Antakya	08.04.1951	5.8	Xm,Mw	36.58	35.85
İskenderun/Antakya	12.07.1951	4.9	Xm,Mw	36.60	36.30
Ceyhan/Adana	22.10.1952	5.7	Xm,Mw	37.25	35.65
Osmaniye	07.04.1967	4.9	Xm,Mw	37.43	36.17
Hatay	30.05.1968	4.3	Xm	36.30	36.20
Hatay	01.01.1975	5.2	xM	36.67	36.49
Hatay	02.01.1980	4.6	xM	36.56	36.38
Hatay	24.02.1981	4.4	xM	36.44	36.18
Hatay	19.02.1981	4.6	xM	36.35	36.42
Antakya	30.06.1981	4.7	xM	36.17	35.89
Hatay	11.02.1982	4.2	xM	36.08	35.89
Hatay	11.08.1991	4.0	xM	36.15	35.90
Antakya	22.01.1997	5.0	xM	36.13	36.08
Hatay	23.01.1997	4.0	xM	36.16	36.33
Ceyhan/Adana	27.06.1998	6.3	xM	36.96	35.52
Osmaniye	25.06.2001	5.5	xM,Mw	37.12	36.28
Adana	18.10.2001	4.8	xM	36.78	35.37
Hatay	22.11.2002	4.2	xM	35.96	36.31
Osmaniye	17.01.2009	4.6	xM	37.0867	36.3592



Table 4.1cont. Distribution of the ground movements having a magnitude of  $M \geq 4.0$  occurred between 1915-2019 in the study area and its immediate surrounding.

Samandağ/Hatay	17.06.2009	4.5	MI	36.1321	36.0173
Kozan/Adana	24.07.2009	4.7	xM	37.4913	35.7431
Aladağ/Adana	05.08.2010	4.4	xM	37.724	35.5513
Osmaniye	16.11.2010	4.5	xM,MI	37.3082	36.4127
Kozan/Adana	29.06.2011	4.5	xM	37.36	35.87
Kozan/Adana	23.04.2011	4.0	xM	37.47	35.58
Andırın/Kahramanmaraş	07.09.2011	4.2	xM,MI	37.3697	36.3235
Kilis	04.04.2012	4.3	xM,MI	36.9585	37.0245
İskenderun	12.07.2012	4.0	xM	36.5533	35.901
Merkez/Kahramanmaraş	22.07.2012	5.0	xM,MI	37.542	36.3795
Kozan/Adana	16.09.2012	4.7	xM,MI	37.4525	35.7538
Pazarcık/Kahramanmaraş	19.09.2012	5.1	xM,MI	37.3203	37.1173
Pazarcık/Kahramanmaraş	19.09.2012	4.1	xM,MI	37.46	35.87
Pazarcık/Kahramanmaraş	16.10.2012	4.5	xM,MI	37.3067	37.1233
Pazarcık/Kahramanmaraş	16.10.2012	4.6	xM,MI	37.26	37.20
Düziçi/Osmaniye	12.12.2012	4.1	xM,MI	37.30	36.2708
Şehitkamil/Gaziantep	25.04.2013	4.3	xM	37.3148	37.1367
Pazarcık/Kahramanmaraş	01.05.2013	4.0	xM,MI	37.304	37.1215
Pazarcık/Kahramanmaraş	06.05.2013	4.0	xM,MI	37.3063	37.1468
Ekinözü/Kahramanmaraş	16.06.2013	4.2	MI	38.05	37.07
Kadirli/Osmaniye	07.11.2013	4.0	xM,MI	37.396	36.2358
Kadirli/Osmaniye	10.01.2014	4.4	xM,Mw	37.3065	36.2035
Andırın/Kahramanmaraş	22.01.2015	4.0	xM,MI	37.3995	36.3053
Samandağ/Hatay	10.02.2015	4.6	xM,MI,Mw	36.0278	35.975
Andırın/Kahramanmaraş	28.03.2015	4.1	xM,MI,Mw	37.482	36.4072
Pazarcık/Kahramanmaraş	26.08.2015	4.2	xM,MI	37.303	36.975
Ceyhan/Adana	31.03.2016	4.1	xM	36.9658	35.8467
Erzin/Hatay	25.02.2017	4.5	xM,Mw	36.9255	36.0902
Araban/Gaziantep	18.08.2017	4.4	xM,MI	37.494	37.6171
Samandağ/Hatay	20.02.2019	4.1	xM,MI,Mw	36.0668	35.8865

Earthquake magnitudes which have the magnitude of  $M \geq 4$  can be reclassified in order to count the number of earthquakes by using later analysis. Reclassification groups are selected as  $4.0 \leq M < 4.5$ ,  $4.5 \leq M < 5.0$ ,  $5.0 \leq M < 5.5$ ,  $5.5 \leq M < 6.0$  and  $6.0 \geq M$ . Figure 4.4 shows that relation between the reclassification groups and their occurrence numbers.

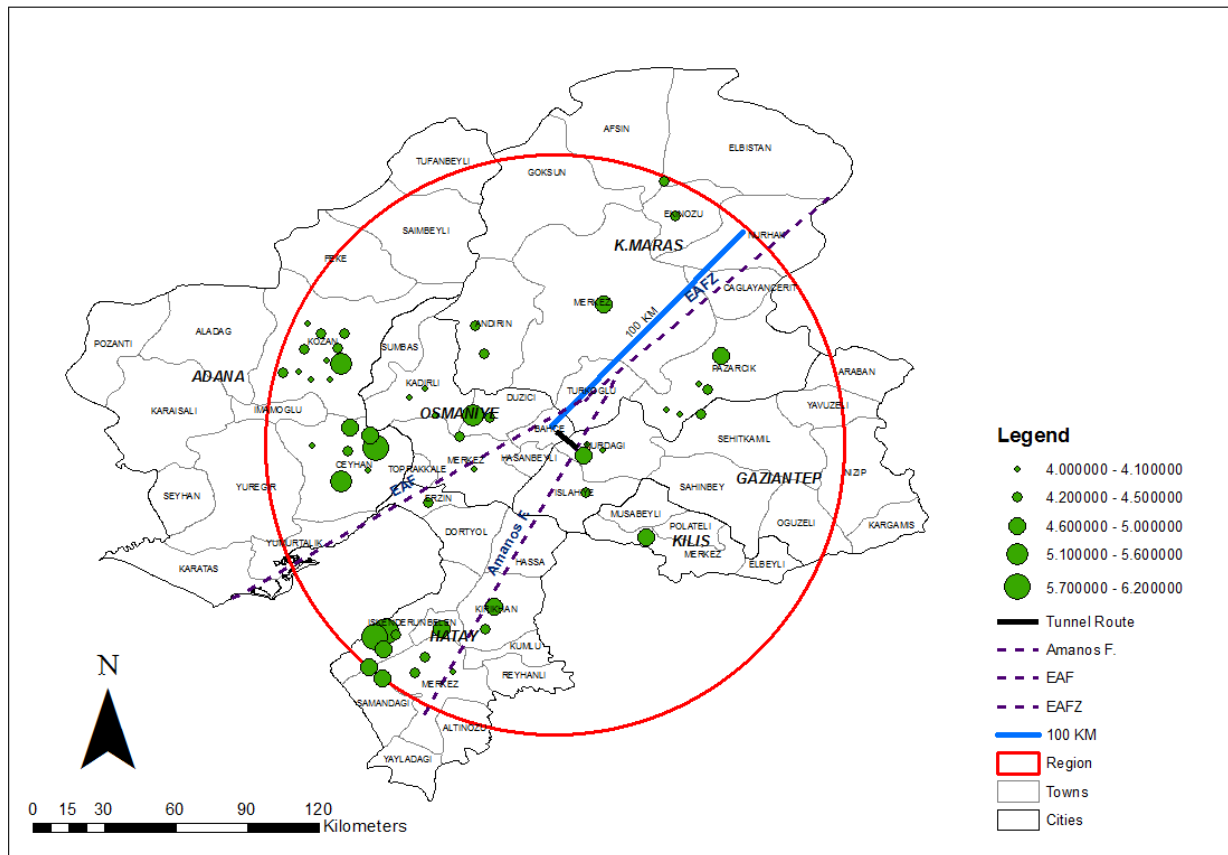


Figure 4.3. Active faults observed in the study area and it surrounding and distribution of the ground movements having a magnitude of  $M \geq 4$  occurred between 1915-2019.

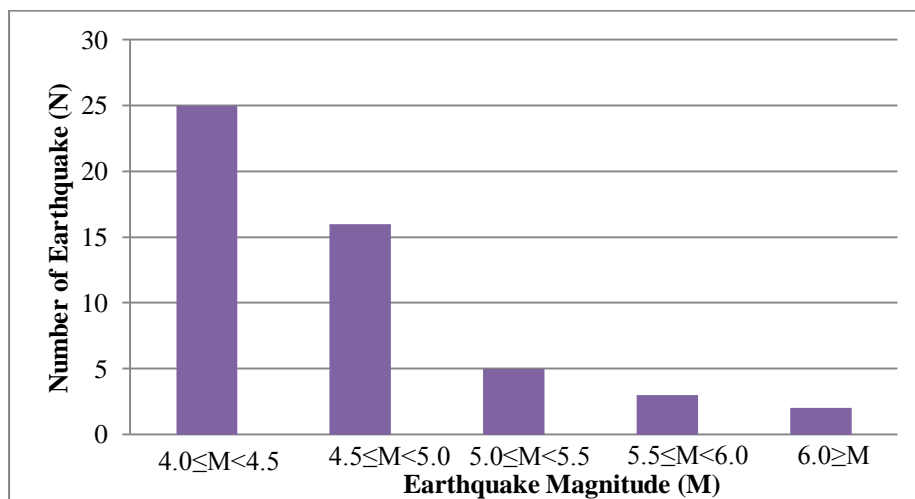


Figure 4.4. Frequency distribution relating to the strong ground movements occurred in the study area and its surrounding between the years 1915-2019 (distribution is given for  $M \geq 4.0$ ).

Law of the Gutenberg and Richter (1954) is evaluation of uncertainties with respect to earthquake magnitudes data sets. Equation 4.1 clarifies the law of Gutenberg and Richter.

$$\log N = a - bM \quad (4.1)$$

Figure 4.3 was prepared, according to Gutenberg and Richter laws employing magnitude of  $M \geq 4$  between the years 1915-2019 in the area and its surrounding. When the Figure 4.5 is considered, the expression of the Gutenberg and Richter equation is also given in Equation 4.2.

$$\log(\Sigma N/t) = -0.4232M_{avg} + 2.413 \quad (4.2)$$

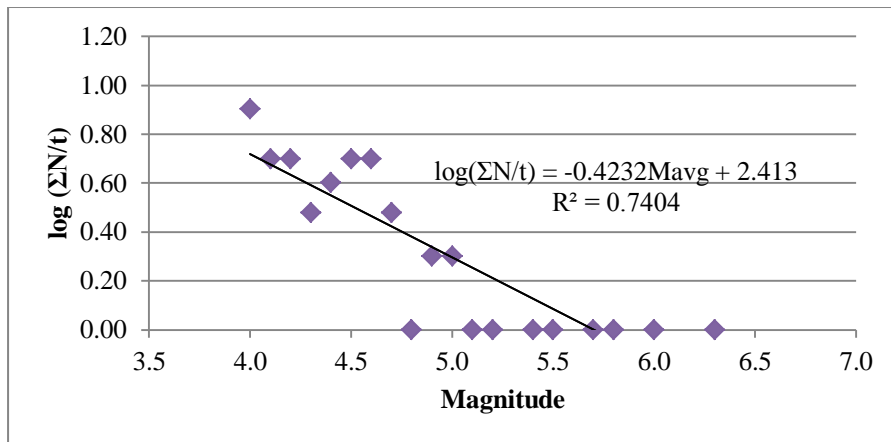


Figure 4.5. Average earthquake magnitude relating to the strong ground movements occurred in the study area and its surrounding between the years 1915-2019 and  $\log(\Sigma N/t)$  relationships.

Furthermore, Poisson probability model is also significant in terms of evaluation of temporal uncertainty relating the earthquake magnitudes which have a probability of possible occurrence of the specific magnitudes in the study area and its surroundings. It is also used for calculating of average return periods. Poisson probability equation is shown in Equation 4.3. In this equation,  $P_n(t)$  is the probability of numbers of  $n$  earthquakes within the time and  $v$  is number of the average occurrence of earthquakes in unit of time.

$$P_n(t) = \frac{e^{-vt}(vt)^n}{n!} \quad (4.3)$$

By using Gutenberg and Richter equation values obtained from earthquake data sets between the period of 1915-2019, the probability of occurrence and the average return periods of the are calculated for the specific earthquake magnitudes which are 5.0, 5.5, 6.0, 6.5, 7.0 and 7.5 in the study area and its surrounding within 100 km for 1, 10, 50, 75 and 100 years that are exhibited in Table 4.2. According to Table 4.2, the probabilities of occurrence of the earthquakes with a magnitude of M = 5, 5.5, 6.0, 6.5 and 7.0 in the area and its immediate surrounding within 100 years are calculated as 85.9, 69.9, 52.2, 36.5 and 24.3 % respectively. Nevertheless, the probability of occurrence of an earthquake with a magnitude of M = 7.5 in the area and its close surrounding within 100 years is obtained as 15.7 %. The average return periods of the subject earthquake magnitudes calculated in the area and its immediate surrounding are calculated as 51, 83, 136, 221, 359 and 585 years, respectively.

Table 4.2. The probabilities of occurrence of the specific earthquake magnitudes and the average return periods in the study area and its surrounding calculated for 1, 10, 50, 75 and 100 years.

MAGNITUDE	PROBABILITY OF EARTHQUAKES OCCURENCE (%)					Return Period (Years)
	1(Year)	10(Years)	50(Years)	75(Years)	100(Years)	
5.0	1.9	17.8	62.4	76.9	85.9	51
5.5	1.2	11.3	45.2	59.4	69.9	83
6.0	0.7	7.1	30.9	42.5	52.2	136
6.5	0.5	4.4	20.3	28.8	36.5	221
7.0	0.3	2.8	13.0	18.9	24.3	359
7.5	0.2	1.7	8.2	12.0	15.7	585

Finally, calculations of peak ground acceleration value separately for rock, ground and loose ground from these information sets are last stage to analyse the scope of the seismicity of area. These acceleration calculations were studied by considering the recommendation of Ulusay et al. (2004). Peak ground accelerations were calculated in case of occurrence of an earthquake with a magnitude of M = 7.5 depending on the fracture of the EAFZ in this study area. Table 4.3

manifests PGA values for loose ground, ground and rock were calculated as 442 gal, 347 gal and 293 gal from Equation 4.4.

$$PGA = 2.18e^{0.0218(33.3M_w - R_E + 7.8427S_A + 18.9282S_B)} \tag{4.4}$$

$S_A = S_B = 0$  (*rock*);  $S_A = 1, S_B = 0$  (*ground*);  $S_A = 0, S_B = 1$  (*loose ground*) (*Ulusay et al., 2004*)

Table 4.3. The peak ground acceleration values that will be effective in the study area in case of realization of the highest moment magnitudes evaluated in the study area and its surrounding.

	<b>PGA (gal)</b>
<b>loose ground</b>	442
<b>ground</b>	347
<b>rock</b>	293

## **5. GEOTECHNICAL SITE CHARACTERIZATION**

This section of the thesis consists of assessment of data. Laboratory test results were rigorously examined to figure out geotechnical conditions of the study area. Quantitative classification systems which are Rock Mass Rating (RMR) and Geological Strength Index (GSI) were also used for evaluation of geotechnical parameters in this chapter.

### **5.1. Laboratory Test**

Some laboratory tests which are Unit Weight, Uniaxial Compressive Strength (UCS), Elasticity Modulus, Poisson's Ratio, Brazilian Test and Point Load Test were carried out by TCDD (2014) for clarifying the geotechnical properties of tunnel which will be used in modelling stages. This study focuses on landslide - TBM relationships in the Bahçe portal part; hence, Table 5.1 exhibits that SK7A, SK8, SK8Y, SK9, SK9Y, SK10 and SK11 are also evidence to identify of geotechnical parameters in between 3+510 Km and 4+110 Km. Information about laboratory test standards are also given in Appendix. Figure 5.1, Figure 5.2, Figure 5.3, Figure 5.4 and Figure 5.5 indicate the graphical representation of test results performed by TCDD (2014) which are prepared according to boreholes data.

Table 5.1. Laboratory test results (TCDD, 2014).

BH ID	Depth (m)		Lithology	Unit Weight (kN/m <sup>3</sup> )	UCS (MPa)	Elasticity Modulus (GPa)	Poisson's ratio	Brazilian Test	Point Load Strength (MPa)
	From	To							
SK7A	18.00	18.25	Heavily Jointed Metasandstone-Metamudstone	27	26.7	9.53	0.23	-	-
	25.05	25.23		-	-	-	-	-	-
	25.35	25.45		-	-	-	-	-	-
	26.00	26.17		27	157.4	-	-	2.72	-
	29.05	29.25		26	21.6	-	-	-	-
	35.75	35.90		26	16.9	4.05	0.26	-	-
SK8	15.30	15.39	Heavily Jointed Metasandstone-Metamudstone	-	-	-	-	-	-
	15.39	15.48		-	-	-	-	7.7	-
	16.60	16.73		-	-	-	-	-	4
	31.50	31.65	Metasandstone-Metamudstone	27	70.55	-	-	-	-
	33.15	33.37		27	63.19	-	-	-	-
	34.60	34.85		27	44.9	12.6	0.29	-	-
SK8Y	16.00	16.50	Heavily Jointed Metasandstone-Metamudstone	25	68	10.1	0.1	-	-
	22.00	22.50		25	36.2	16.4	0.11	-	-
	29.50	30.00		25	31.7	15	0.13	-	-
	38.00	38.50		-	110.7	-	-	-	5.2
SK9	17.25	17.37	Metasandstone-Metamudstone	-	-	-	-	-	5.55
	23.70	23.82		-	-	-	-	19.85	-
	23.82	23.95		26	64.38	-	-	-	-
	23.82	23.95		-	-	-	-	-	-
	24.30	24.52		27	324.7	33.2	0.2	-	-
	30.75	30.90		26	126.5	26.2	0.17	-	-
	33.80	38.80		-	-	-	-	-	1.28

Table 5.1 cont. Laboratory test results (TCDD, 2014).

<b>SK9Y</b>	12.30	12.50	Heavily Jointed Metasandstone- Metamudstone	-	10.7	-	-	-	0.51
	14.50	15.00		-	16.5	-	-	-	0.78
	20.50	21.00		-	91	-	-	-	4.33
	26.50	27.00		26	49.3	21.9	0.13	-	-
	34.50	35.00		-	36.2	-	-	-	1.72
	49.50	50.00		20	178.9	-	-	-	8.46
<b>SK10</b>	25.15	25.30	Metasandstone- Metamudstone	26	121.6	20.7	0.1	-	-
	25.30	25.43		-	-	-	-	17.57	-
	25.30	25.43		-	-	-	-	27.2	-
	25.30	25.43		-	-	-	-	21.89	-
	27.86	27.95		-	-	-	-	-	-
	36.00	36.10		-	-	-	-	-	6.46
	36.00	36.10		-	-	-	-	-	8.43
	40.05	40.15		-	-	-	-	-	5.18
<b>SK11</b>	68.78	68.85	Metasandstone- Metamudstone	-	-	-	-	-	-
	74.00	74.13		-	-	-	-	-	3.47
	74.00	74.13		-	-	-	-	-	1.2
	83.00	83.13		26	151.4	22.5	0.26	-	-
	92.00	92.20		26	265.1	41.4	0.42	-	-



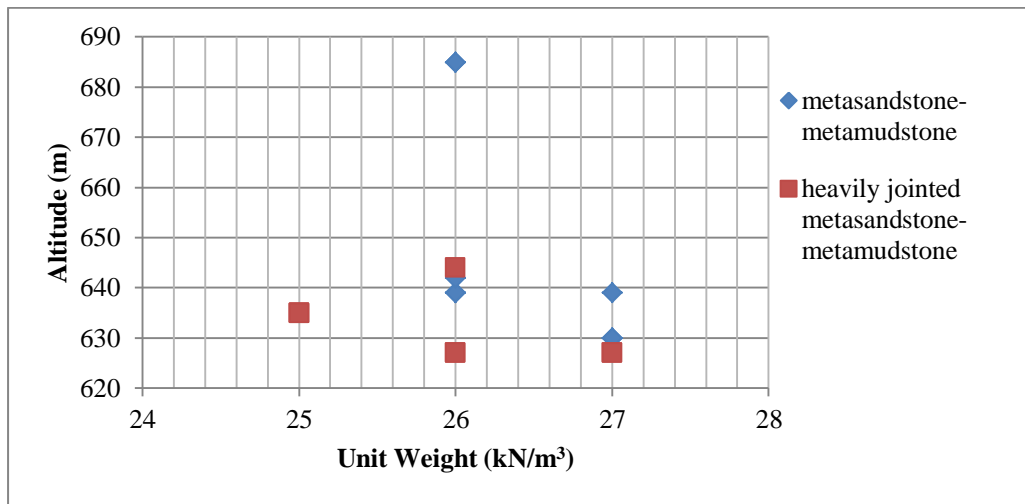


Figure 5.1. Unit weight test results graph (TCDD, 2014).

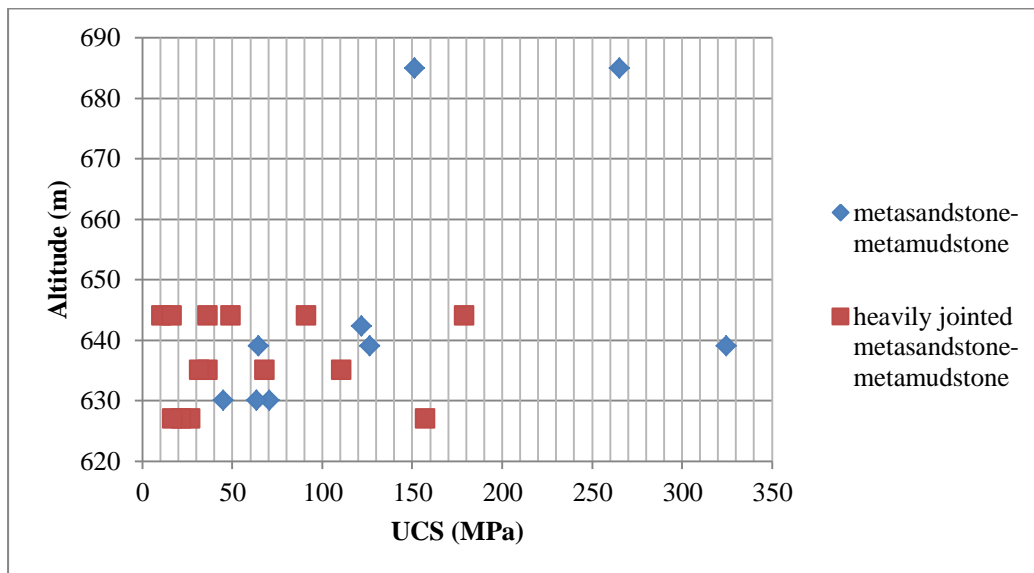


Figure 5.2. UCS test graph Km: 3+510 and 4+110 (TCDD, 2014).

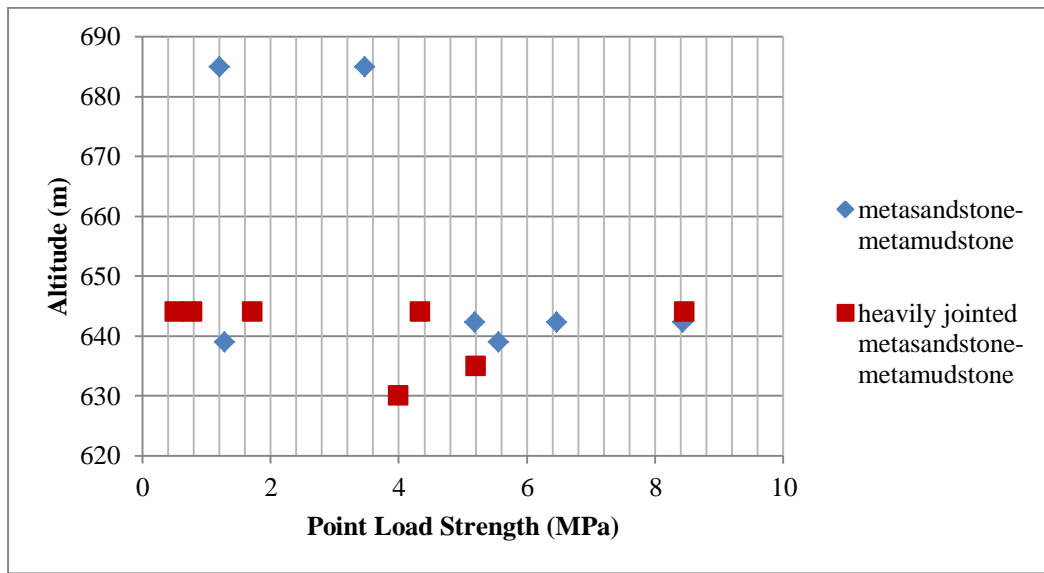


Figure 5.3. Point load strength graph Km: 3+510 and 4+110 (TCDD, 2014).

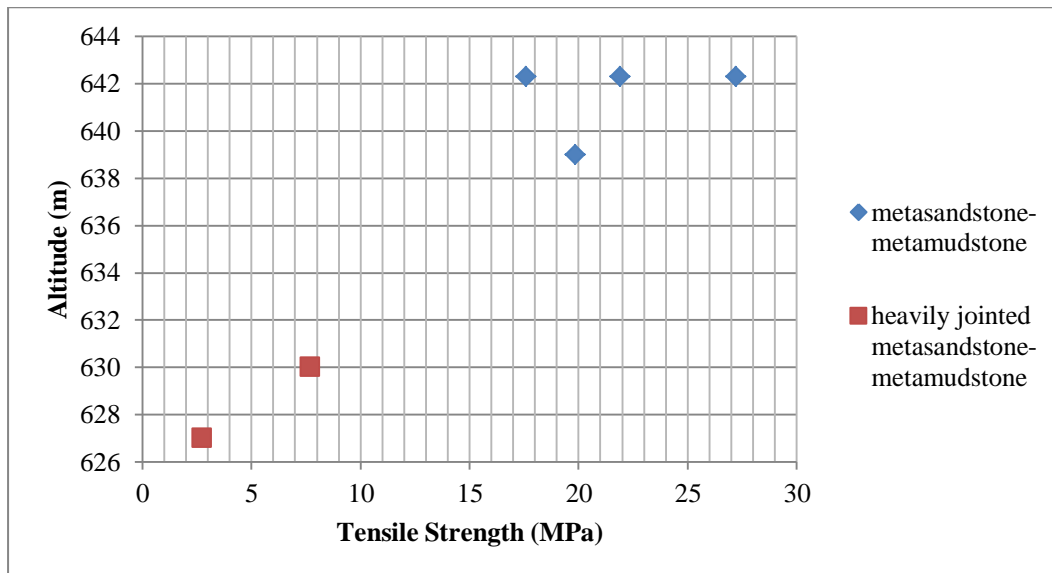


Figure 5.4. Brazillian test graph for Km: 3+510 and 4+110 (TCDD, 2014).

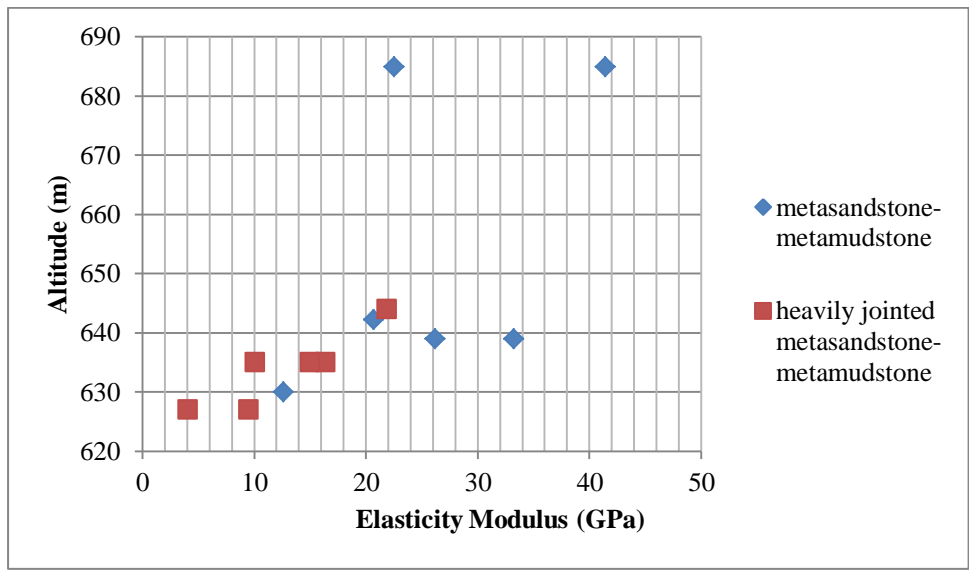


Figure 5.5. Elasticity modulus graph for Km: 3+510 and 4+110 (TCDD, 2014).

## 5.2. Rock Mass Rating (RMR) Classification

Six rock mass parameters such as uniaxial compressive strength of intact rock material, rock quality designation (RQD), spacing of discontinuities, condition of discontinuities, given as: persistence, roughness, aperture, infilling and alteration/weathering), groundwater conditions and orientation of discontinuities are used to classify rock mass (Bieniawski, 1989). Borehole information of SK1, SK2, SK7A, SK8, SK8Y, SK9, SK9Y, SK10 and SK11 are employed to reveal rock mass rating. Metasandstone-metamudstone and heavily jointed metasandstone-metamudstone are classified employing RMR and the results which are presented in Table 5.2 which was prepared according to considering Fugro Sial (2014) and Progeo Proje (2018) information. It should be noticed that UCS values which were interpreted from UCS graph were calculated as the range of 50-100 MPa and 5-25 MPa. Furthermore, considering boring log information sheets, RQD (%) values were also calculated as 50-75 and 25-50. Given these consideration, orientations of discontinuities were assigned as moderate for both lithology. Discontinuity surface properties for the metasandstone-metamudstone are generally fair. These class discontinuity properties are defined as moderately weathered surfaces and between these surfaces have generally soft infilling. On the contrary, heavily jointed metasandstone metamudstone mass discontinuity surface properties are described as poor.

Table 5.2. RMR parameters for heavily jointed metasandstone-metamudstone and metasandstone-metamudstone.

<b>Classification of Rock Mass Rating (RMR)</b>				
<i>Parameters</i>	<b>Metasandstone-Metamudstone</b>		<b>Heavily Jointed Metasandstone-Metamudstone</b>	
	<i>Description</i>	<i>Rate</i>	<i>Description</i>	<i>Rate</i>
UCS (MPa)	50-100	7	5-25	2
RQD (%)	50-75	13	25-50	8
Spacing of discontinuities (mm)	60-200	8	60-200	8
Persistence	1-3 m	4	10-20 m	1
Aperture	0.1-1 mm	4	0.1-1 mm	4
Roughness	Slightly rough	4	Slightly rough	4
Infilling	Soft filling	2	Soft filling	2
Weathering	Moderate	4	Moderate	3
Groundwater	Dripping	4	Dripping	4
Orientation of discontinuities	Moderate	-5	Moderate	-5
<b>RMR</b>	<b><i>Fair rock</i></b>	<b>45</b>	<b><i>Poor rock</i></b>	<b>31</b>

### 5.3. Geological Strength Index (GSI)

Hoek–Brown criterion of GSI value enables to interpret the strength and deformation modulus of the jointed rock masses. SK1, SK2, SK7A, SK8, SK8Y, SK9, SK9Y, SK10 and SK11 and were utilized to calculate GSI for this tunnel route by Fugro Sial (2014) considering discontinuity sets interval. Contrary to Fugro Sial (2014), recommendation of Palmstrom (2005) was also employed to reach GSI in this research.

GSI was empirically determined by considering borehole data according to GSI classification system which was modified by Sönmez and Ulusay (2002). They suggested that GSI is based on surface condition rating (SCR) and structure rating (SR). While SCR equals to sums of values of  $R_f$ ,  $R_w$  and  $R_r$ , SR is decided by using the following expression (Sönmez and Ulusay, 2002) which is defined in Equation 5.1.

$$SR = -17.5 \ln(J_v) + 79.8 \quad (5.1)$$

Volumetric joint count ( $J_v$ ) and estimated from the input parameters of RMR scheme (e.g. roughness, weathering and infilling) have very close relationships to define SR and SCR. Volumetric Joint Count ( $J_v$ ) is required for calculation of the SR. Thus,  $J_v$  is obtained by Palmstrom (2005) equation which is shown in Equation 5.2. In order to reach large spectrum of view, max and min RQD values were chosen to calculate  $J_v$ .

$$RQD = 110 - 2.5 \times J_v \quad (5.2)$$

RQD = 75 for metasandstone-metamudstone;

- $J_v = 14$ .
- $SR = -17.5 \ln(J_v) + 79.8 = 34$ .
- $SCR = (R_r=4 + R_w=4 + R_f=2) = 10$ .

RQD = 25 for heavily jointed metasandstone-metamudstone;

- $J_v = 43$ .
- $SR = -17.5 \ln(J_v) + 79.8 = 14$ .
- $SCR = (R_r=4 + R_w=3 + R_f=2) = 9$ .

In Figure 5.6, GSI assignment was exhibited by considering classification system of GSI Sönmez and Ulusay (2002). GSI was calculated as 41 and 33 for metasandstone-metamudstone and heavily jointed metasandstone-metamudstone, respectively (Figure 5.6). It should not be neglected that while metasandstone-metamudstone GSI values may locate between the range of 40 and 45, heavily jointed metasandstone-metamudstone GSI value may have range between 30 and 35.

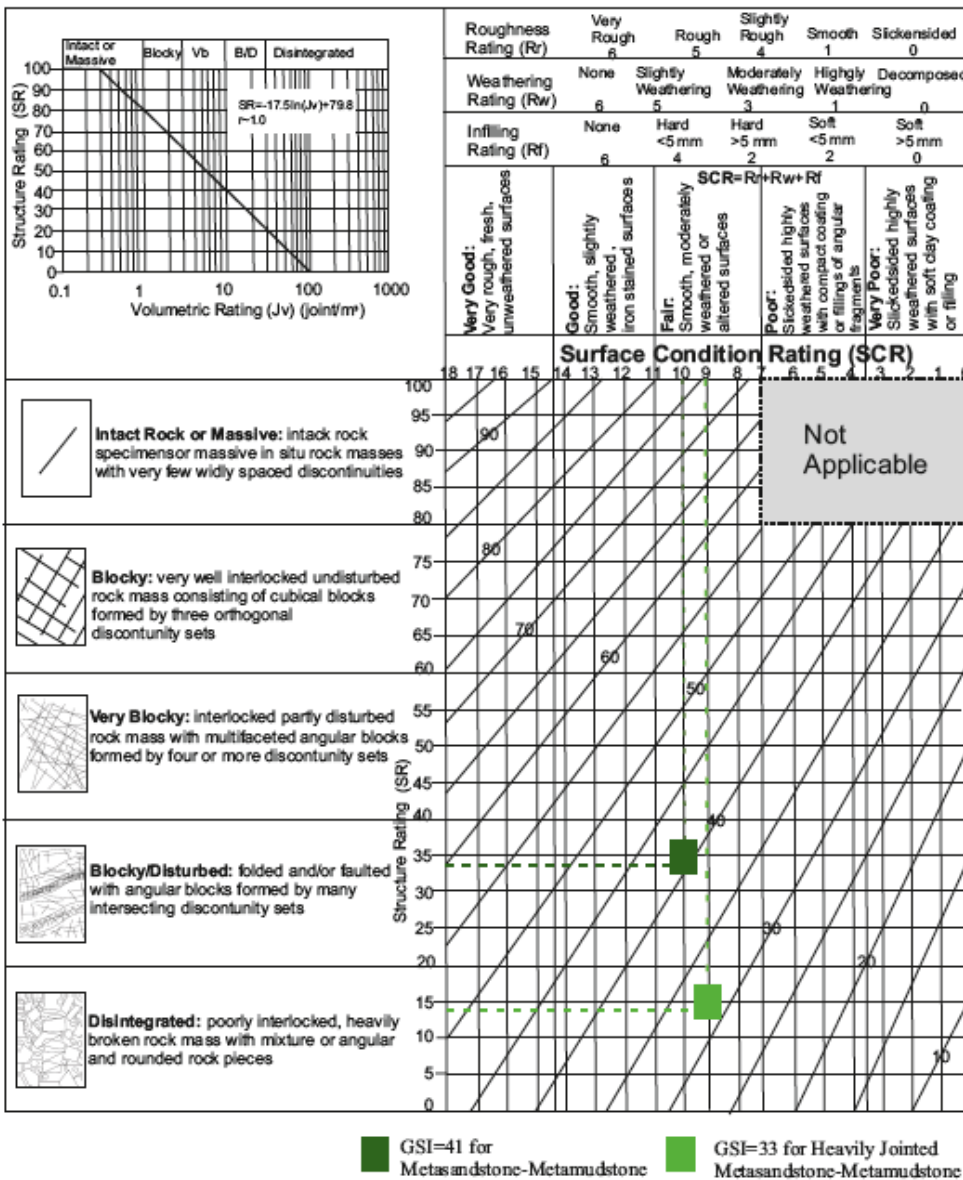


Figure 5.6. The modified GSI classification suggested by Sönmez and Ulusay (2002) for metasandstone-metamudstone and heavily jointed metasandstone-metamudstone.

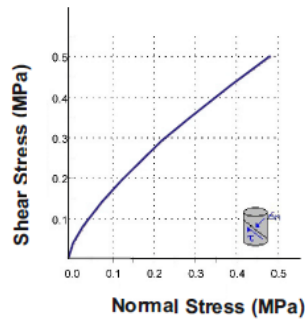
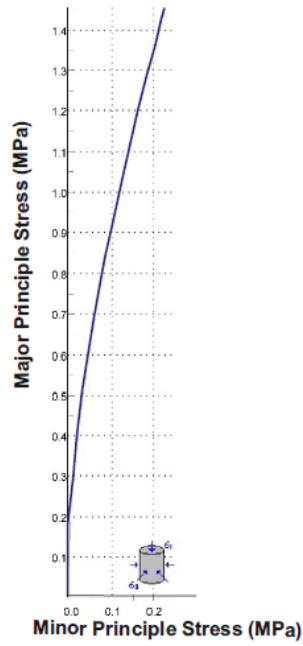
#### 5.4. Geotechnical Parameters

Models showing interactions of rock/rock mass and TBM need to be set up identifying geotechnical parameters of tunnel route. Geotechnical parameters must be used to evaluate prediction of TBM-performance. Estimation of tunnel performance is very difficult, if rock has some properties which having low strength and high deformation risk and being heterogeneous (Schubert et al., 1995). Study area has extremely heterogonous nature in terms of its complex geology. Therefore, decided geotechnical parameters were carefully checked again in order to prepare realistic design of model.

Accurate determination of geotechnical parameters for Bahçe-Nurdağ Tunnel in between 3+510 and 4+110 Km is critical in accordance with reviewing of borehole information of SK1, SK2, SK7A, SK8, SK8Y, SK9, SK9Y, SK10 and SK11 because they will be used in modelling stages of in MIDAS GTS NX considering of two failure criteria which are Mohr-Coulomb and Hoek-Brown. When parameters are decided, they should also be correlated with literature information. First, according to modified classification system of GSI (Sönmez and Ulusay, 2002), GSI was decided as 41 by Fugro Sial (2014) for metasandstone-metamudstone. When literature information is reviewed, Marinos and Hoek (2001) propose that jointed rocks for weak siltstone or clayey shale with sandstone'- which are poor, very smooth, occasionally slickenside surfaces with compact coatings or fillings with angular fragments- GSI value equals to 40. Additionally, GSI was calculated as 33 by Fugro Sial (2014) in the interval of Km: 3+510 and 4+110 for heavily jointed metasandstone-metamudstone. Tectonically deformed, intensively folded and faulted, sheared clayey shale or siltstone with jointed and deformed sandstone layers forming an almost chaolitic structure which are smooth, moderately weathered and altered surfaces' GSI value equals to 30 (Marinos and Hoek, 2001). Hence, it can be understood that literature information of GSI values are very close the calculated GSI values. Second,  $m_i$  is an important parameter in the use of the Hoek–Brown failure criterion (Arshadnejad, 2018). While  $m_i$  is chosen as 9 for heavily jointed metasandstone-metamudstone, it is preferred as 13 for metasandstone-metamudstone. The parameter  $m_i$  is given by Marinos and Hoek (2001) as  $12 \pm 3$  for schist. In addition, the parameter  $m_i$  for schist is defined in the range of 4-8 by Hoek and Brown (1997). Given these considerations, it is clear that the parameters  $m_i$  were realistically chosen. Rock mass parameters Disturbance factor (D) is equal to 0 or 0.5. If TBM excavation causes minimal disturbance to the confined rock mass surrounding a tunnel, disturbance factor

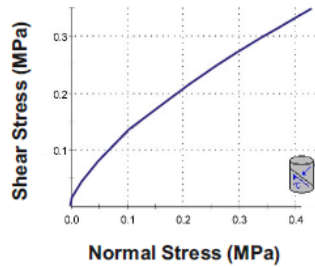
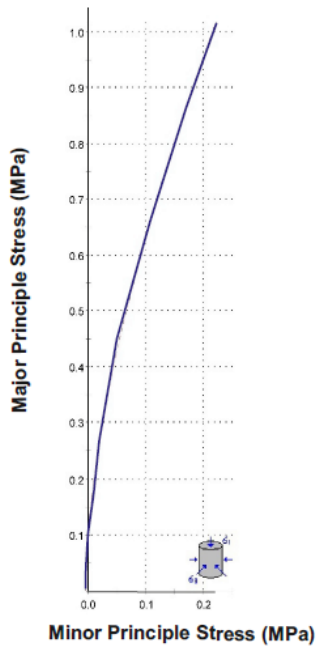
(D) is defined as 0 (Hoek et al., 2002). D is equal to 0.5, if squeezing problems are current (Hoek et al., 2002). Accordingly, the uniaxial compressive strength values of heavily jointed metasandstone-metamudstone and metasandstone-metamudstone were taken as 9 MPa and 50 MPa, respectively. It is also possible to determine geotechnical design parameters by using RocLab software. RocLab was used to decide rock mass parameters depend on Hoek-Brown criteria (Rocscience, 2019). Roclab software utilized the input parameters of UCS, GSI,  $m_i$  and D in order to decide Hoek-Brown strength parameters of a rock mass:  $m_b$ ,  $s$  and  $a$ . Mohr-Coulomb parameters of cohesion and internal friction angle which are also obtained from Roclab are important because of being used as input for numerical models. Thus, the other parameters which are shown in Figures 5.7, 5.8, 5.9 and 5.10 were detected using Roclab program after Progeo (2018). It is also important to emphasize that Roclab program uses Generalized Hoek & Diederichs (2006) method in order to calculate deformation modulus.





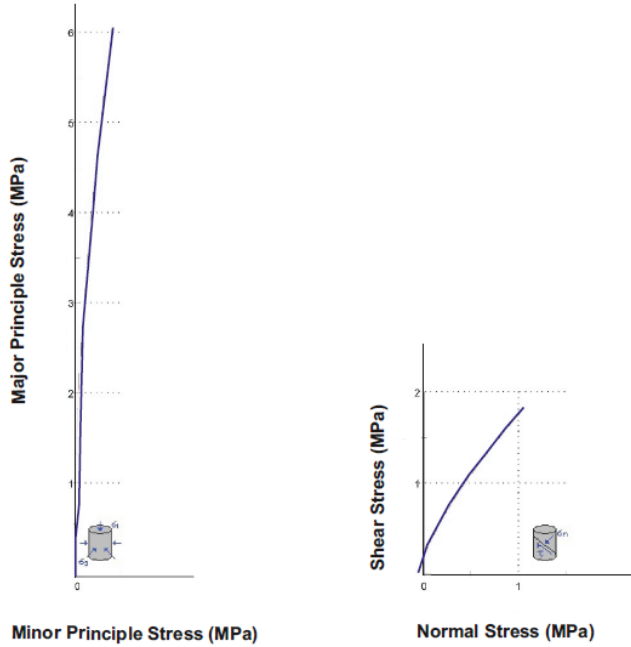
Hoek - Brown Classification	
Intact uniaxial compressive strength	9 MPa
GSI	33
mi	9
Disturbance factor (D)	0
Intact Modulus (Ei)	1800 MPa
Hoek - Brown Criterion	
mb	0.822
s	0.0006
a	0.518
Mohr - Coulomb Fit	
cohesion	0.073 MPa
internal friction angle	42.9 deg
Rock Mass Parameters	
tensile strength	-0.006 MPa
uniaxial compressive strength	0.190 MPa
global strength	1.010 MPa
deformation modulus	178.36 MPa

Figure 5.7. Results of Roclab for heavily jointed metasandstone-metamudstone when D=0



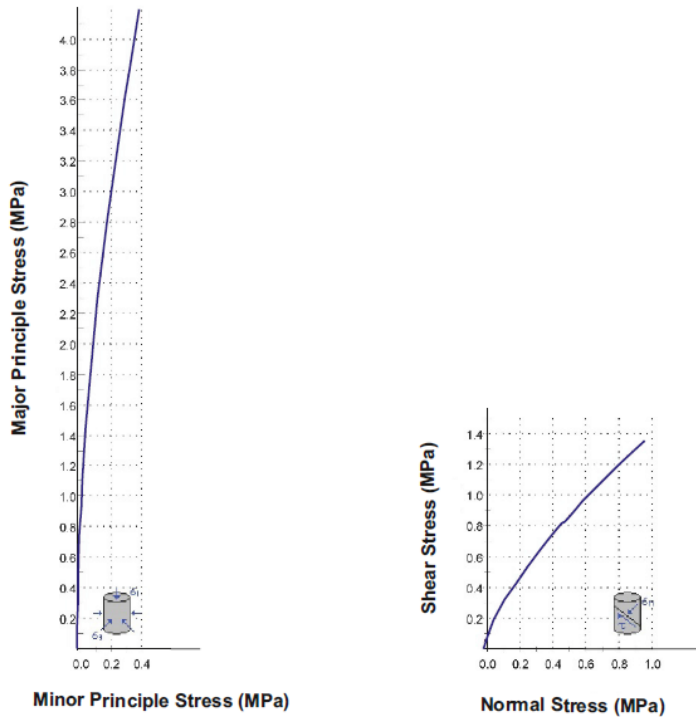
Hoek - Brown Classification	
Intact uniaxial compressive strength	9 MPa
GSI	33
mi	9
Disturbance factor (D)	0.5
Intact Modulus (Ei)	1800 MPa
Hoek - Brown Criterion	
mb	0.370
s	0.0001
a	0.518
Mohr - Coulomb Fit	
cohesion	0.053 MPa
internal friction angle	36.13 deg
Rock Mass Parameters	
tensile strength	-0.003 MPa
uniaxial compressive strength	0.088 MPa
global strength	0.664 MPa
deformation modulus	92.20 MPa

Figure 5.8. Results of Roclab for heavily jointed metasandstone-metamudstone when D=0.5.



Hoek - Brown Classification	
Intact uniaxial compressive strength	50 MPa
GSI	41
mi	13
Disturbance factor (D)	0
Intact Modulus (Ei)	8750 MPa
Hoek - Brown Criterion	
mb	1.581
s	0.0014
a	0.511
Mohr - Coulomb Fit	
cohesion	0.285 MPa
internal friction angle	56.92 deg
Rock Mass Parameters	
tensile strength	-0.045 MPa
uniaxial compressive strength	1.759 MPa
global strength	8.137 MPa
deformation modulus	1495.70 MPa

Figure 5.9. Results of Roclab for metasediment-metamudstone when D=0



Hoek - Brown Classification	
Intact uniaxial compressive strength	50 MPa
GSI	41
mi	13
Disturbance factor (D)	0.5
Intact Modulus (Ei)	8750 MPa
Hoek - Brown Criterion	
mb	0.783
s	0.0004
a	0.511
Mohr - Coulomb Fit	
cohesion	0.200 MPa
internal friction angle	52.07 deg
Rock Mass Parameters	
tensile strength	-0.024 MPa
uniaxial compressive strength	0.900 MPa
global strength	5.651 MPa
deformation modulus	716.29 MPa

Figure 5.10. Results of Roclab for metasediment-metamudstone when D=0.5.

## 6. TUNNELLING EXCAVATION METHOD

This chapter gives brief information about tunnel excavation method of TBM is often applied. Introducing of this tunnelling method is critical for following chapters to explain the reasons of inactivation applying of this tunnel method in between KM: 3+510 and 4+110.

Tunnel Boring Machines (TBMs) have positive impacts on tunnel constructions because tunnels can quickly be completed with TBM. On the other hand, if tunnel is especially constructed with TBM in adverse conditions, ground should be realistically characterized to avoid the unrecoverable economical loses. Spencer et al. (2009) conducted that TBM has been enhanced the tunnelling industry with respect to economic and safe tunnelling in difficult grounds where it could not be practicable. TBM is the best choice for constructing long tunnels in terms of less noise and disturbance to surrounding structures. Tunnelling construction with TBM is advantageous because TBM has high performance and low labor costs (Girmscheid and Schexnayder, 2002; Abdallah and Marzouk, 2013). The major disadvantages of TBM are its lack of versatility with regards to tunnel shape and its inadaptability in varying or mixed geological conditions (Phadke and Titirmare, 2017). TBM excavation represents a big investment in an inflexible but potentially very fast method of excavating and supporting a rock tunnel (Barton, 1996).

Phadke and Titirmare (2017) state that TBM is designed based on the geological conditions, for hard rock condition, soft rock conditions or mixed conditions requirement torque, thrust type cutter head and many parameters are dissimilar; hence, geological and geotechnical analyses are crucial for predetermination of TBM type. Spencer et al. (2009) express that there are three common types: Earth pressure balance (EPB), Bentonite slurry (BS) sometimes called hydro shield, and compressed air (CA). Earth Pressure Balance Shield is frequently chosen for soft ground conditions. Herrenknecht Tunnelling System (2019) explains that EPB Shield is type of the TBM aims to stabilize the earth pressure during excavation in soft ground conditions containing water under pressure.

Brabant and Duhme (2017) state that hard rock TBMs can be classified as single shield, double shield and gripper TBM. Considering the tunnel route geological and geotechnical conditions, single shield TBM and double shield TBM were chosen for this tunnelling project by TCDD. According to Robbins (2019), single shield TBM is generally used in mixed ground conditions quickly. Robbins (2019) declares that not only it enables to work fast in difficult ground conditions, but also its system also decreases the amount of mud or water to work safely. Robbins (2019) also claims that double shield TBM can be chosen for large sections of fractured rock condition. Double shield allows increasing rate of TBMs in fractured rock (Brabant and Duhme, 2017). It should also remarked that thickness of segments are 35 cm for TBM. Given these considerations, it can be understood that TBM technology has been improved in difficult condition in recent years. Safety construction is important in terms of cost, moral and schedule; hence, applied numerical analyses which will be displayed in subsequent chapter will be helpful to discuss whether tunnels can be finalized with TBM or not.

## **7. MODEL DEVELOPMENT AND CALIBRATION**

### **7.1. Numerical Model**

Numerical methods have a significant role in simulating conditions for different adverse geotechnical studies; consequently, nowadays numerical methods are very popular to create beneficial geotechnical solutions. Numerical methods are also recently widespread in geotechnical studies of tunnel design due to generating user-friendly model. Potts and Zdravkovic (2001) state that the field conditions can be simulated more accurately if the utilized constitutive models can accurately represent ground behaviour and if the boundary conditions set are correct. Gnisen (1989) proposed that numerical methods are divided as 3 main models which are continuum model, discontinuum model and subgrade reaction model in tunnel engineering. Continuum Model consists of Finite Element Method (FEM), Finite Difference Method (FDM) and Boundary Difference Method (BDM). While discrete element is a method of discontinuum model, beam element method with elastic support is a method of subgrade reaction model. For the purpose of the study, FEM is chosen to create 3D numerical analysis model to understand the TBM-landslide relationships.

#### **7.1.1. Finite Element Method (FEM)**

FEM is commonly preferred in order to figure out stresses and deformations around an underground structure. FEM solutions are also practical applications in complex area; hence, FEM was chosen to handle with the problem studied in this thesis. Discretized homogenous elements are used in finite element method. Jing and Hudson (2002) claimed that FEM is very popular numerical method to study on non-homogeneity method, complex boundary conditions and non-linear deformability. In the FEM, the body to be analysed is divided into a number of discrete homogeneous elements- which are generally preferred as triangles or tetrahedrons have nodes. The finite element mesh comprises collection of elements and nodes. In addition, FEM was used with the software of MIDAS in this study in order to calculate deformations.

## **7.2. Midas Software**

In this study, MIDAS GTS NX software was chosen for modelling because this software has high capability to deal with highly complex problems. This software works with using finite element method to display realistic 3D tunnel models. Indeed, MIDAS (2019) state that MIDAS GTS NX is a geotechnical and tunnel analysis system which is founded on the expert analysis and exceptional graphic technologies. Having sophisticated technology, it can provide modelling strategies on unfavourable geological area. Application of the 3D finite element analysis is critical in geotechnical and tunnel engineering. MIDAS GTS NX has been designed for the deformation and stability analyses of underground works and geotechnical structures (MIDAS, 2019).

## **7.3. Modelling of Bahçe - Nurdağ Tunnel**

The aim of this subchapter is to provide a better understanding of modelling stages of Bahçe-Nurdağ Tunnel for Bahçe portal. Determination of model size is critical to reduce the boundary impacts on the analysis outcomes while allowing the analysis to be accomplished coherently. For this purpose, terrain which is part of between 3+510 Km and 4+110 Km was modelled in order to evaluate possible landslide problem Bahçe on the tunnel. In this study, using software is also very critical because it helps to work quickly and accurately. MIDAS GTS NX software with trial license which enables engineers to solve complex geotechnical problems and support valuable technical solutions was used to develop finite element model by creating mesh automatically in this study. All interaction impacts are monitored with complex FEM analyses in order to estimate landslide-tunnel relationships in unfavourable region.

Modelling stages are composed of six steps which are exhibited in Figure 7.1. The first step is to define terrain and tunnel geometry. The second step is to assign geotechnical parameters. Third step is development of the meshed model. Besides, construction stage analyses were also done to obtain the most realistic numerical model representing the field conditions. Additionally, model scenarios were generated to examine deformations results. Last step is to evaluate and compare model results.

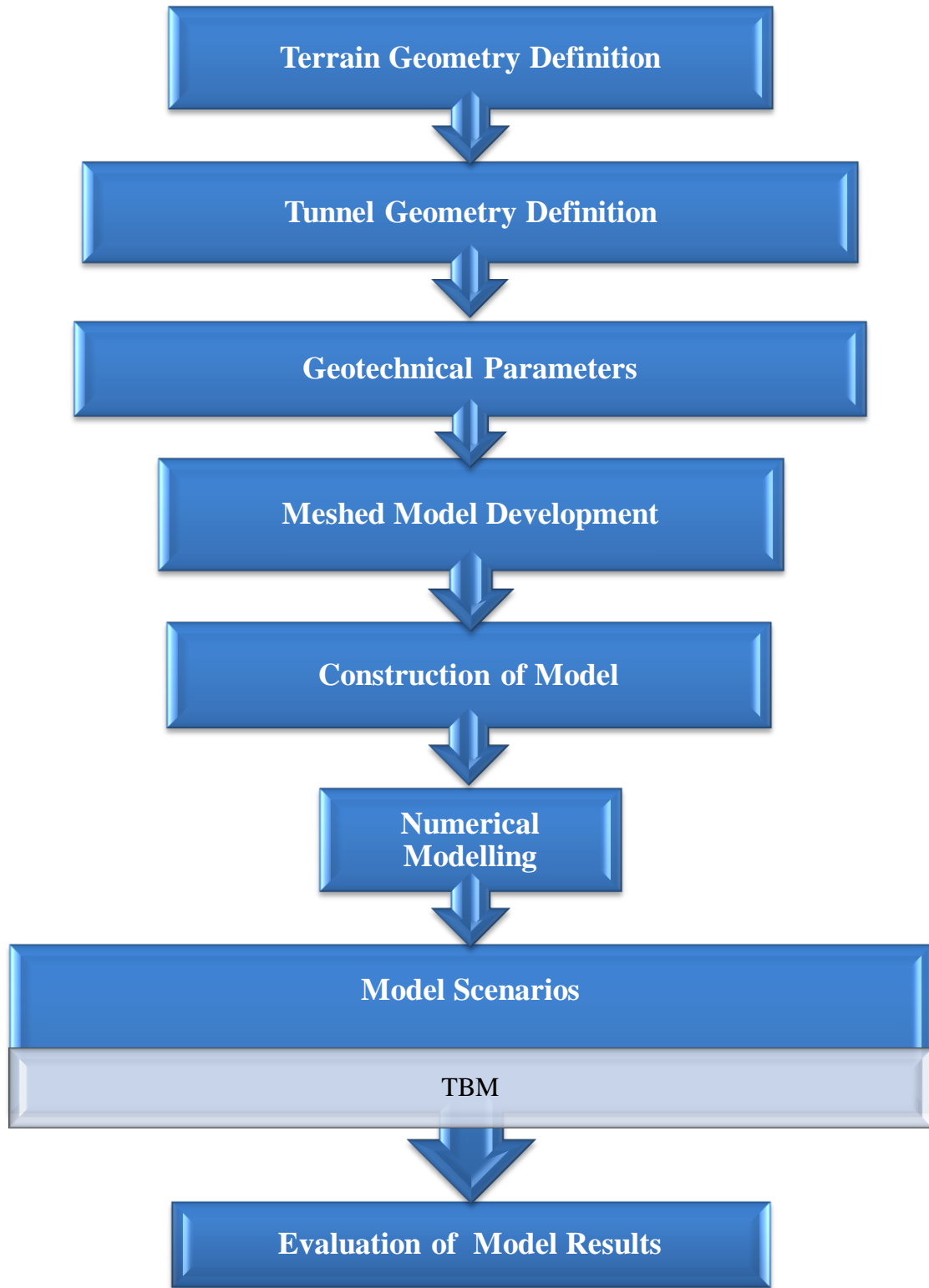


Figure 7.1. Flow chart of the model construction.

### **7.3.1. Definition of Terrain and Tunnel Geometry**

First of all, terrain geometry (Figure 7.2) and tunnel geometry (Figure 7.3) were created by using the software of AUTOCAD. Then, they were imported via “*dxf*” files from AUTOCAD. When *dxf* files are imported in the MIDAS, wireframes can be created on the tunnel drawings by considering the plan dimensions. They were also combined with boreholes information. Nine boreholes information, which were given in Chapter 3, was used to identify the study area conditions to create a model. Figure 7.4 manifests that terrain topography which was created by considering contour line from the *dxf* files. Therefore, contour lines help to define terrain geometry in the MIDAS software program. When tunnel geometry preparing stage is completed, its surfaces should be extended in accordance with suitable direction and length. Ground region should be defined as solid for 3D numerical analyses. Figure 7.5 and Figure 7.6 show the stage of creating tunnel geometry by making solid and extending the direction and length. Figure 7.7 schematically represents the developed conceptual model of the Bahçe portal which was constructed by using MIDAS GTS NX 3D software for the purpose of the analysis.



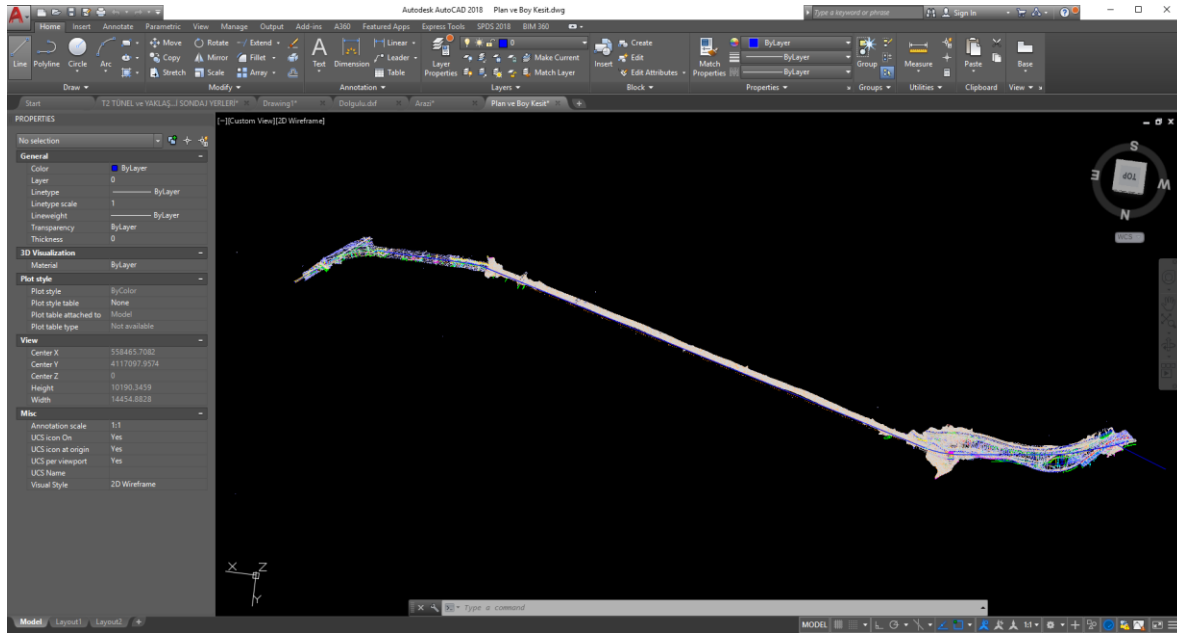


Figure 7.2. Terrain geometry in AUTOCAD.

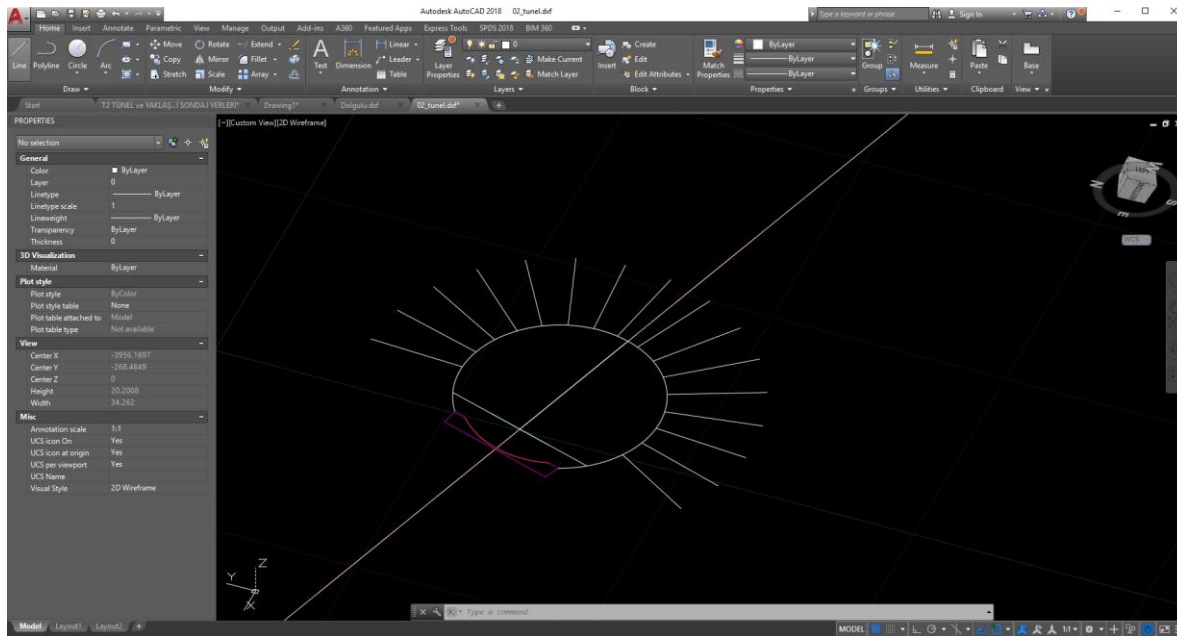


Figure 7.3. Tunnel geometry in AUTOCAD.

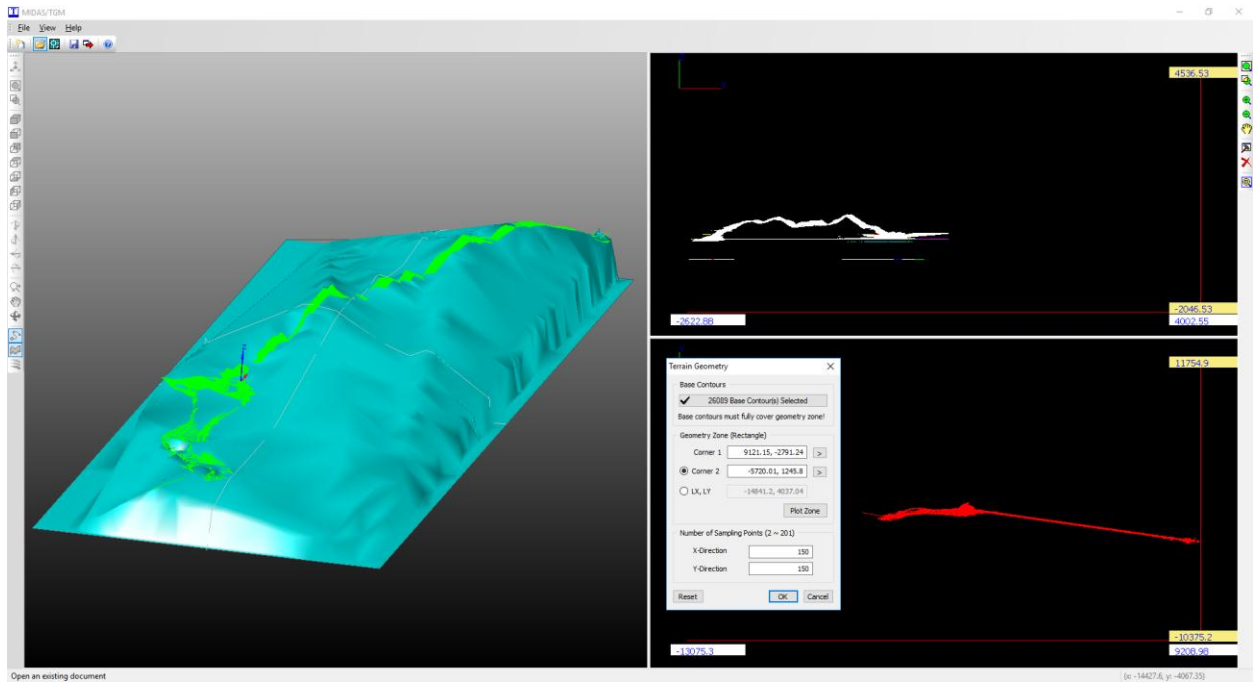


Figure 7.4. Stage of creating terrain topography in MIDAS GTS NX.

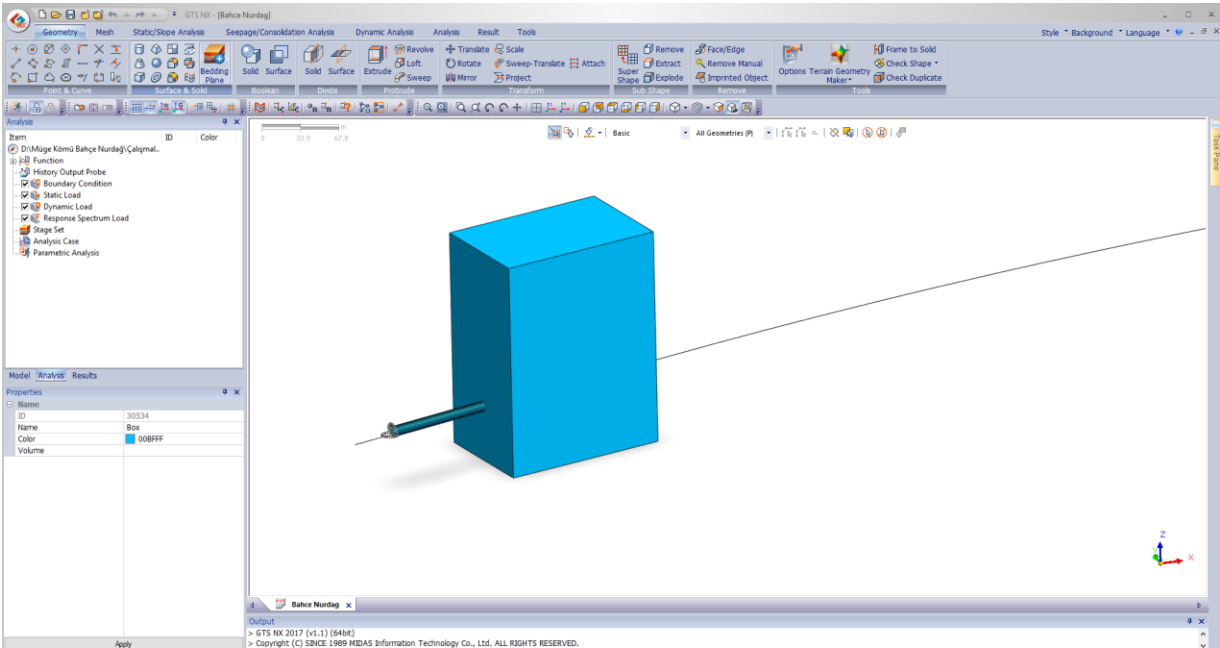


Figure 7.5. Stage of creating tunnel geometry in MIDAS GTS NX.



Basic All Geometries (P)

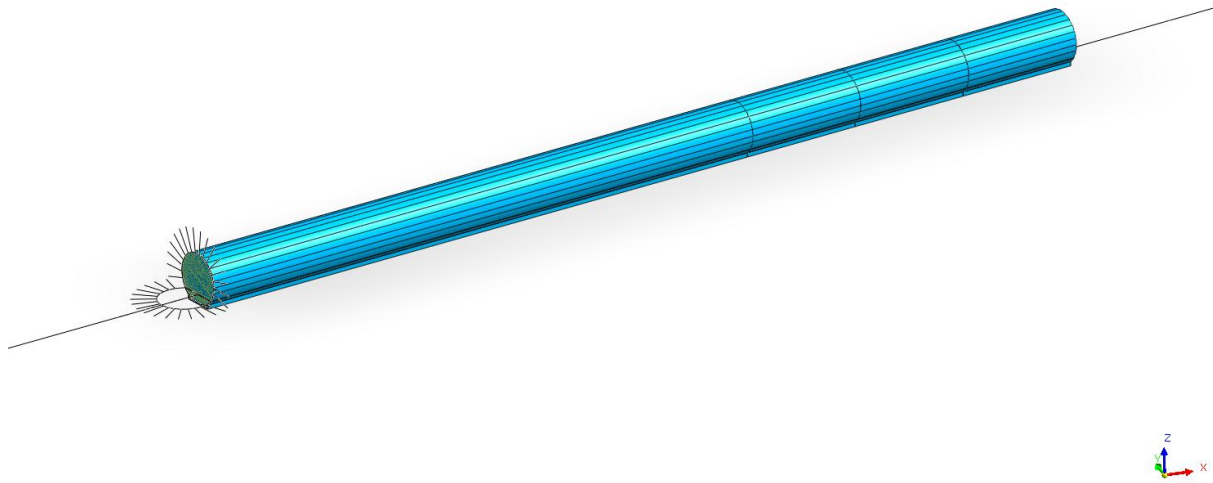


Figure 7.6. Tunnel geometry in MIDAS GTS NX.

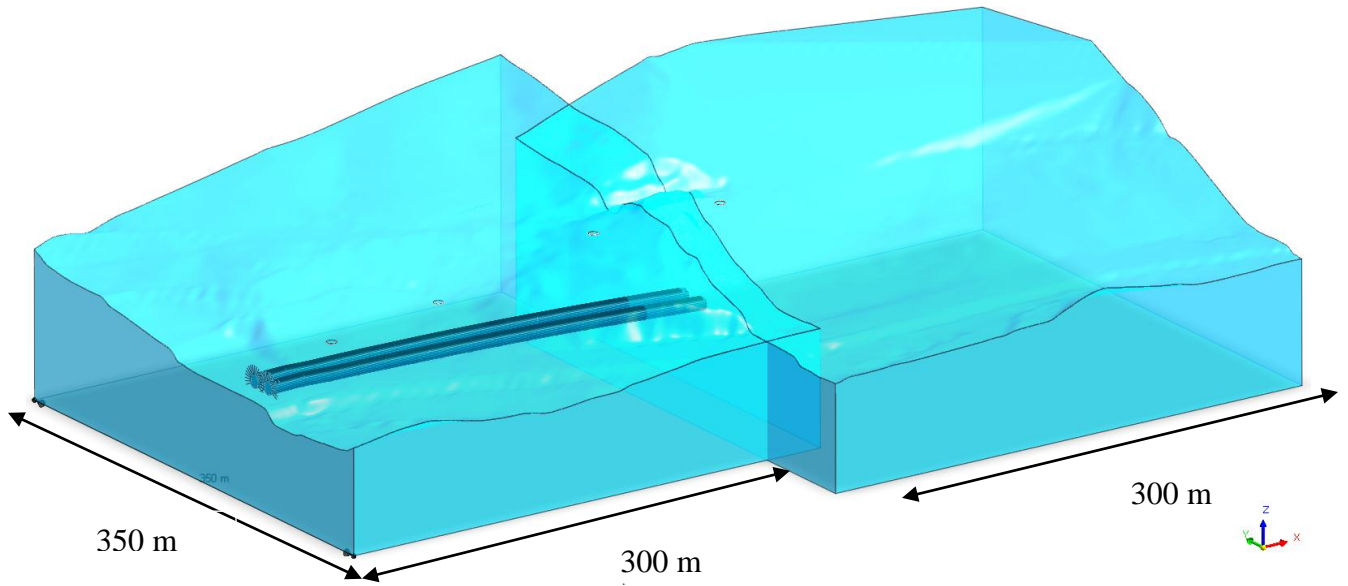


Figure 7.7. Conceptual 3D model of the Bahçe portal in MIDAS GTS NX.

### 7.3.2. Geotechnical Parameters

This part of study enlightens geotechnical parameters assigned to MIDAS software. This stage is the previous stage of the model meshing and construction of the model. Model type is selected as Mohr-Coulomb or Hoek-Brown by taking into account lithology. Considering of the criterion of Mohr-Coulomb, the behaviour of the debris was described as a perfectly plastic elastic model. The Hoek-Brown is used to model the behaviour of a jointed rock mass (which can be considered homogeneous and isotropic) in a response to induced stresses (MIDAS, 2019). Therefore, rock mass was defined as homogenous and isotropic for this aims of the study. Materials are linearly-elastic. Names, colors, model type, elastic modulus ( $E_m$ ), poisson's ratio, unit weight are assigned for each lithology in the MIDAS software. Figure 7.8, Figure 7.9 and Figure 7.10 show the assignment of the parameters for debris, heavily jointed metasandstone-metamudstone and metasandstone-metamudstone. Assigned parameters (Table 7.1) and their literature correlation are presented in below:

Table 7.1. Model parameters.

	<b>Model Type</b>	$\gamma$ (kN/m <sup>3</sup> )	<b>c</b> (kPa)	$\Phi$ (°)	<b>v</b>	<b>E</b> (MPa)
Debris	Mohr-Coulomb	20	5	32	0.3	60
Heavily Jointed Metasandstone-Metamudstone	Hoek-Brown	23	-	-	0.25	60-100-150
Metasandstone-Metamudstone	Hoek-Brown	24	-	-	0.25	700-1500-2900

First, cohesion ( $c$ ) and internal friction angle ( $\phi$ ) of debris were assigned as 5 kPa and  $32^\circ$ , respectively. Literature have very close approach that debris cohesion was chosen as 4 kPa, internal friction angle was used as  $30^\circ$  by Delmonaco et al. (2003). Moreover, Iverson (1997) also evaluated debris internal friction angle as  $30^\circ$ . Cohesion was also taken as 6.7 kPa by Hu et al. (2010) for debris. Second, poisson's ratio ( $\nu$ ) was detected as 0.3, 0.25, 0.25 for debris, heavily jointed metasandstone-metamudstone, metasandstone-metamudstone, respectively. Poisson's ratio was preferred as 0.3 for debris (Hu et al., 2010; Kanungo et al., 2012). Hoek (2001) also assigned as 0.3 for very poor quality rock mass. Moreover, Meng and Xian (2013) chose as 0.24 for poisson's ratio of mudstone. Hoek (2001) detected as 0.25 for average quality rock mass poisson's ratio. Therefore, assigned poisson's ratio parameters are suitable for literature. Third, Roclab software results -which were presented in geotechnical site characterization chapter- were also considered the assesment of the deformation modulus in MIDAS. Debris deformation modulus ( $E$ ) was considered as 60 MPa. While deformation modulus of heavily jointed metasandstone-metamudstone was preferred as 60, 100 and 150 MPa, deformation modulus of metasandstone-metamudstone was chosen as 700, 1500 and 2900 MPa. They were also calculated according to Generalized Hoek & Diederichs (2006) method considering to maximum and minimum values. One of the other significant parameters is unit weight ( $\gamma$ ). Debris, heavily jointed metasandstone-metamudstone and metasandstone-metamudstone unit weight were also chosen as  $20 \text{ kN/m}^3$ ,  $23 \text{ kN/m}^3$  and  $24 \text{ kN/m}^3$ , respectively. While heavily jointed metasandstone-metamudstone and metasandstone-metamudstone unit weight were determined by considering laboratory test results, debris unit weight was decided according to literature because debris unit weight labrotary results are not existed at hand. Unit weight of debris was determined to be  $20 \text{ kN/m}^3$  by Hu et al. (2010). Liu et al. (2012) was used as  $22.3 \text{ kN/m}^3$  for debris unit weight. It should also be stated that the coefficient of earth pressure ( $K_0$ ) was detected automatically for this study.

After assigning of the parameters, MIDAS GTS NX enables to obtain high quality mesh generation in unfavourable geometries. Mesh generation is time consuming without using software program. MIDAS GTS NX simplifies the problem of mesh with help of auto mesh tool so 3D auto mesh was applied for each model.

**Material** ✕

ID  Name  Color

Model Type   Structure

General **Porous** Non-Linear Thermal Time Dependent

Elastic Modulus(E)  kN/m<sup>2</sup> ...

Inc. of Elastic Modulus  kN/m<sup>3</sup>


Inc. of Elastic Modulus Ref. Height  m

Poisson's Ratio(Nu)

Unit Weight(Gamma)  kN/m<sup>3</sup>

Initial Stress Parameters

Ko Determination

Automatic  Manual  Anisotropy 

Thermal Parameter

Thermal Coefficient  1/[T]

Molecular vapor diffusion coefficient  m/sec<sup>2</sup>

Thermal diffusion enhancement

Damping Ratio(For Dynamic)

Damping Ratio

Safety Result(Mohr-Coulomb)

Cohesion(C)  kN/m<sup>2</sup>

Frictional Angle(Phi)  [deg]

Tensile Strength  kN/m<sup>2</sup>

Figure 7.8. Assigning the parameters for debris.

Material ×

ID  Name  Color

Model Type   Structure

General Porous Non-Linear Thermal Time Dependent

Elastic Modulus(E)  kN/m<sup>2</sup> ...

Inc. of Elastic Modulus  kN/m<sup>3</sup>

Inc. of Elastic Modulus Ref. Height  m


Poisson's Ratio(Nu)

Unit Weight(Gamma)  kN/m<sup>3</sup>

Initial Stress Parameters

Ko Determination

Automatic

Manual  Anisotropy 

Thermal Parameter

Thermal Coefficient  1/[T]

Molecular vapor diffusion coefficient  m/sec<sup>2</sup>

Thermal diffusion enhancement

Damping Ratio(For Dynamic)

Damping Ratio

Safety Result(Mohr-Coulomb)

Cohesion(C)  kN/m<sup>2</sup>

Frictional Angle(Phi)  [deg]

Tensile Strength  kN/m<sup>2</sup>

Figure 7.9. Assigning the parameters for heavily jointed metasandstone-metamudstone.

Material ×

ID  Name  Color

Model Type   Structure

General Porous Non-Linear Thermal Time Dependent

Elastic Modulus(E)  kN/m<sup>2</sup> ...

Inc. of Elastic Modulus  kN/m<sup>3</sup>

Inc. of Elastic Modulus Ref. Height  m


Poisson's Ratio(Nu)

Unit Weight(Gamma)  kN/m<sup>3</sup>

Initial Stress Parameters

Ko Determination

Automatic

Manual  Anisotropy 

Thermal Parameter

Thermal Coefficient  1/[T]

Molecular vapor diffusion coefficient  m/sec<sup>2</sup>

Thermal diffusion enhancement

Damping Ratio(For Dynamic)

Damping Ratio

Safety Result(Mohr-Coulomb)

Cohesion(C)  kN/m<sup>2</sup>

Frictional Angle(Phi)  [deg]

Tensile Strength  kN/m<sup>2</sup>

Figure 7.10. Assigning the parameters for metasandstone-metamudstone.



### 7.3.3. Construction of Model

In this part, construction of models was performed in the software. It includes many stages which are element groups, boundary conditions and load conditions. First, three set assignment rules which are mesh set, boundary set and load set were defined in Midas stage definition wizard. Software enables to change them at the start of each stage. Therefore, they have chance to be activated/deactivated at any time during construction stages. It should be noticed that stage type is preferred as stress. Boundary conditions were decided as fixed. When solution is applied, it is also important to determine the loading of the on the supporting system. Static loads were primarily applied during the construction stage process. TBM face loads are applied as 4500 kPa, 1000 kPa, 200 kPa and 50 kPa, respectively. Initial steps shows initial stress model before excavating the tunnel. Unlike initial stages, following stages consist of face pressure of load application. Figure 7.11 reveals the example of summarized construction stages analyses for this study. It indicates the activation and the re-activation of the structural elements during construction stages done in the software to prepare 3D FEM model. The deformation results were separately also displayed in next subchapter.

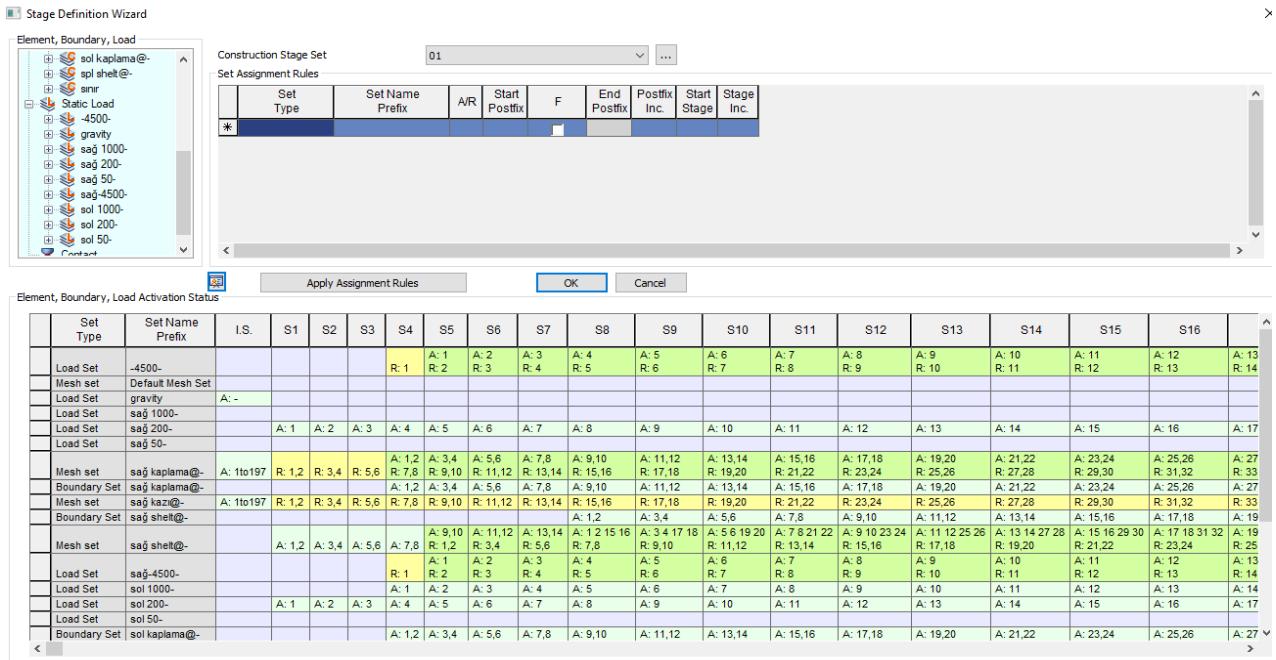


Figure 7.11. Construction stages analyses.

#### 7.3.4. Modelling Scenarios

Adhering to the purpose of the study, obtained results have been presented in this section. Model scenarios assess the possible effects of TBM tunnelling by using inclusive 3D MIDAS GTS NX FEM. Region is critical in terms of landslide. Tunnel is also very long to be completed with TBM so determination of TBM stop point is very critical to ensure to tunnel stability because of landslide. In order to better understand the mechanisms of the landslides and relationship of them with TBM, displacement analyses results of in the X, in the Y and in the Z directions were determined separately. In particular, meshed models, probable deformation results, stress models and material output models are also demonstrated for each specific interval within the scope of this thesis. Four intervals determined as Km: 3+810-4+110, 3+710-3+810, 3+660-3+710 and 3+510-3+660 during the software analyses.

Firstly, there are two units which are slope debris and metasandstone-metamudstone between Km: 3+810-4+110. On the upper level of the model debris was modelled, at the bottom of the model metasandstone-metamudstone can be observable. Mesh was applied for model between Km: 3+810-4+110 (Figure 7.12). Mesh size are automatically assigned.

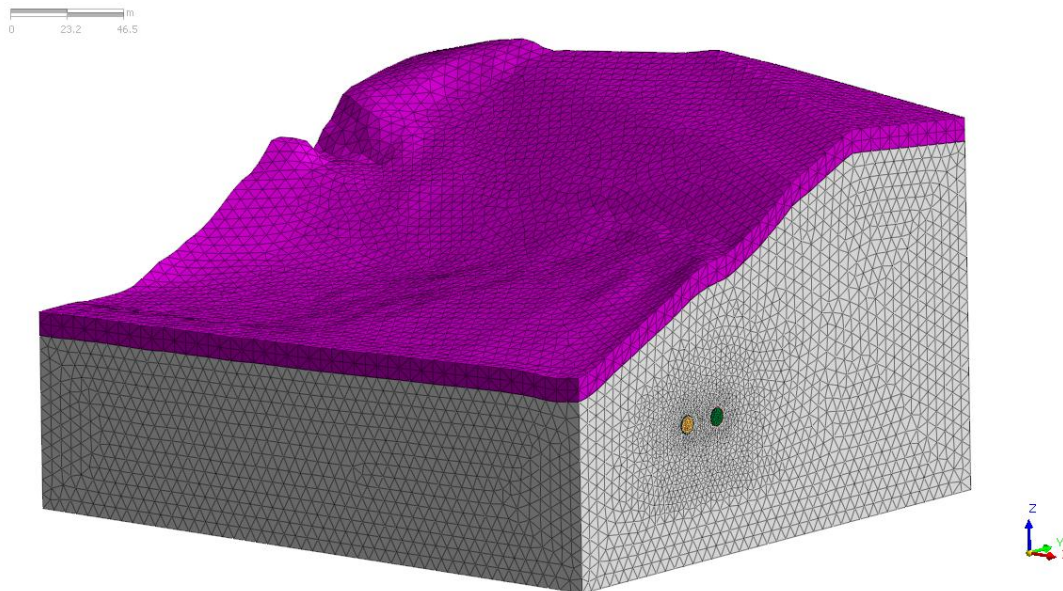


Figure 7.12. Meshed model for Km: 3+810 - 4+110.

Table 7.2 is the representation of maximum and minimum displacement results in the total (Figure 7.13), X (Figure 7.14), Y (Figure 7.15) and Z (Figure 7.16) directions. Results clarify that maximum vertical displacement is bigger than maximum horizontal displacement. It is shown that the landslide is activated from the toe up to the crest of the slope. This shows that landslide is closely related to topography formation with hills and hollows. The main cause of movements is debris occurrence in the toe section.

Table 7.2. Maximum and minimum displacement values for Km: 3+810 - 4+110.

<i>KM: 3+810 - 4+110</i>	<i>Displacement</i>	<i>Max (cm)</i>	<i>Min (cm)</i>
Figure 7.13	Total	3.72	0.310
Figure 7.14	X	1.22	0.076
Figure 7.15	Y	3.55	0.128
Figure 7.16	Z	1.74	0.041

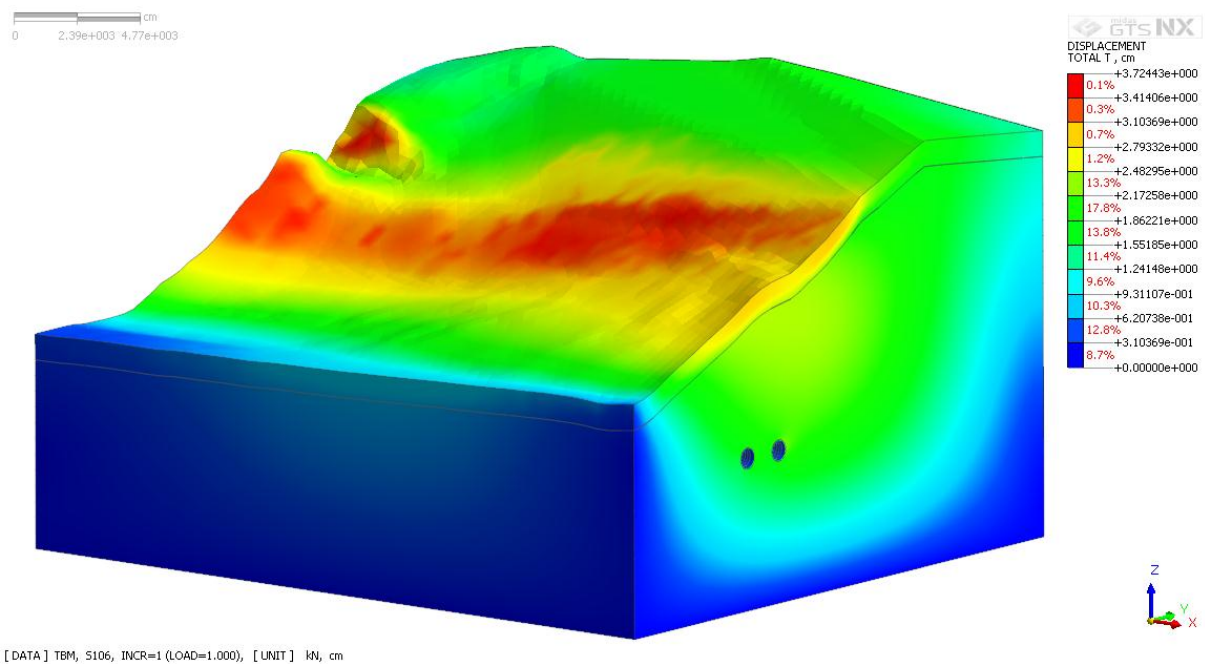


Figure 7.13. Total displacement model for Km: 3+810 - 4+110.

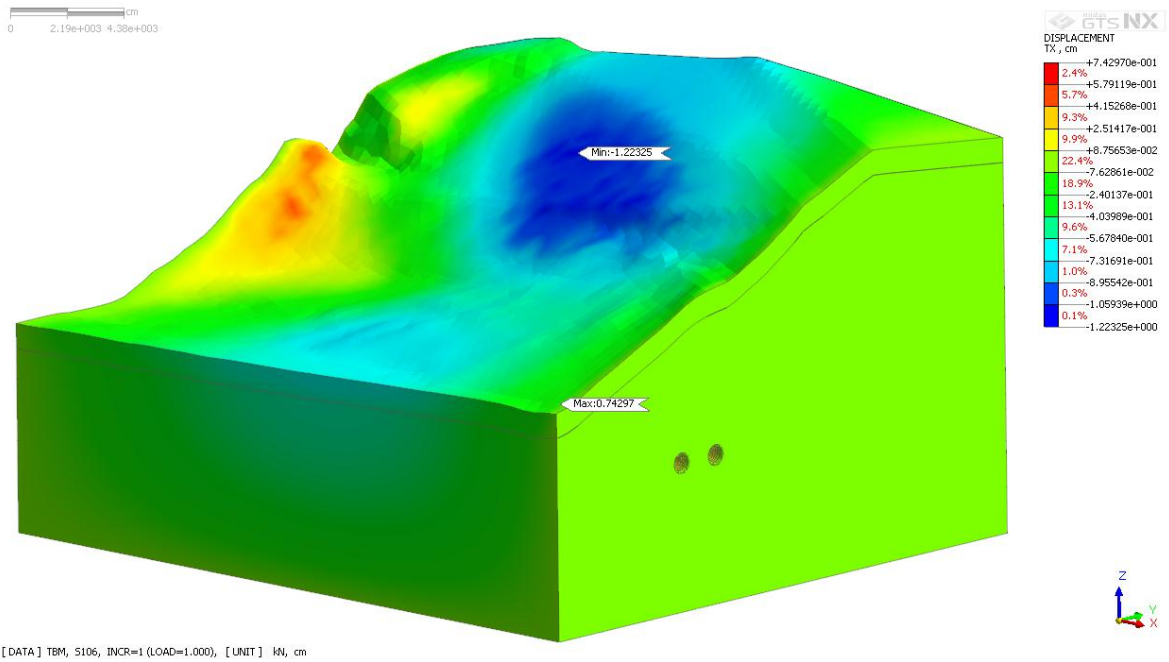


Figure 7.14. Horizontal displacement model for Km: 3+810 - 4+110.

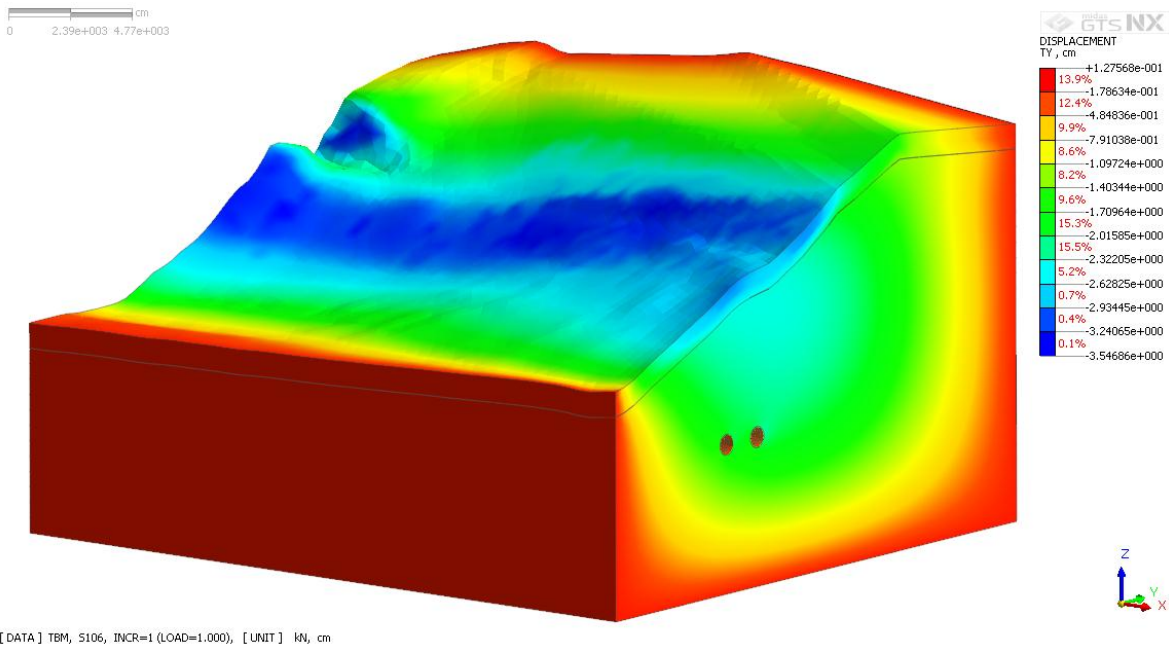


Figure 7.15. Displacement model along Y axis for Km: 3+810 - 4+110.

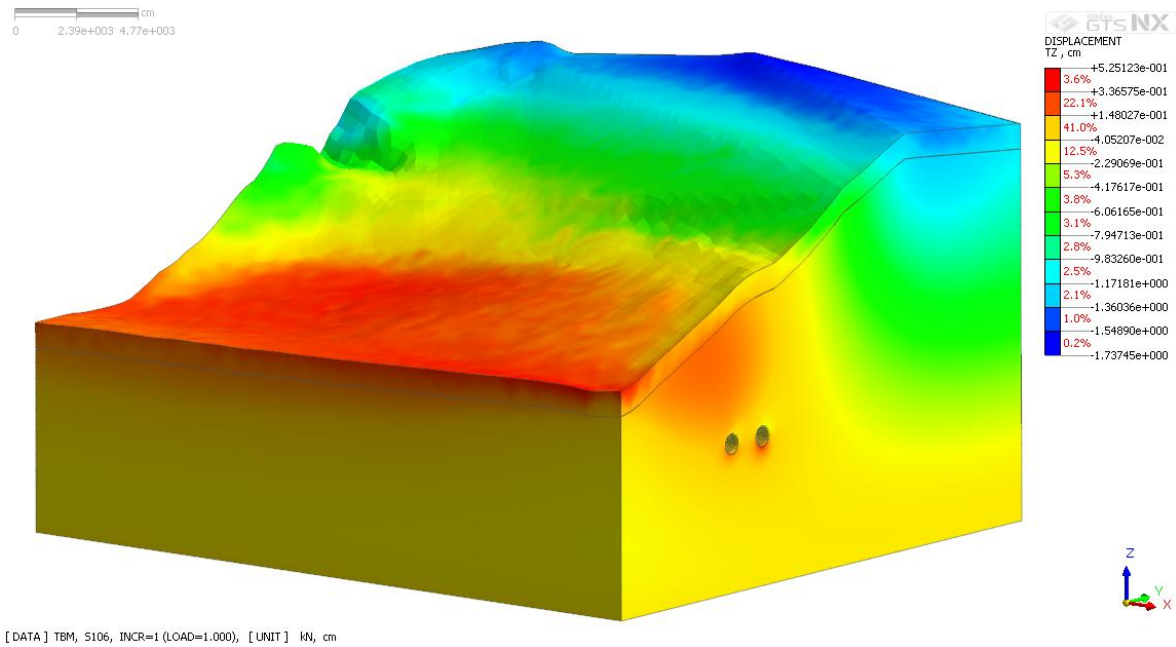


Figure 7.16. Vertical displacement model for Km: 3+810 - 4+110.

Following four models give information about stress values for Km: 3+810 - 4+110. Table 7.3 displays maximum and minimum stress values for this interval. Maximum stress is 6543 ( $\text{kN/m}^2$ ) in green regions which are seen around the tunnels (Figures 7.17 and 7.21). Figures 7.18, 7.19, 7.20 also manifest that high stress values are also examined around the tunnels.

Table 7.3. Maximum and minimum stress values for Km: 3+810 - 4+110.

<b><i>KM: 3+810 - 4+110</i></b>	<b><i>Stress</i></b>	<b><i>Max (kN/m<sup>2</sup>)</i></b>	<b><i>Min (kN/m<sup>2</sup>)</i></b>
Figure 7.17	Mean Total	6543	168
Figure 7.18	XX	13414	203
Figure 7.19	YY	12211	49
Figure 7.20	ZZ	13457	11
Figure 7.21	Mean Effective	6543	168

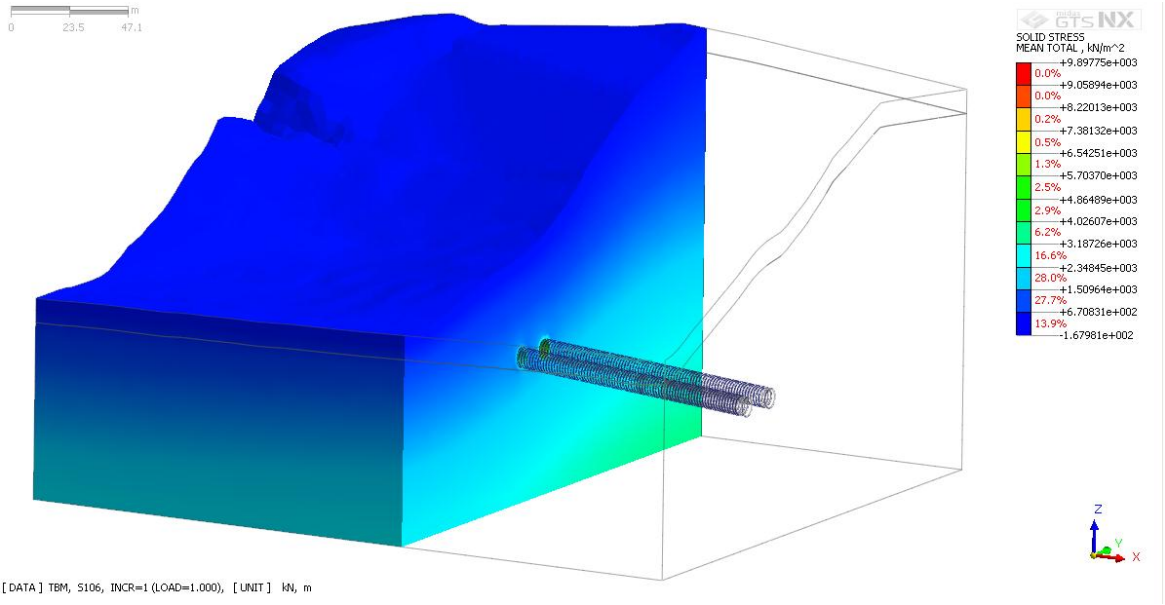


Figure 7.17. Total stress model for Km: 3+810 - 4+110.

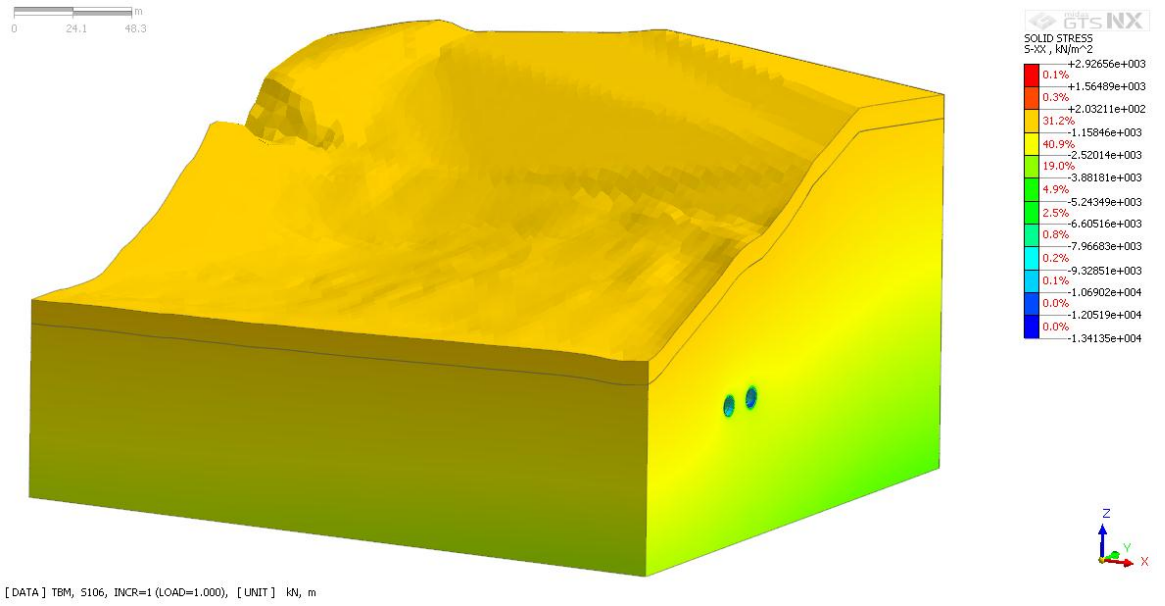


Figure 7.18. XX stress model for Km: 3+810 - 4+110.

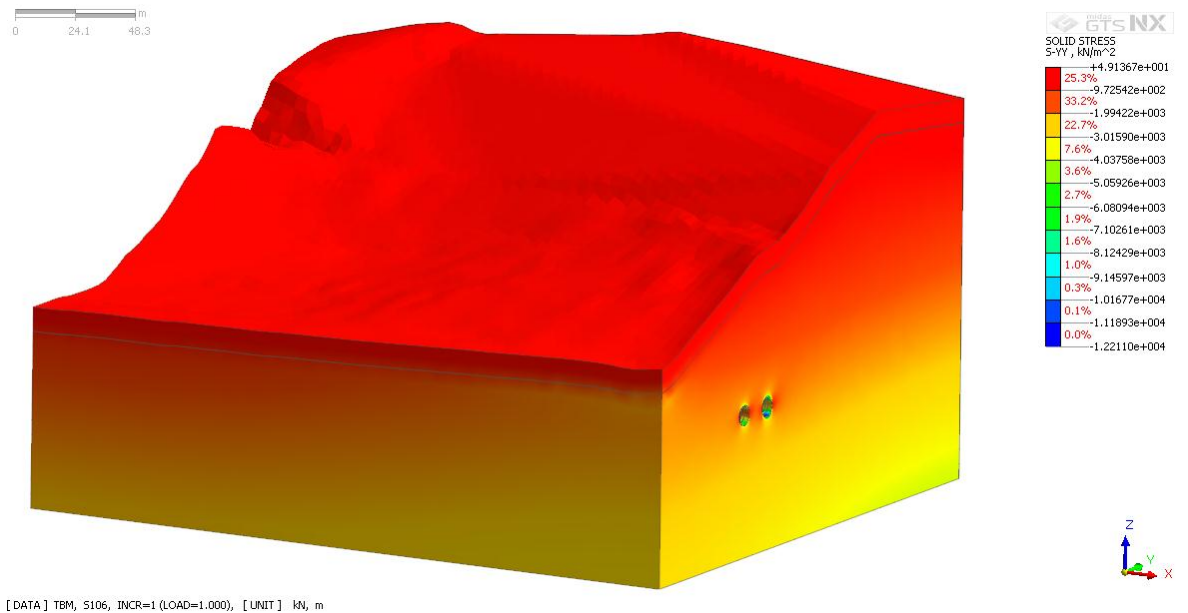


Figure 7.19. YY stress model for Km: 3+810 - 4+110.

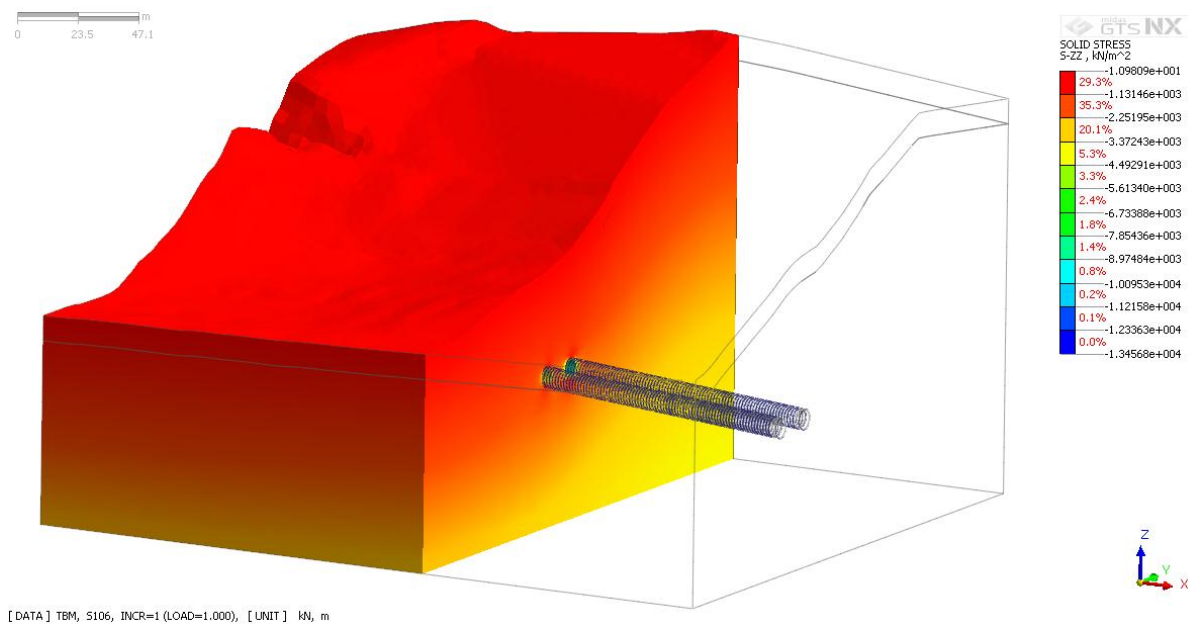


Figure 7.20. ZZ stress model for Km: 3+810 - 4+110.

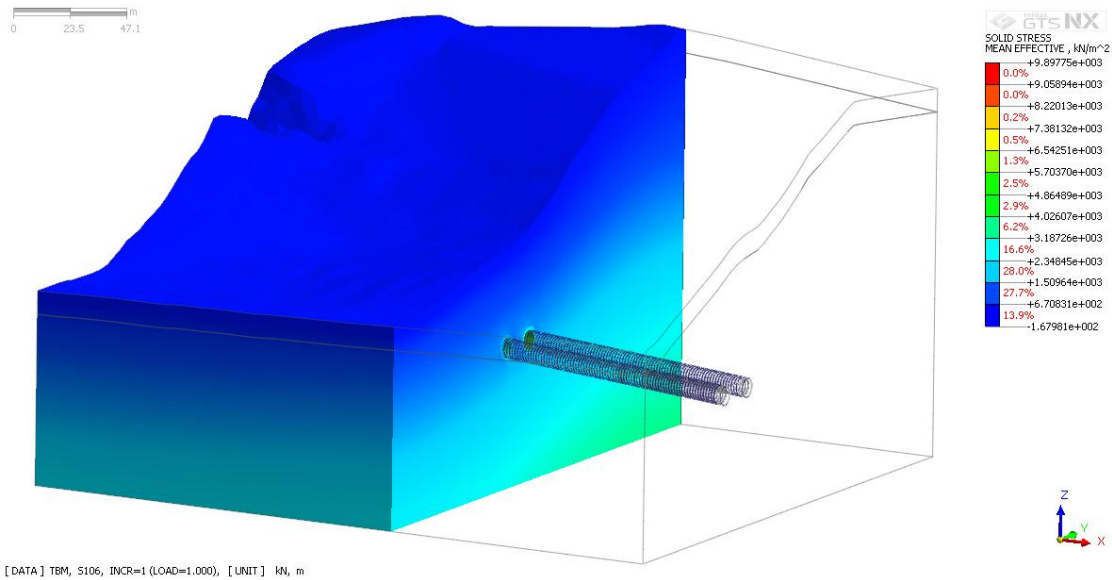


Figure 7.21. Mean effective stress model for Km: 3+810 - 4+110.

Figure 7.22 allows to understand the material behavior for Km: 3+810 - 4+110. As can be deduced from Figure 7.22, while plastic failure materials are shown in red regions, the other failures were displayed in blue region. Failures on tunnel and terrain prove that TBM-tunnelling excavation may not be successful for this interval.

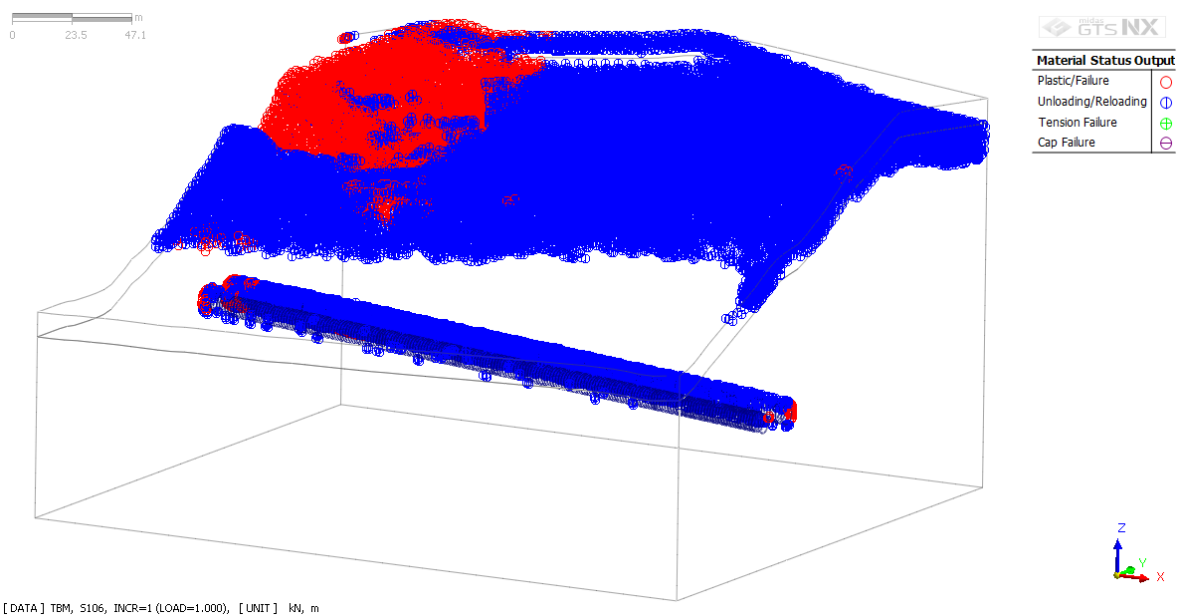


Figure 7.22. Material status model for Km: 3+810 - 4+110.



It is also possible to show tunnel section models in order to understand displacements and failures on tunnels and their surroundings more clearly; hence, following four models (Figures 7.23, 7.24, 7.25 and 7.26) aim to show relationships between tunnel and displacements. Maximum and minimum tunnel section displacement values for Km: 3+810-4+110 are also displayed in Table 7.4. Tunnel section models depict that dark blue and light blue color show deformations on tunnel. In addition, failures on tunnel can be examined from Figure 7.27.

Table 7.4. Maximum and minimum tunnel section displacement values for Km: 3+810 - 4+110.

<b><i>KM: 3+810 - 4+110</i></b>	<b><i>Displacement</i></b>	<b><i>Max (cm)</i></b>	<b><i>Min (cm)</i></b>
Figure 7.23	Total	2.48	0.31
Figure 7.24	X	0.74	0.076
Figure 7.25	Y	2.32	0.13
Figure 7.26	Z	0.53	0.041

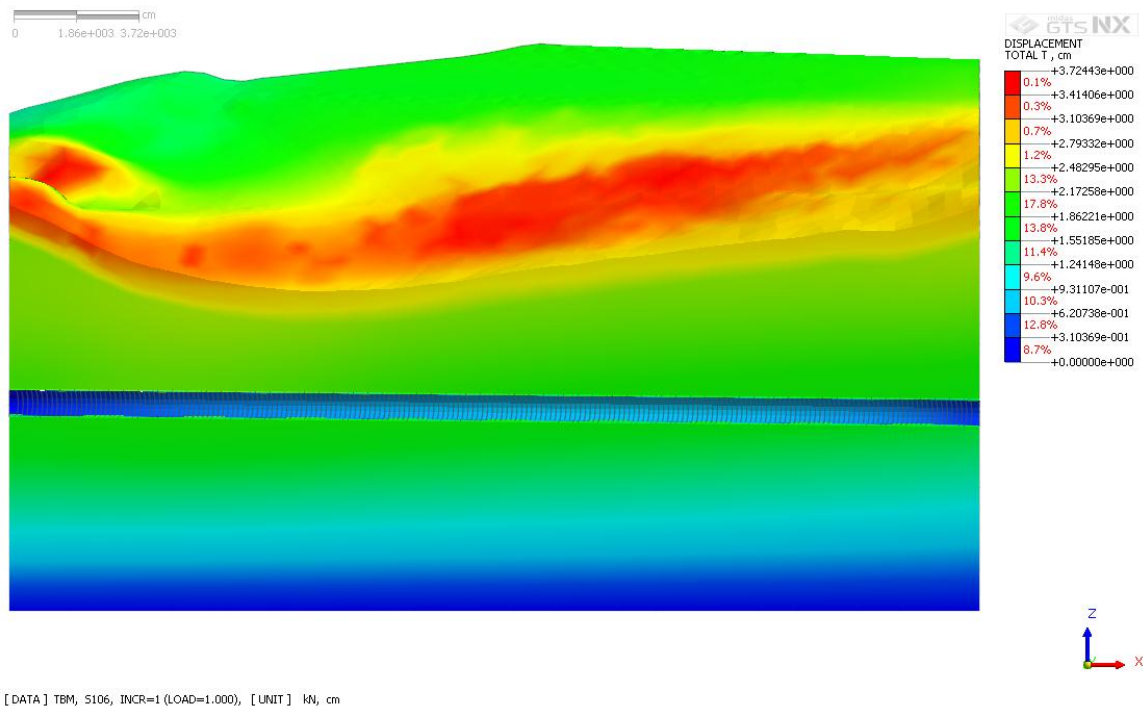


Figure 7.23. Tunnel section of total displacement model for Km: 3+810 - 4+110.

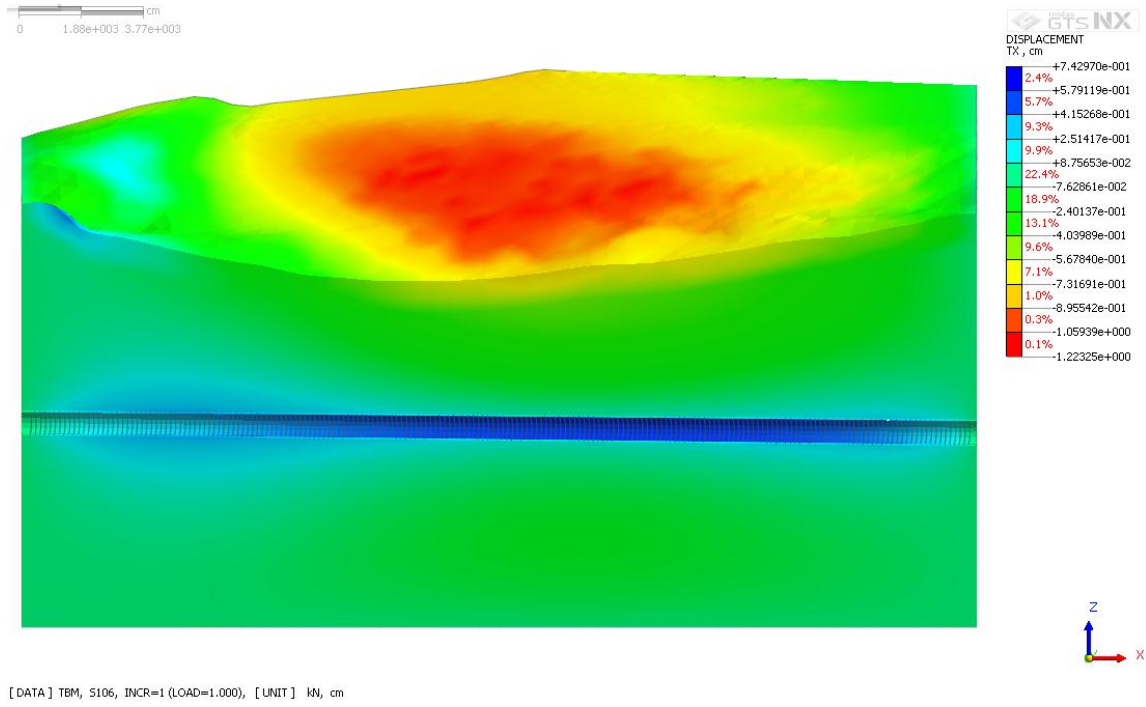


Figure 7.24. Tunnel section of X displacement model for Km: 3+810 - 4+110.

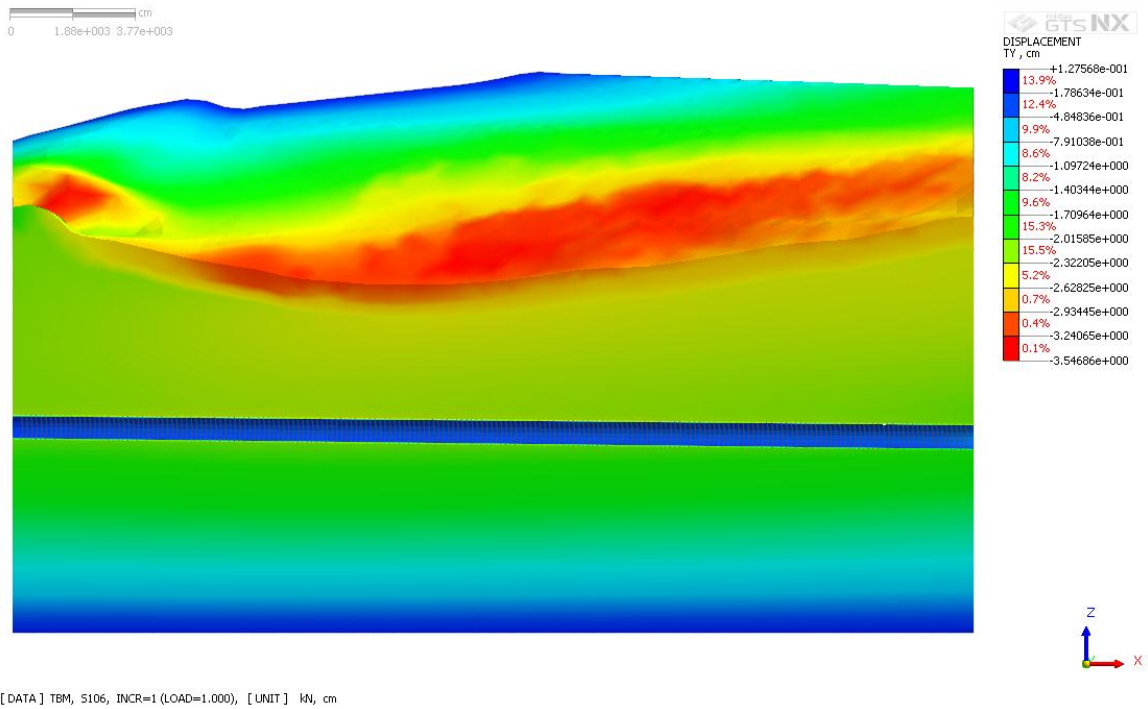


Figure 7.25. Tunnel section of Y displacement model for Km: 3+810 - 4+110.

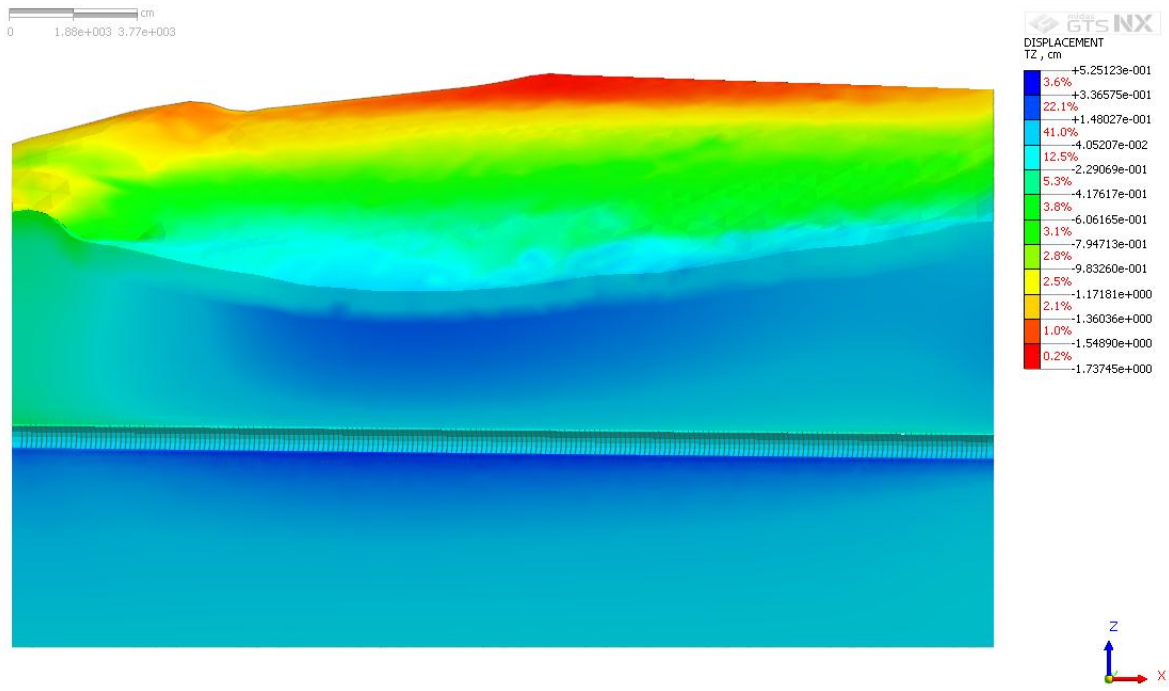


Figure 7.26. Tunnel section of Z displacement model for Km: 3+810 - 4+110.

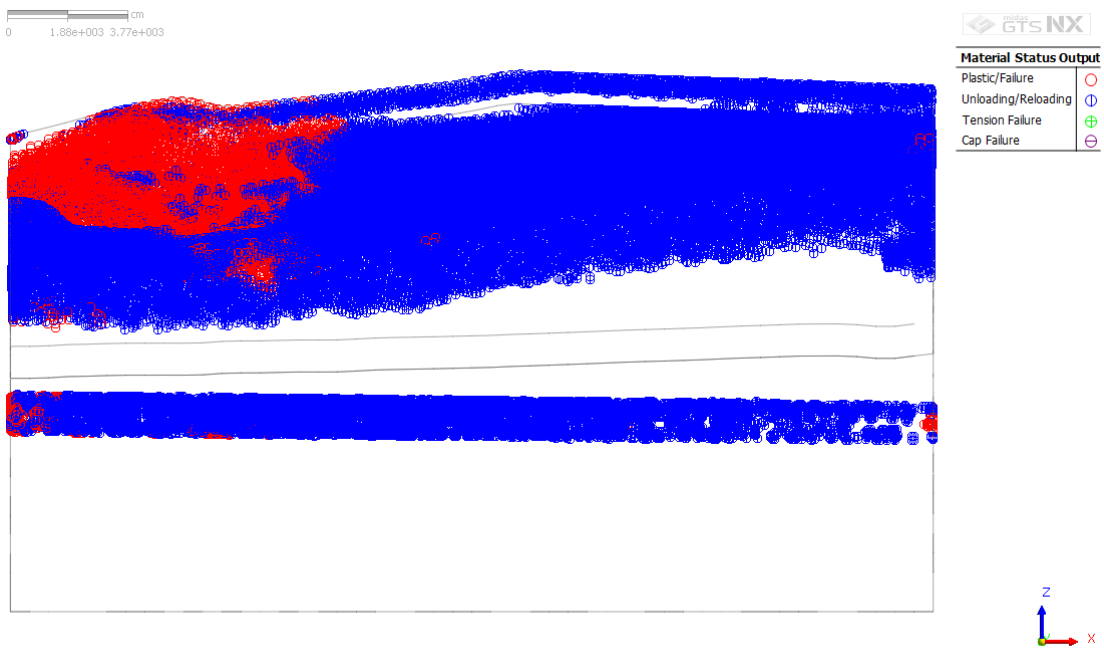


Figure 7.27. Tunnel section of material status model for Km: 3+810 - 4+110.

Secondly, Km: 3+710 - 3+810 will be examined in this part of the thesis. Mesh generation was applied for Km: 3+710 - 3+810 (Figure 7.28).

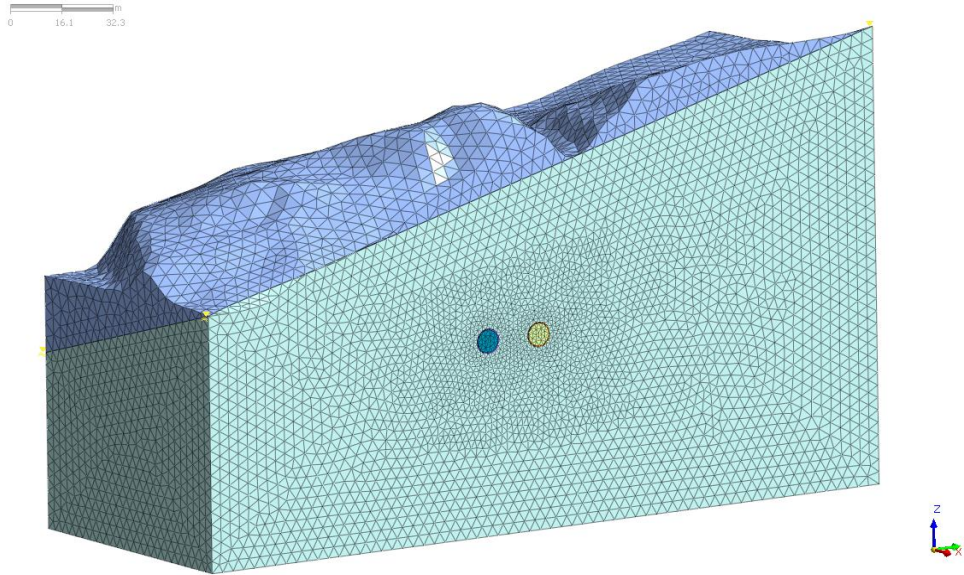


Figure 7.28. Meshed model for Km: 3+710 - 3+810.

Table 7.5 summarizes the maximum and minimum displacement values for this interval. Red regions depict maximum displacement values for total displacement model (Figure 7.29). Unlike total displacement model, maximum displacement locates in blue regions for X (Figure 7.30), Y (Figure 7.31) and Z (Figure 7.32) displacement models.

Table 7.5. Maximum and minimum displacement values for Km: 3+710 - 3+810.

<b><i>KM: 3+710 - 3+810</i></b>	<b><i>Displacement</i></b>	<b><i>Max (cm)</i></b>	<b><i>Min (cm)</i></b>
Figure 7.29	Total	6.90	0.575
Figure 7.30	X	2.57	0.042
Figure 7.31	Y	6.75	0.231
Figure 7.32	Z	2.13	0.062

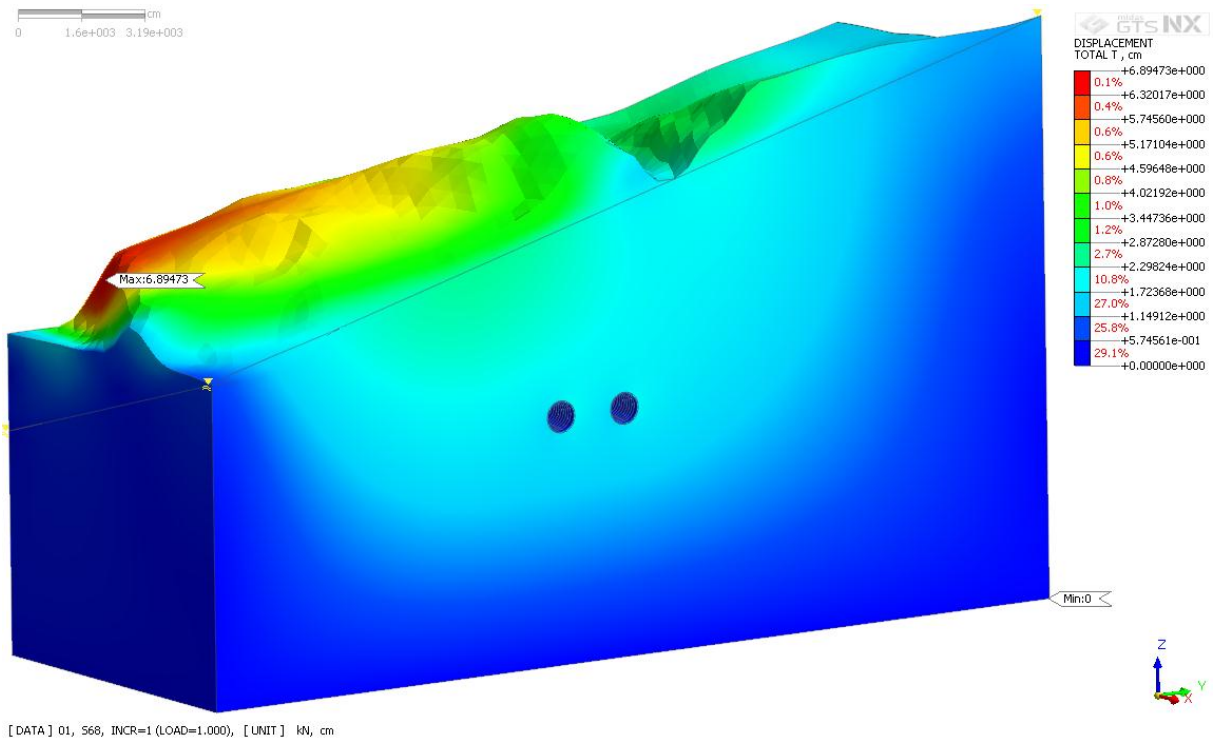


Figure 7.29. Total displacement model for Km: 3+710 - 3+810.

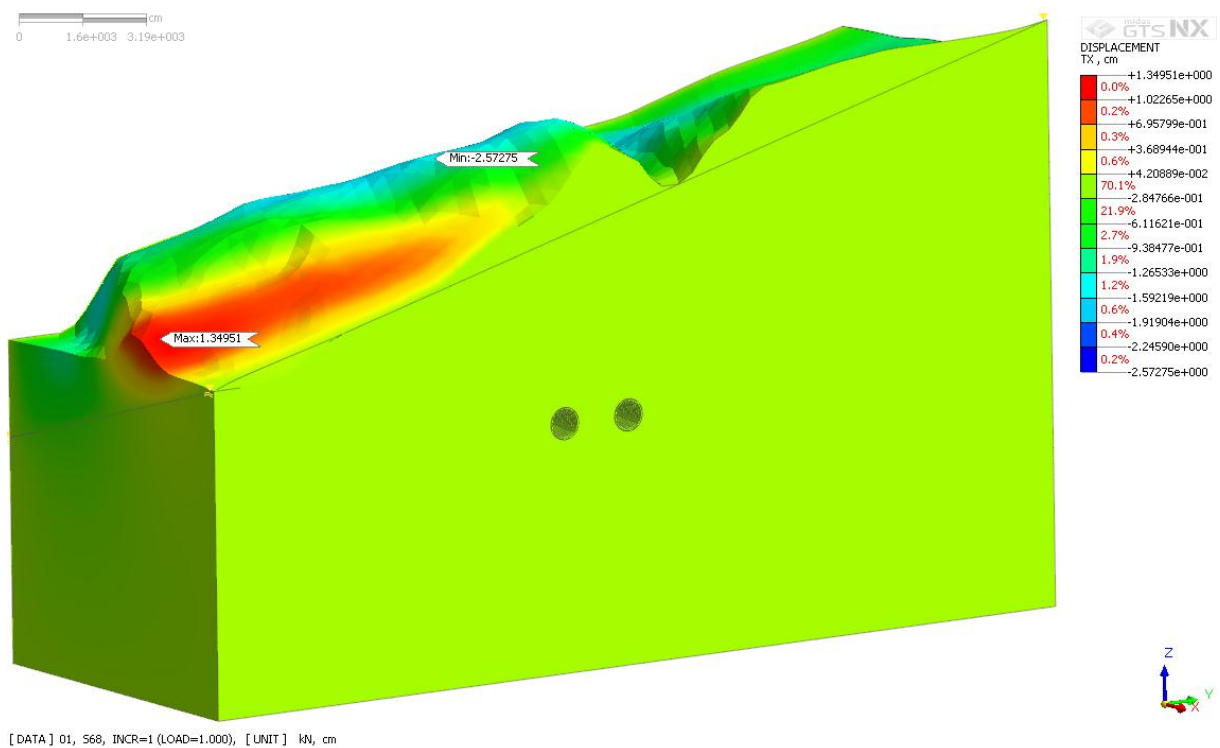


Figure 7.30. Horizontal displacement model for Km: 3+710 - 3+810.

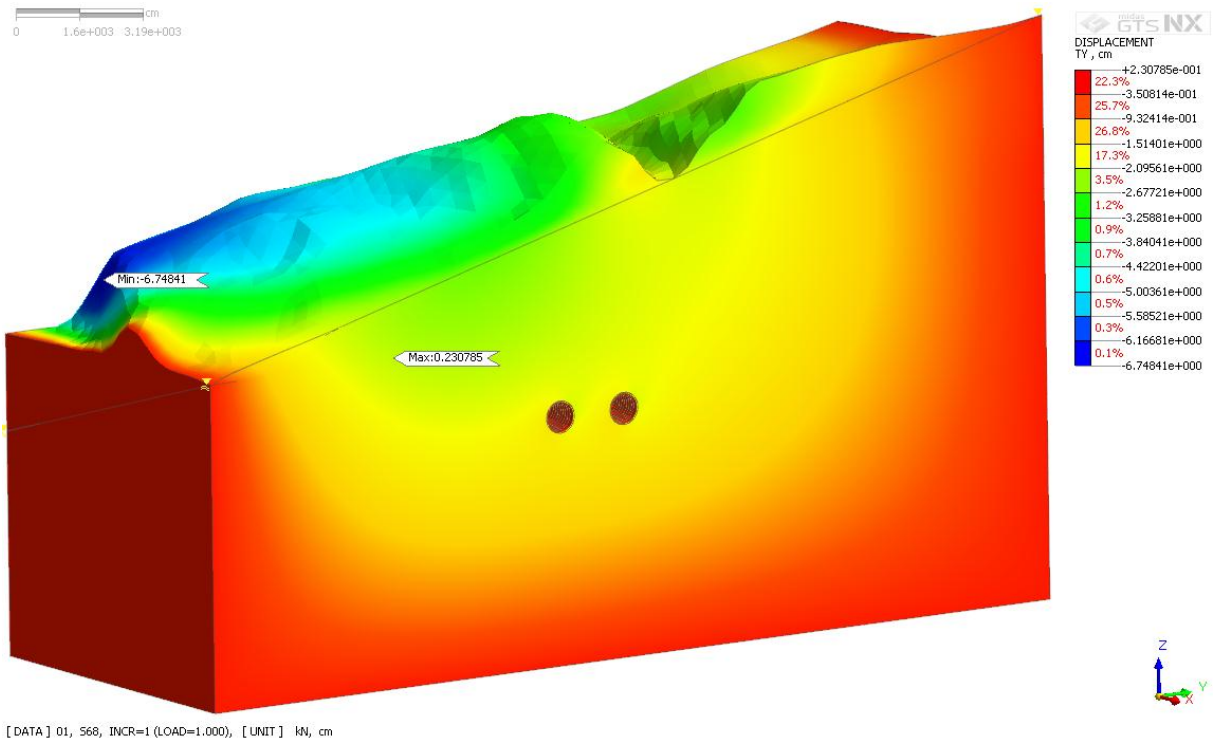


Figure 7.31. Displacement model along the Y-axis for Km: 3+710 - 3+810.

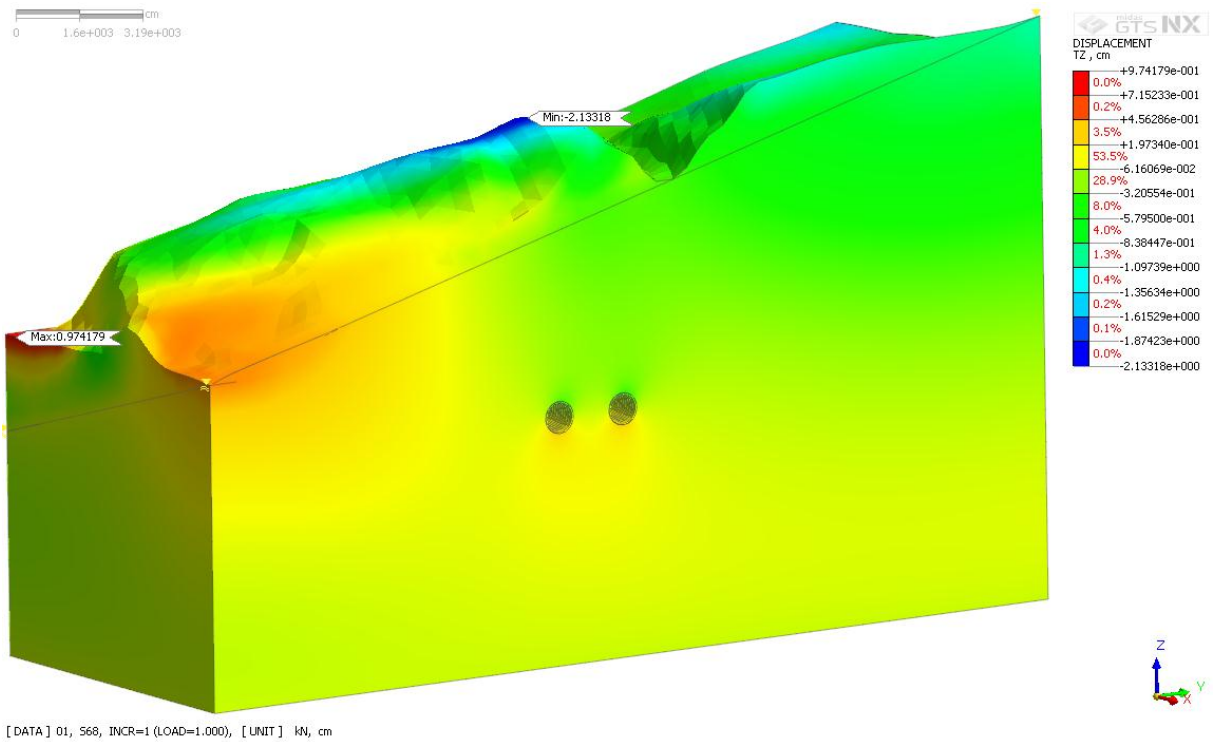


Figure 7.32. Vertical displacement model for Km: 3+710 - 3+810.

Due to necessary of collecting more information, maximum and minimum stress values for Km: 3+710 - 3+810 can be manifested in Table 7.6. It can be described that red color reveals maximum deformations for Figures 7.33 and 7.37. As can be seen from Figure 7.34, XX maximum stress is about 5939 kN/m<sup>2</sup> in light blue region which are seen around tunnel. YY stress model (Figure 7.35) and ZZ stress model (Figure 7.36) display maximum deformations in blue regions which are located in around the tunnels.

Table 7.6. Maximum and minimum stress values for Km: 3+710 - 3+810.

<b>KM: 3+710 - 3+810</b>	<b>Stress</b>	<b>Max (kN/m<sup>2</sup>)</b>	<b>Min (kN/m<sup>2</sup>)</b>
Figure 7.33	Mean Total	7264	0.9
Figure 7.34	XX	5939	5.4
Figure 7.35	YY	12130	5.5
Figure 7.36	ZZ	14597	6.7
Figure 7.37	Mean Effective	7125	4.9

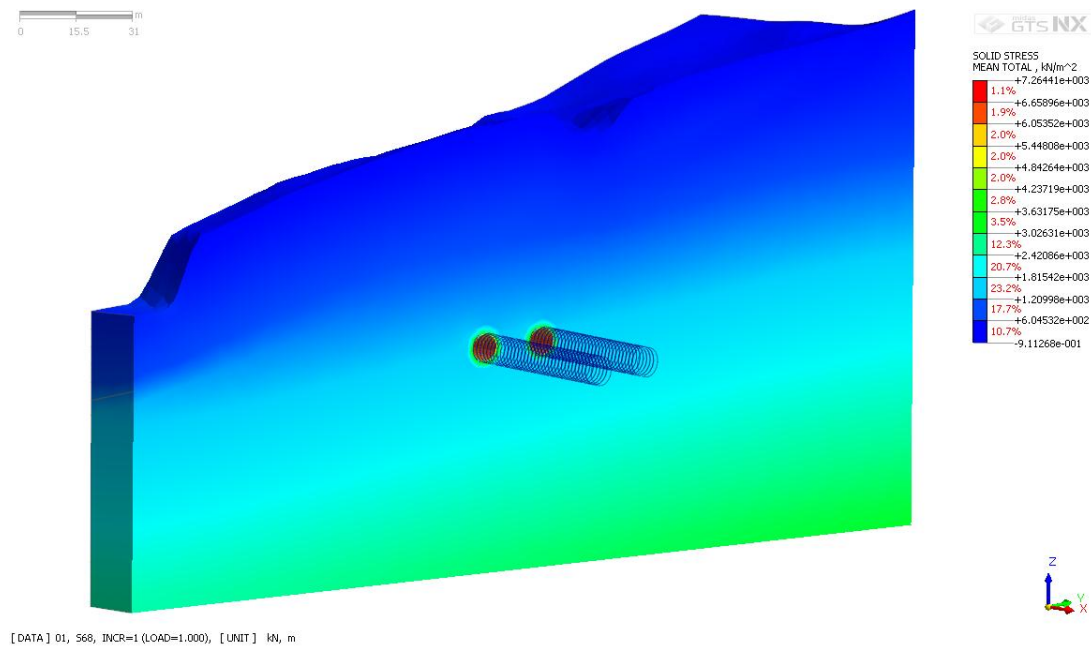
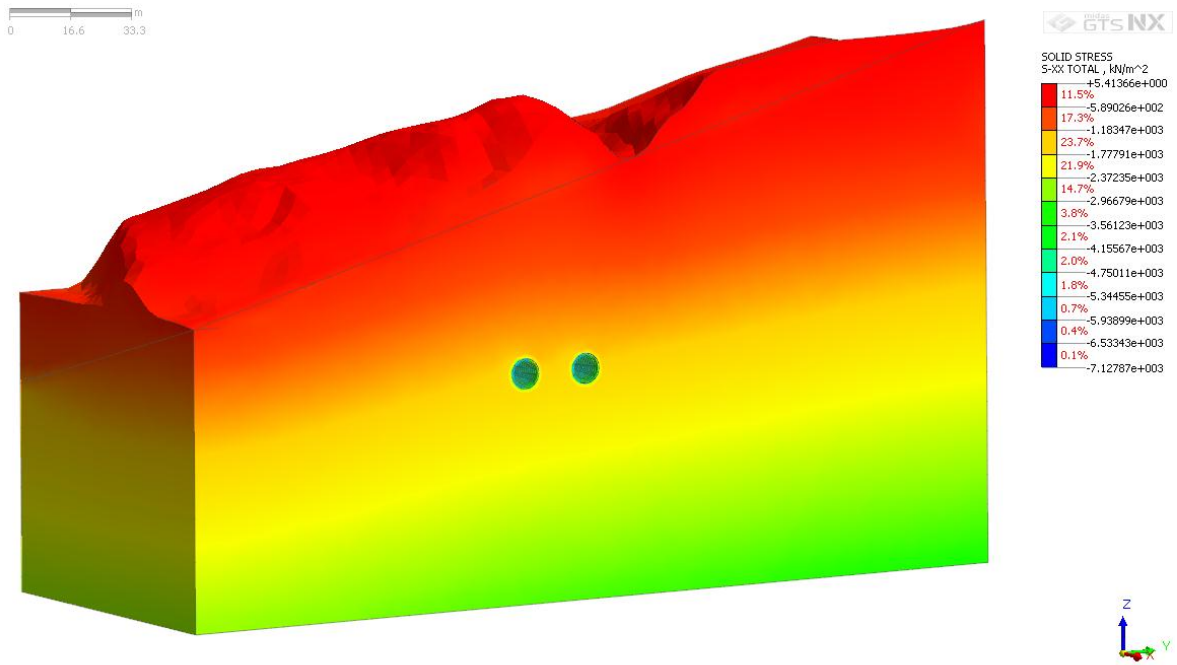
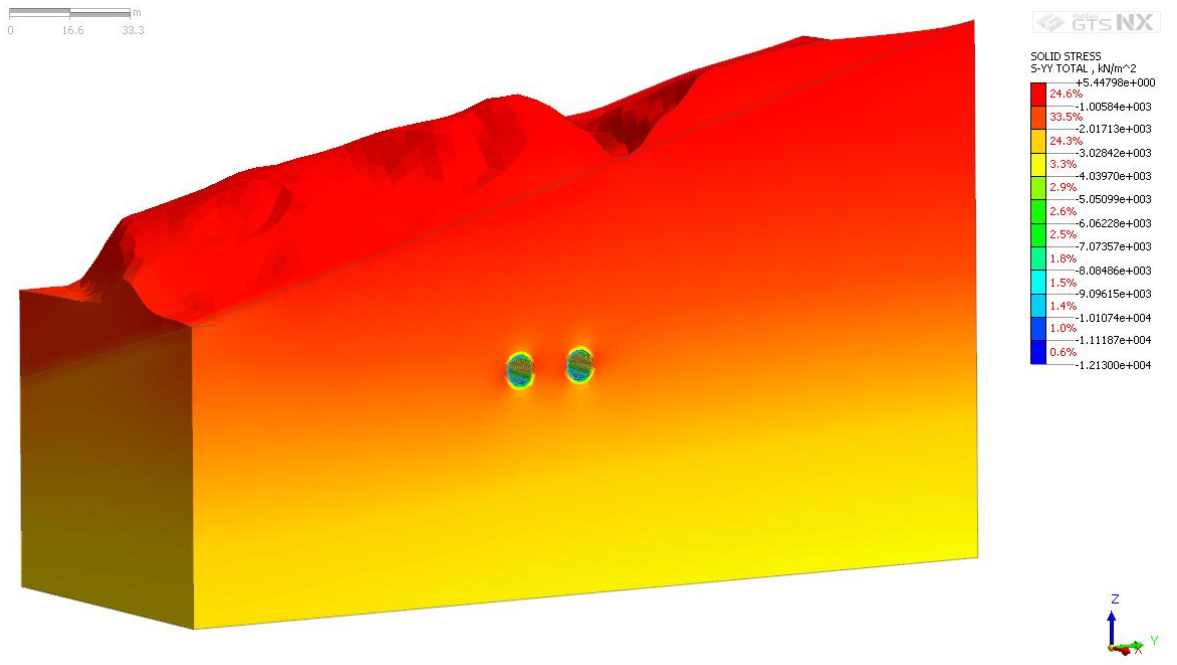


Figure 7.33. Total stress model for Km: 3+710 - 3+810.



[DATA] 01, 568, INCR=1 (LOAD=1.000), [UNIT] kN, m

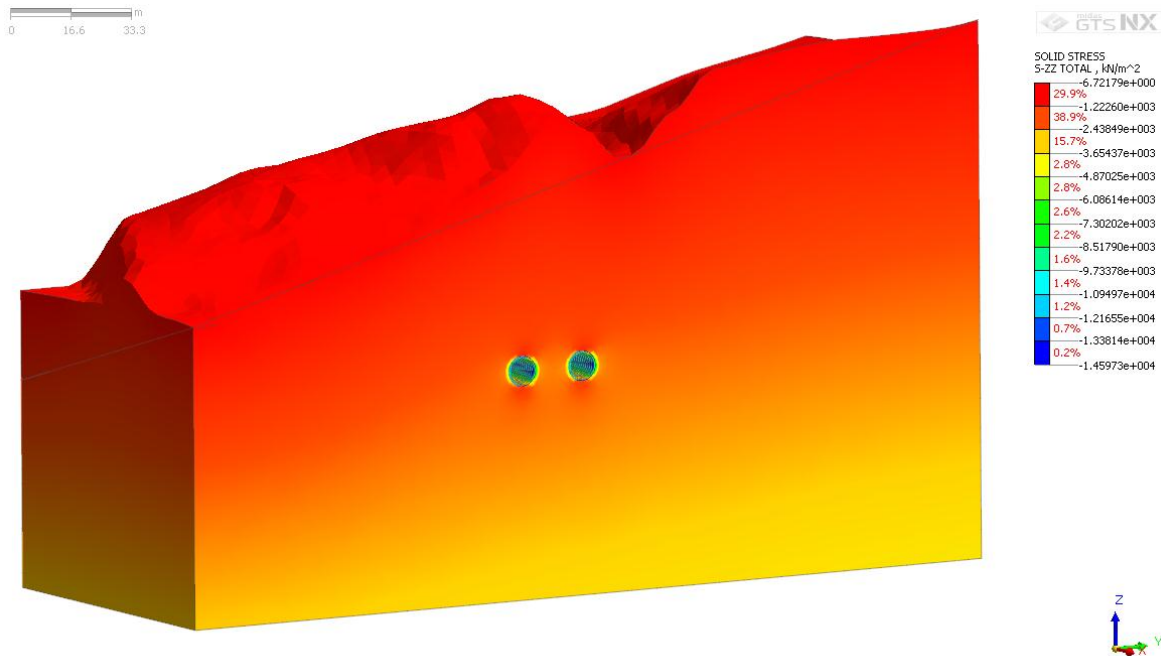
Figure 7.34. XX stress model for Km: 3+710 - 3+810.



[DATA] 01, 568, INCR=1 (LOAD=1.000), [UNIT] kN, m

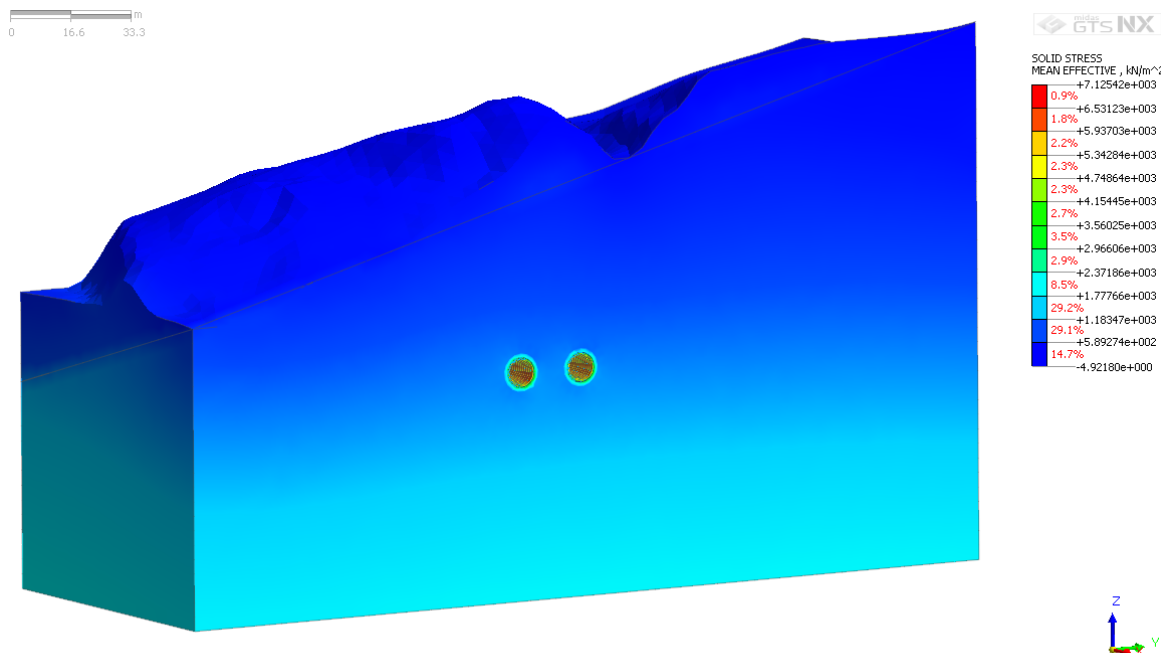
Figure 7.35. YY stress model for Km: 3+710 - 3+810.





[DATA] 01, 568, INCR=1 (LOAD=1.000), [UNIT] kN, m

Figure 7.36. ZZ stress model for Km: 3+710 - 3+810.



[DATA] 01, 568, INCR=1 (LOAD=1.000), [UNIT] kN, m

Figure 7.37. Mean effective stress model for Km: 3+710 - 3+810.

Failures are also clearly observable on the terrain and the tunnels (Figure 7.38).

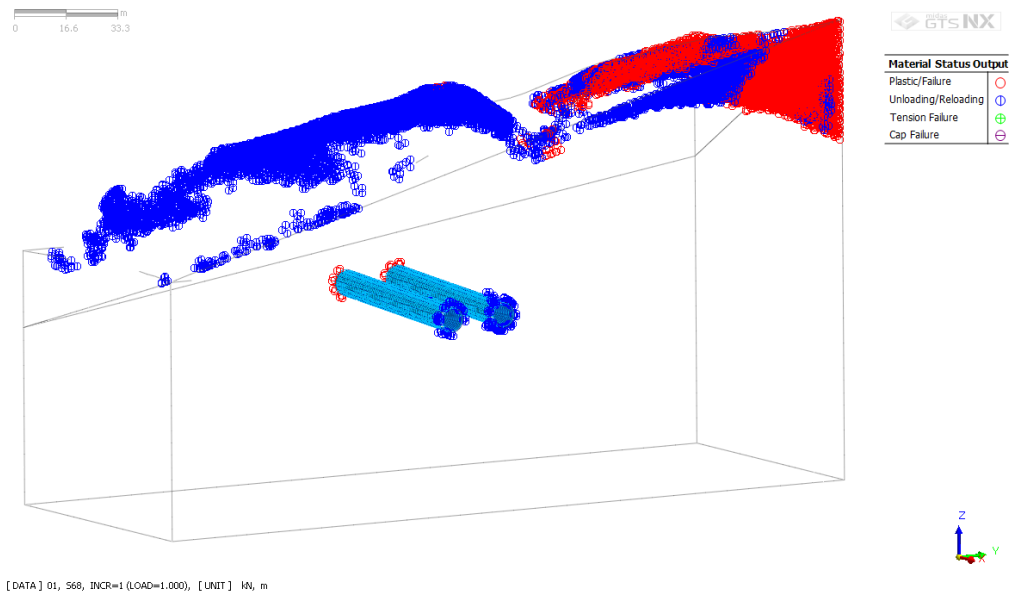


Figure 7.38. Material status model for Km: 3+710 - 3+810.

Maximum and minimum tunnel section displacement values for Km: 3+710-3+810 were presented in Table 7.7. Figures 7.39, 7.40, 7.41 and 7.42 also show tunnel section total, X, Y and Z displacement values. Tunnel section of total (Figure 7.39) and Y (Figure 7.41) displacements can be explained with blue color's range. In addition, tunnel section of X displacement (Figure 7.40) values have range between 1.27 and 0.042. Light blue and green color also show tunnel section displacement ranges in Figure 7.42.

Table 7.7. Maximum and minimum tunnel section displacement values for Km: 3+710 - 3+810.

<b><i>KM: 3+710 - 3+810</i></b>	<b><i>Displacement</i></b>	<b><i>Max (cm)</i></b>	<b><i>Min (cm)</i></b>
Figure 7.39	Total	2.30	0.57
Figure 7.40	X	1.27	0.042
Figure 7.41	Y	2.10	0.23
Figure 7.42	Z	1.10	0.062

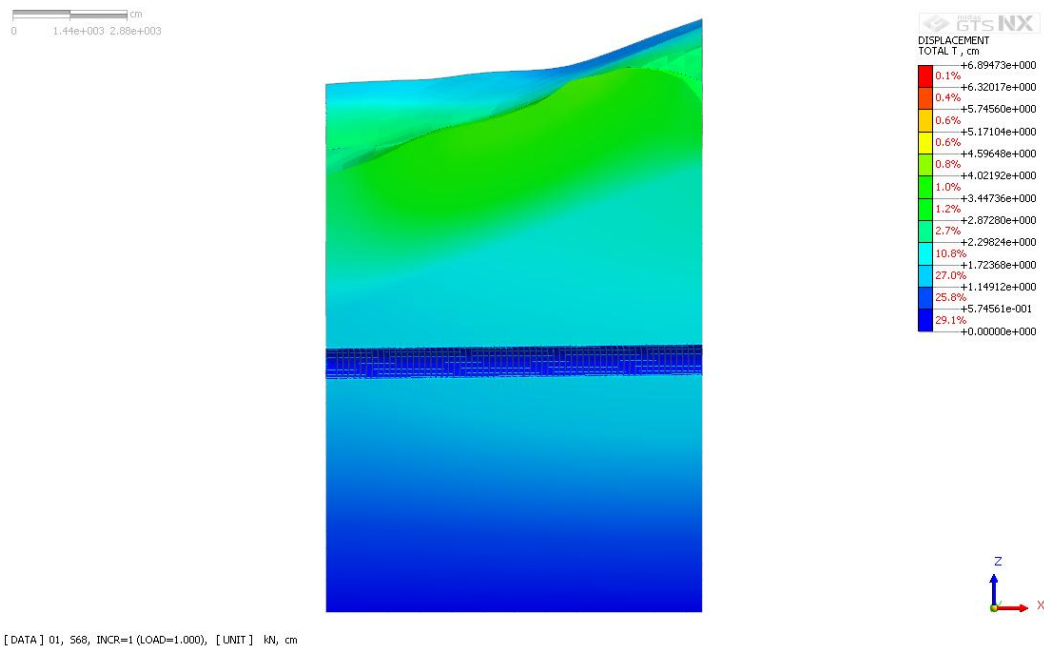


Figure 7.39. Tunnel section of total displacement model for Km: 3+710 - 3+810.

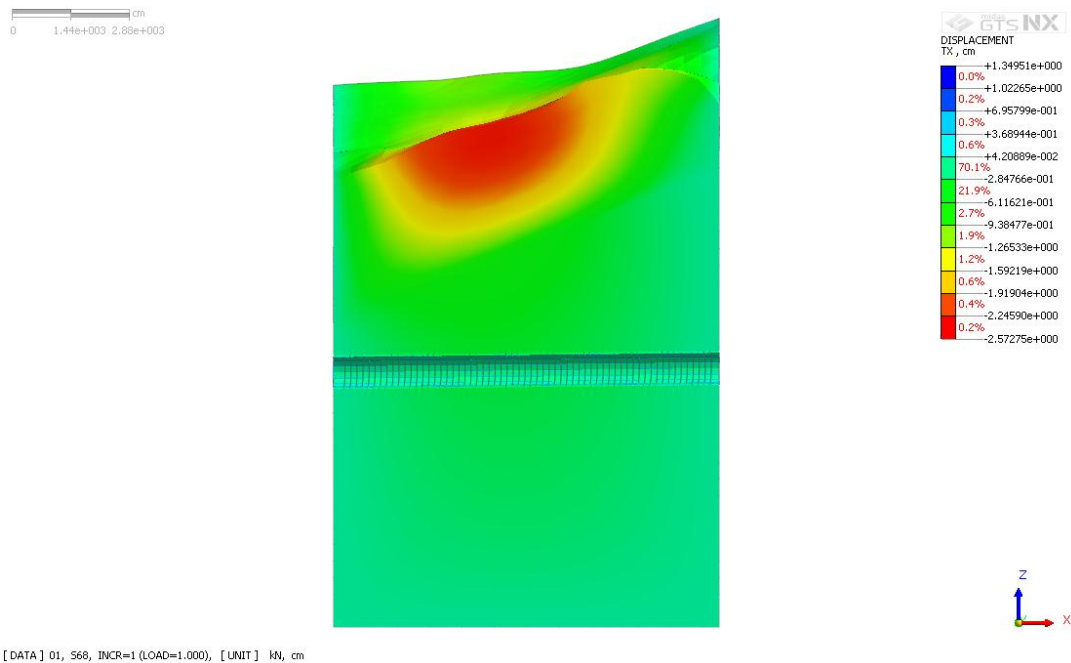


Figure 7.40. Tunnel section of X displacement model for Km: 3+710 - 3+810.

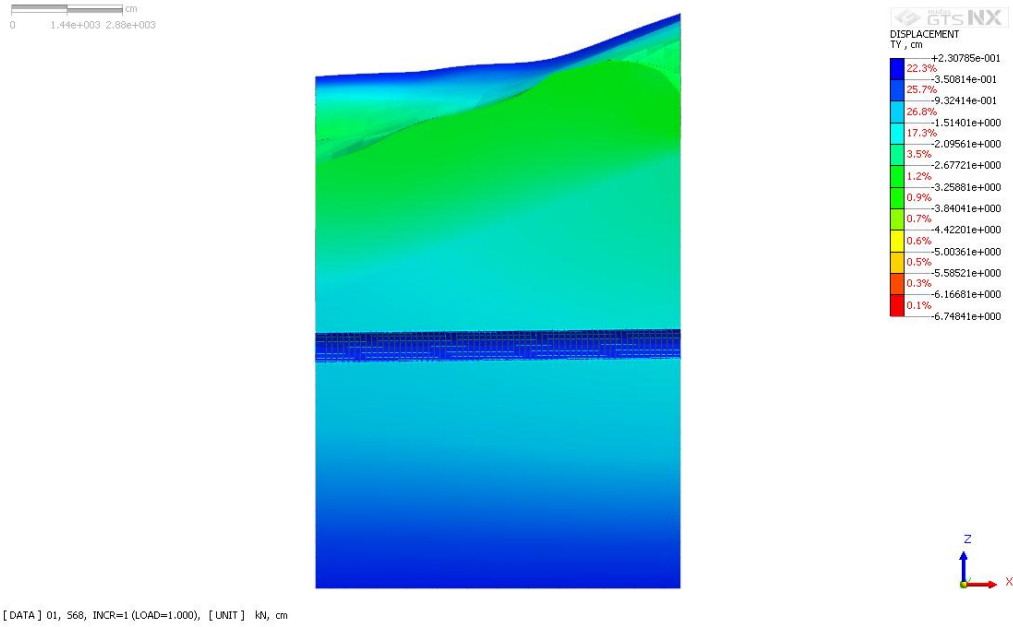


Figure 7.41. Tunnel section of Y displacement model for Km: 3+710 - 3+810.

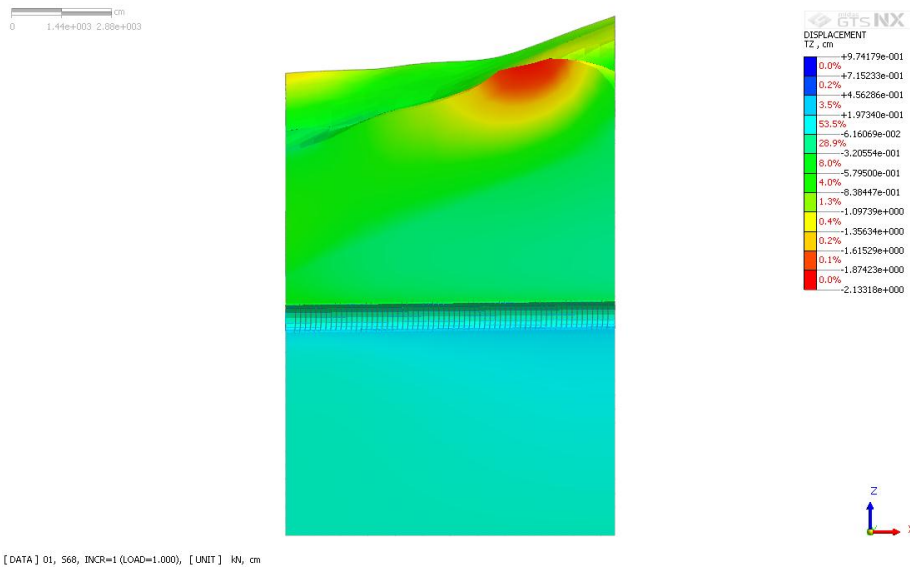


Figure 7.42. Tunnel section of Z displacement model for Km: 3+710 - 3+810.

Failures on tunnel are also presented in Figure 7.43.

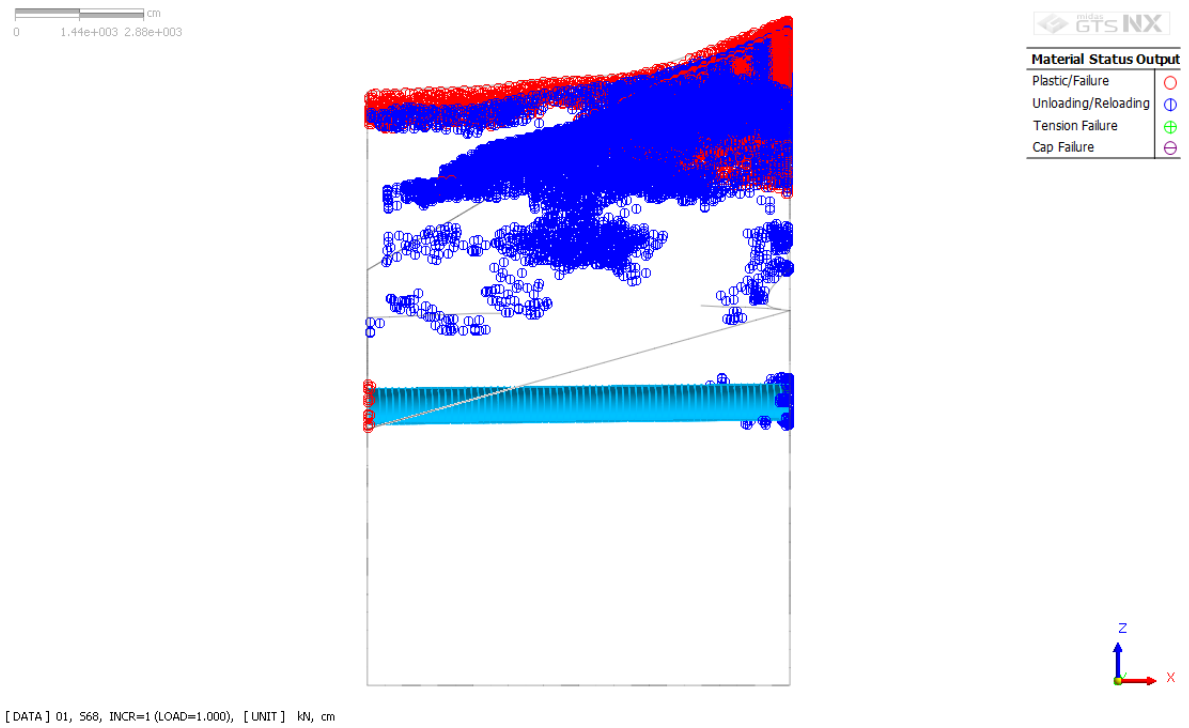


Figure 7.43. Tunnel section of material status model for Km: 3+710 - 3+810.

Thirdly, Km: 3+660 – 3+710 was also modeled in order to reach more information about displacement, stress and failures. Meshed model for Km: 3+660 – 3+710 was illustrated in Figure 7.44.

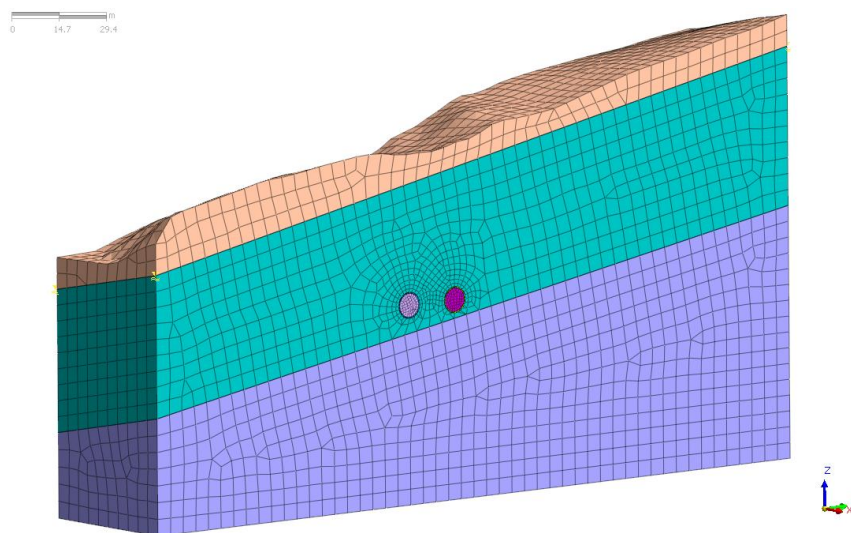


Figure 7.44. Meshed model for Km: 3+660 – 3+710.

Maximum and minimum displacement values for Km: 3+660 – 3+710 can be provided from Table 7.8. While maximum displacements accumulates in red regions for total (Figure 7.45), Y (Figure 7.47) displacements models, dark blue color represents maximum displacement values for X (Figure 7.46) and Z (Figure 7.48) displacement models.

Table 7.8. Maximum and minimum displacement values for Km: 3+660 – 3+710.

<i>KM: 3+660 – 3+710</i>	<i>Displacement</i>	<i>Max (cm)</i>	<i>Min (cm)</i>
Figure 7.45	Total	23.8	0
Figure 7.46	X	7.20	0.27
Figure 7.47	Y	23.7	0.25
Figure 7.48	Z	20.7	1.13

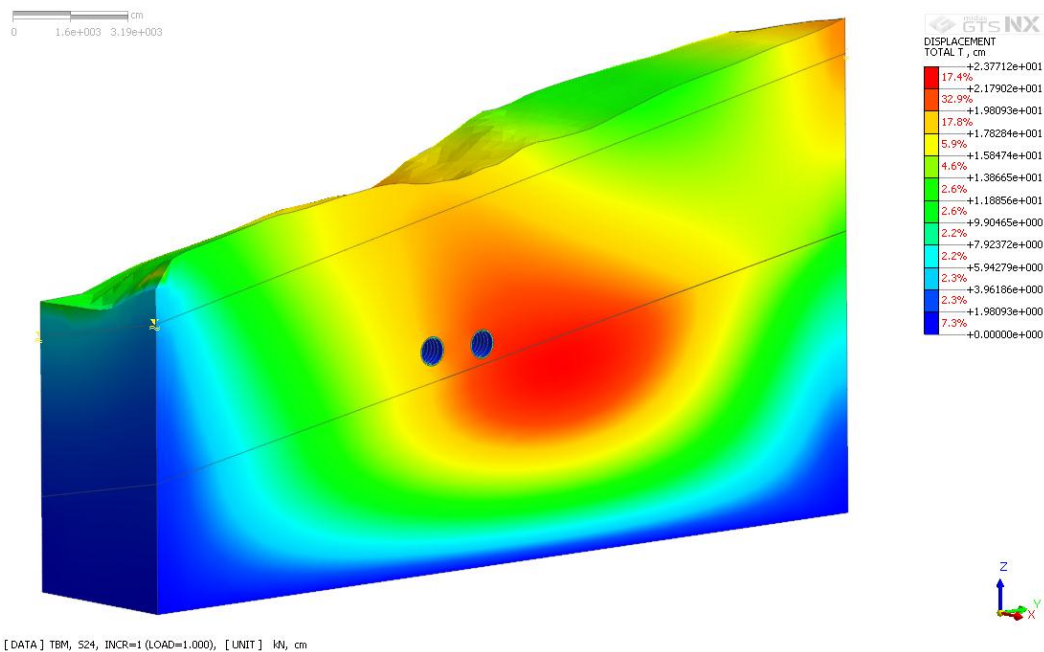


Figure 7.45. Total displacement model for Km: 3+660 – 3+710.

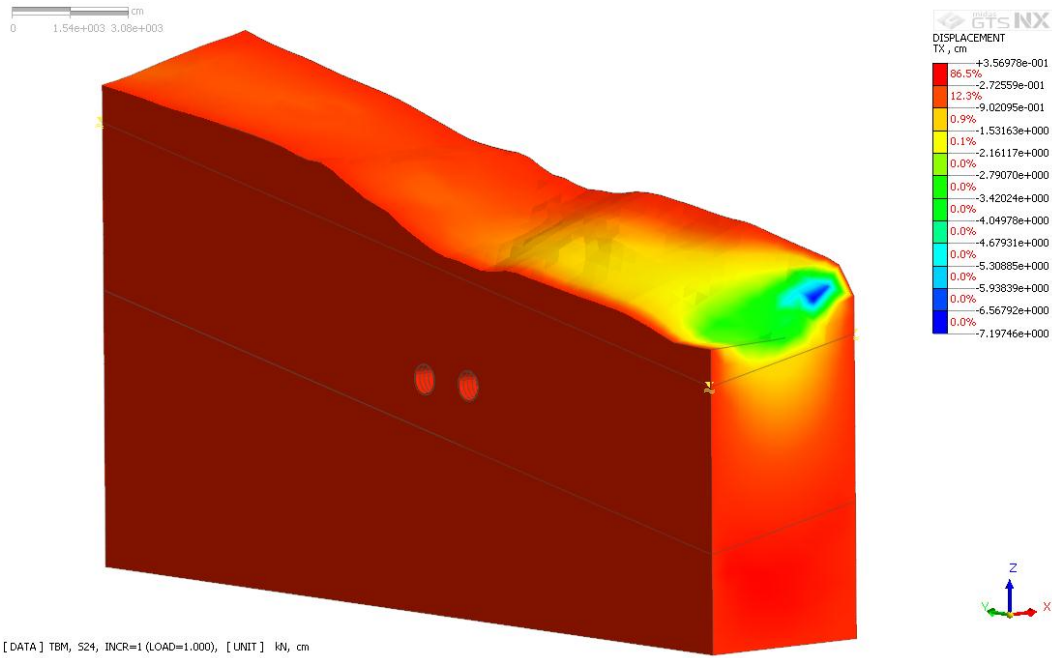


Figure 7.46. Horizontal displacement model for Km: 3+660 – 3+710.

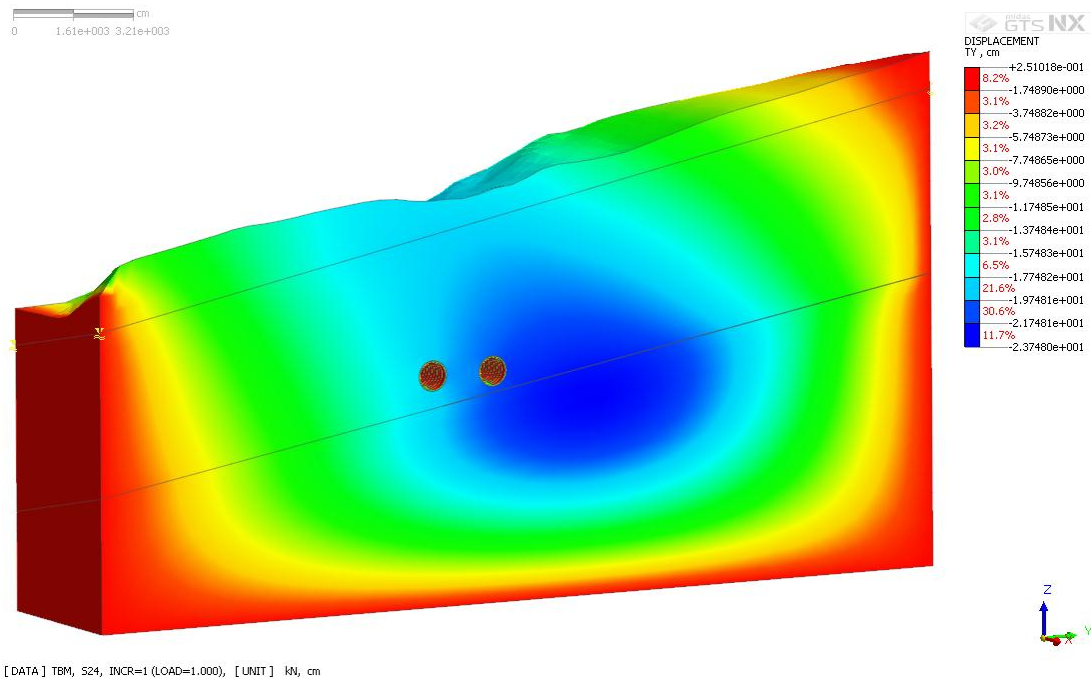


Figure 7.47. Displacement model along the Y-axis for Km: 3+660 – 3+710.

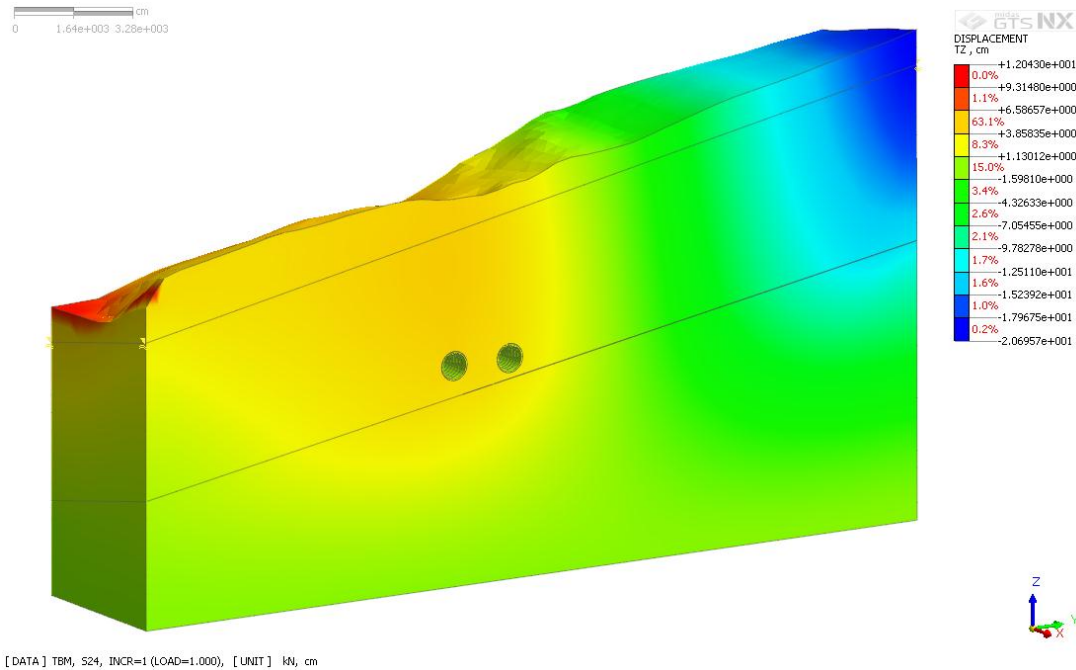


Figure 7.48. Vertical displacement model for Km: 3+660 – 3+710.

After the displacement values was examined for Km: 3+660 – 3+710, maximum and minimum stress values were presented in Table 7.9. Maximum stresses locate in red regions which are examined around the tunnel for Figures 7.49, 7.50 and 7.53. In addition, as can be seen from Figures 7.51 and 7.52, tunnel arounds have maximum stress value in red regions.

Table 7.9. Maximum and minimum stress values for Km: 3+660 – 3+710.

<b><i>KM: 3+660 – 3+710</i></b>	<b><i>Stress</i></b>	<b><i>Max (kN/m<sup>2</sup>)</i></b>	<b><i>Min (kN/m<sup>2</sup>)</i></b>
Figure 7.49	Mean Total	4245	12.3
Figure 7.50	XX	4050	45
Figure 7.51	YY	11444	11.9
Figure 7.52	ZZ	8078	5.9
Figure 7.53	Mean Effective	3891	12.3



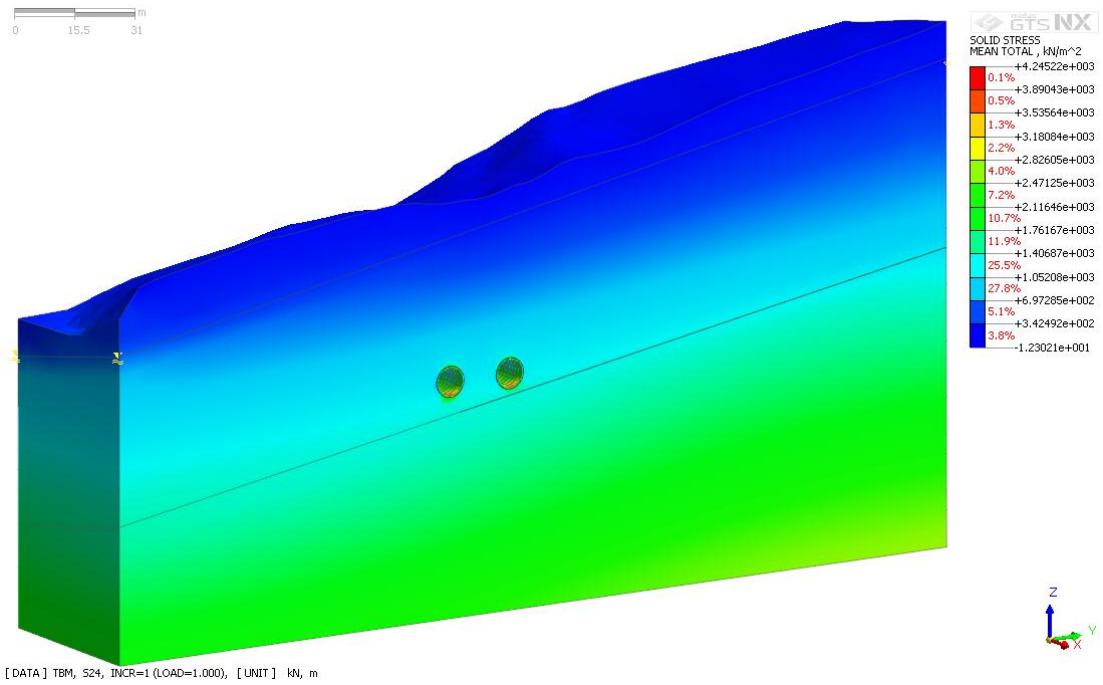


Figure 7.49. Total stress model for Km: 3+660 – 3+710.

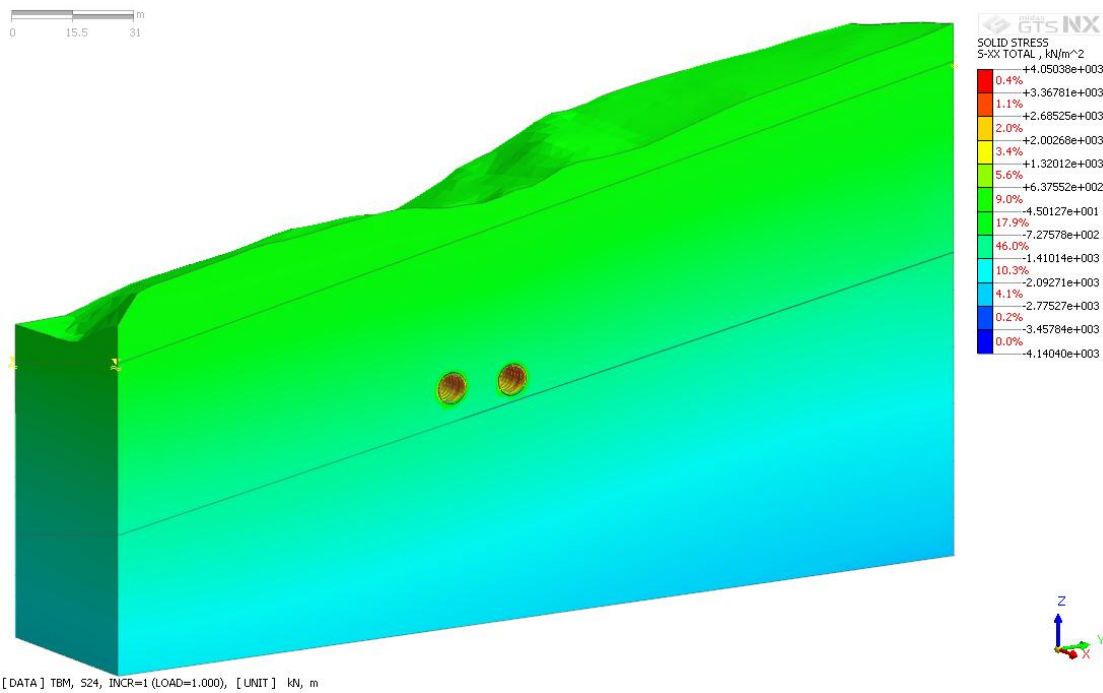


Figure 7.50. XX stress model for Km: 3+660 – 3+710.

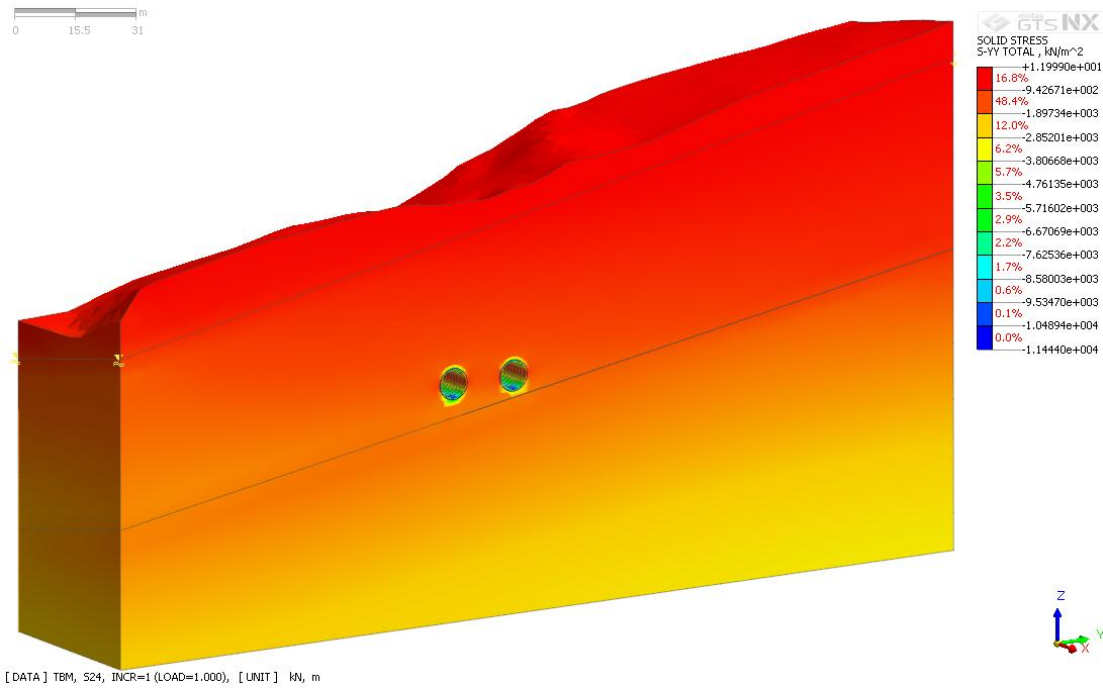


Figure 7.51. YY stress model for Km: 3+660 – 3+710.

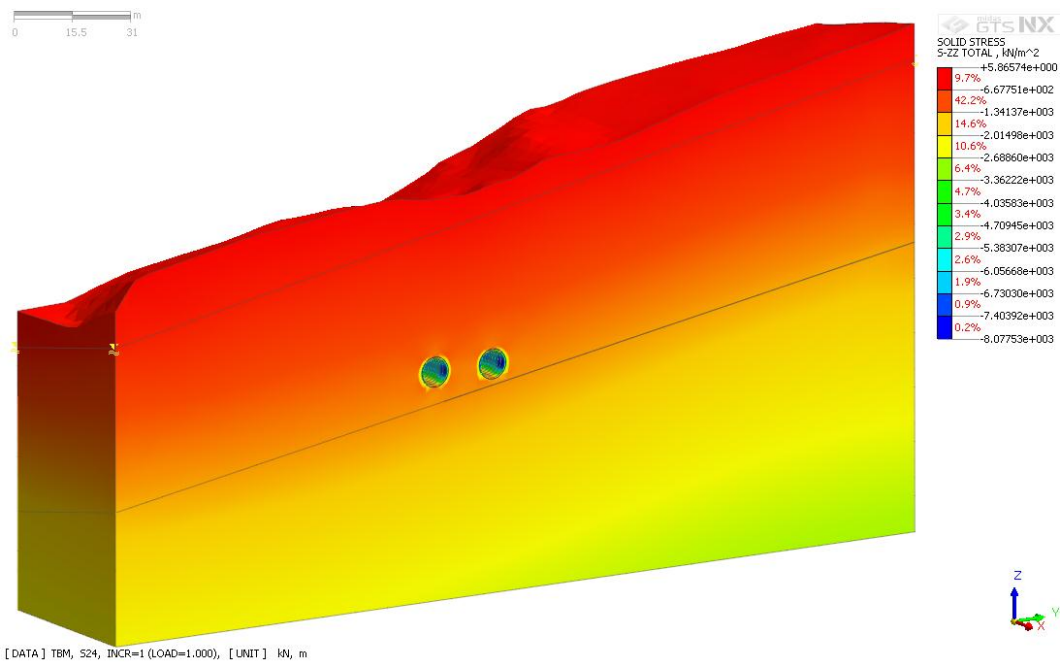


Figure 7.52. ZZ stress model for Km: 3+660 – 3+710.

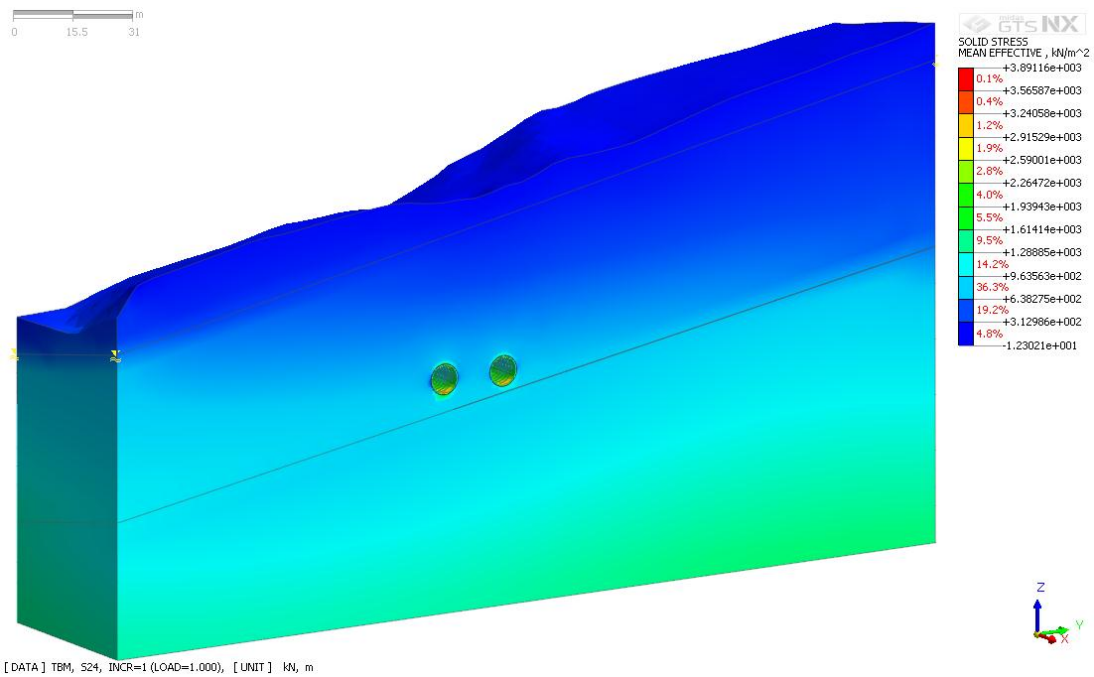


Figure 7.53. Mean effective stress model for Km: 3+660 – 3+710.

Material status output was displayed in Figure 7.54 for Km: 3+660 – 3+710. According to Figure 7.54, plastic material failure can be shown in red region. The other failures were shown in blue areas.

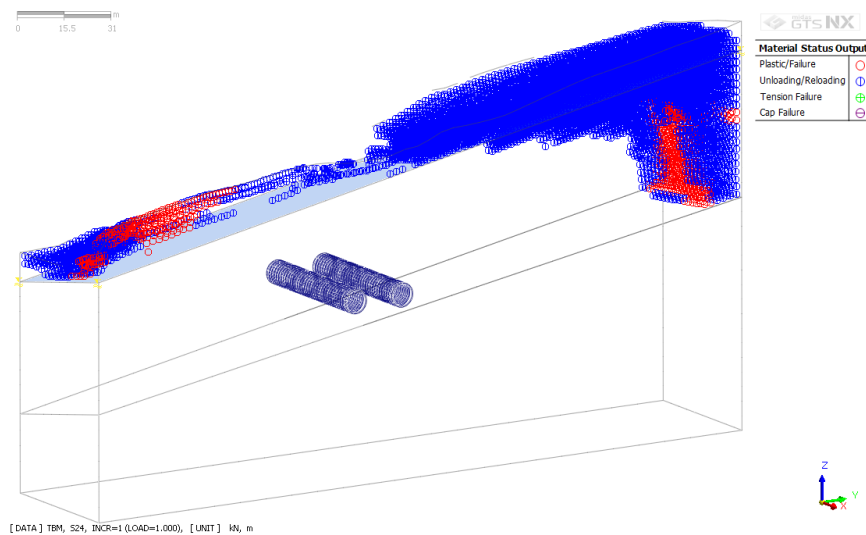


Figure 7.54. Material status model for Km: 3+660 – 3+710.

Table 7.10 is helpful to clarify maximum and minimum tunnel section displacement values for Km: 3+660 – 3+710. Dark blue colors represents deformations on tunnel for Figures 7.55 and 7.57. Furthermore, red colors show deformations around tunnel for both models. While maximum displacement values accumulate in red region for Figure 7.56, maximum displacements are seen in light blue colors for Figure 7.58.

Table 7.10. Maximum and minimum tunnel section displacement values for Km: 3+660 – 3+710.

<i>KM: 3+660 – 3+710</i>	<i>Displacement</i>	<i>Max (cm)</i>	<i>Min (cm)</i>
Figure 7.55	Total	23.8	0
Figure 7.56	X	0.90	0.27
Figure 7.57	Y	23.7	0.25
Figure 7.58	Z	6.59	1.13

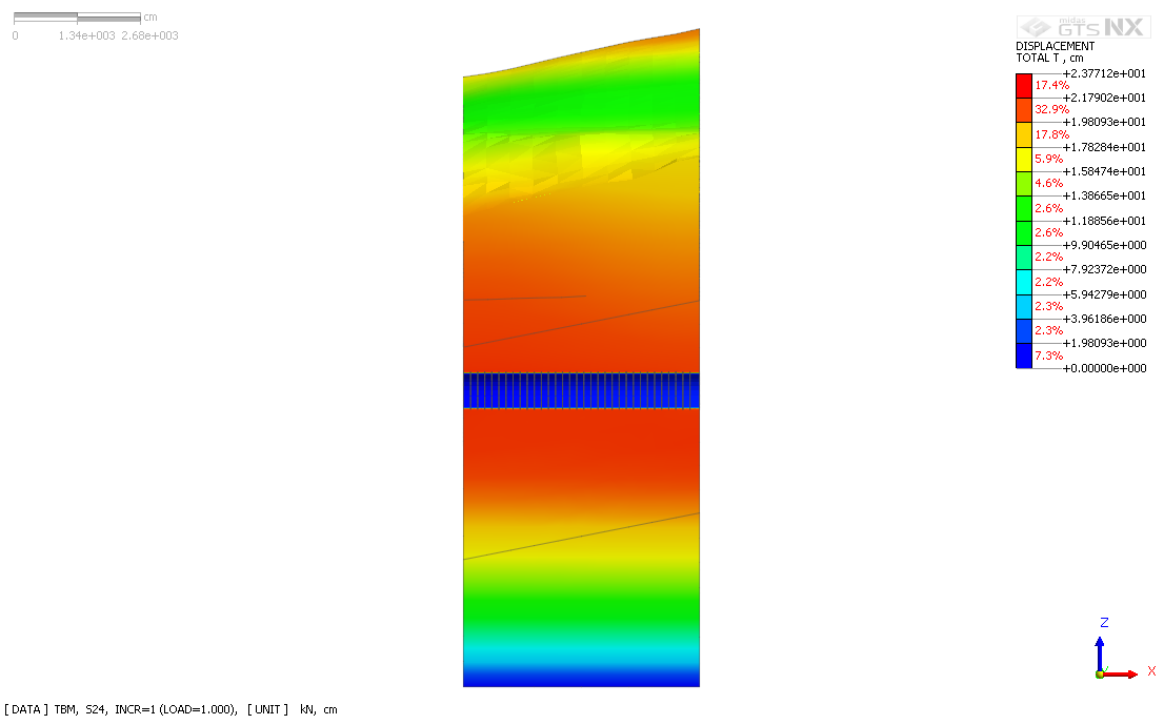


Figure 7.55. Tunnel section of total displacement model for Km: 3+660 – 3+710.

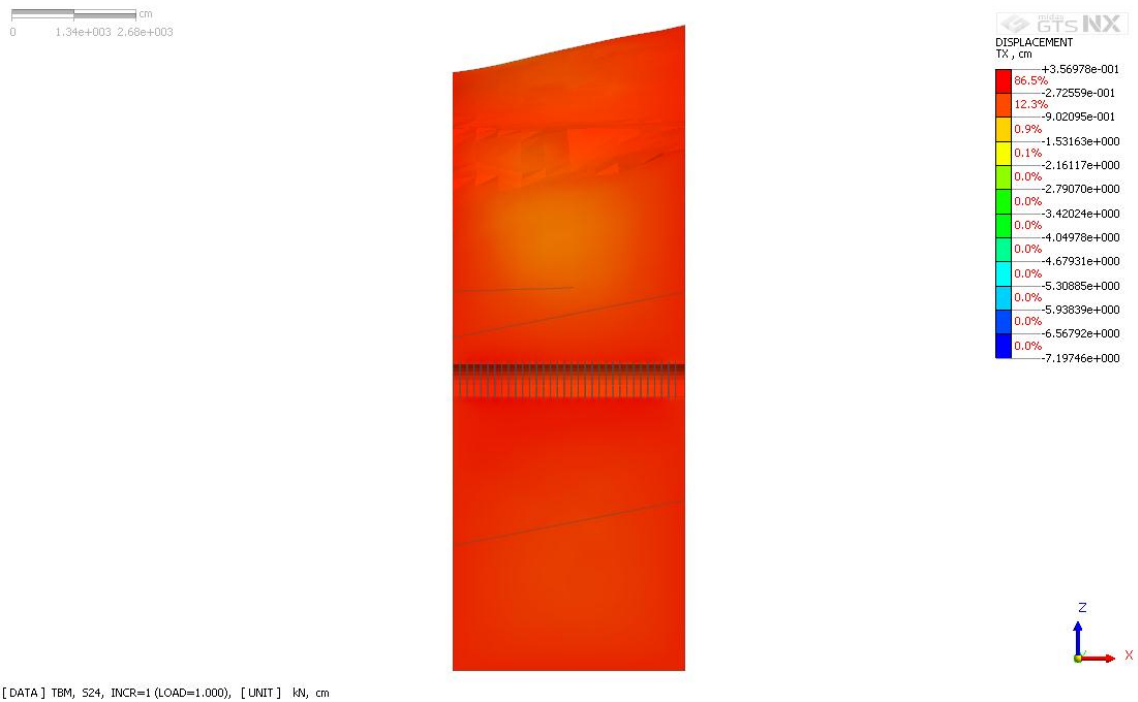


Figure 7.56. Tunnel section of X displacement model for Km: 3+660 – 3+710.

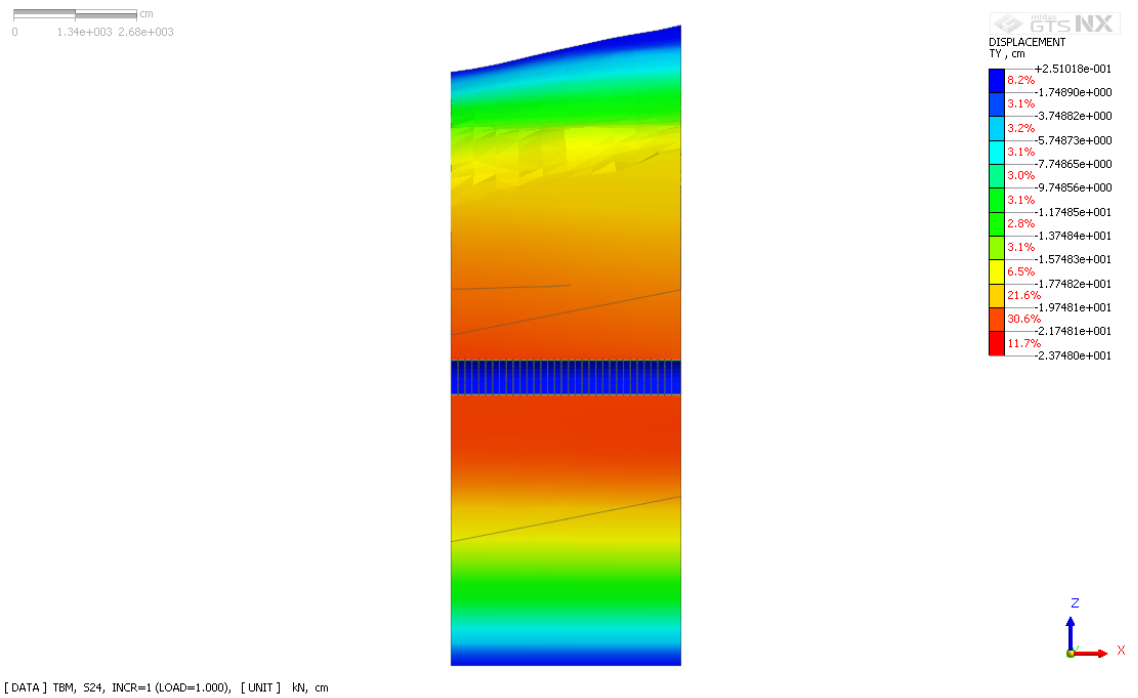


Figure 7.57. Tunnel section of Y displacement model for Km: 3+660 – 3+710.

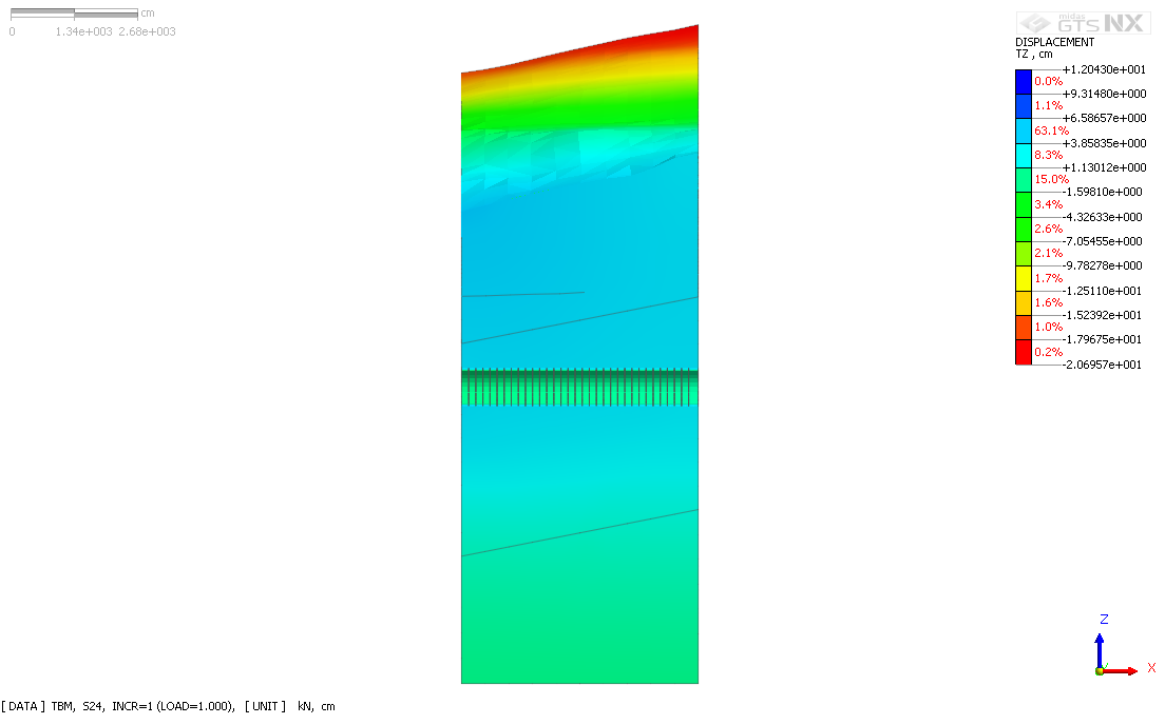


Figure 7.58. Tunnel section of Z displacement model for Km: 3+660 – 3+710.

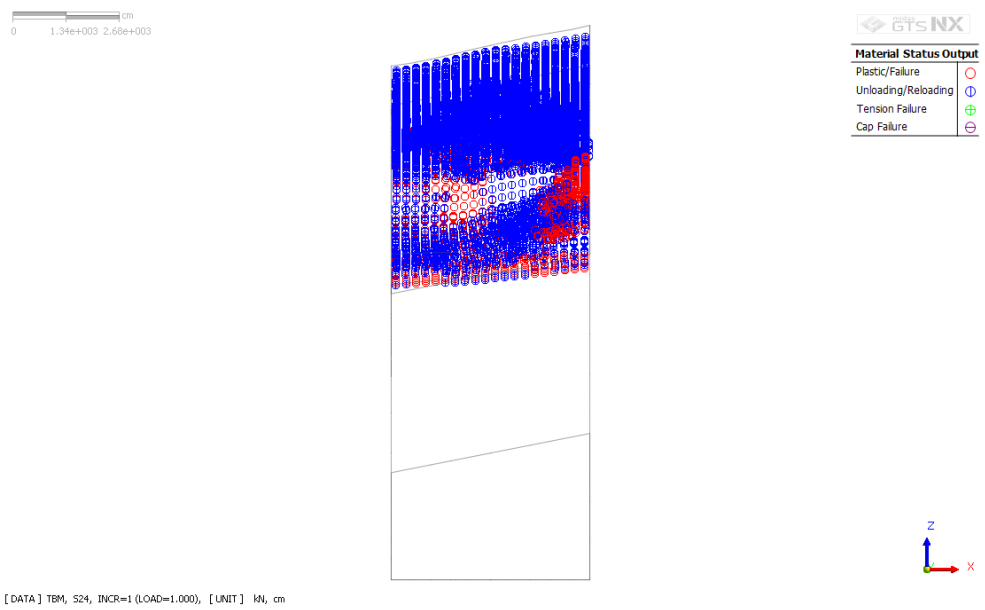


Figure 7.59. Tunnel section of material status model for Km: 3+660 – 3+710.

Finally, examination of displacements, stress and failures models for Km: 3+510 – 3+660 are presented in this part of thesis. Meshed model for Km: 3+510 – 3+660 was also given in Figure 7.60.

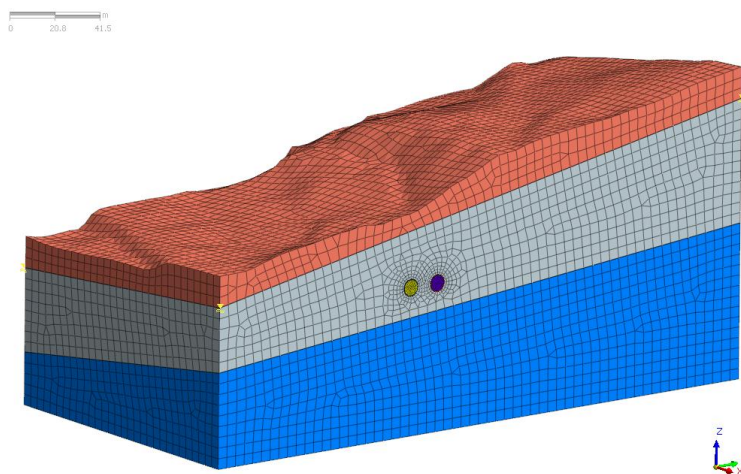
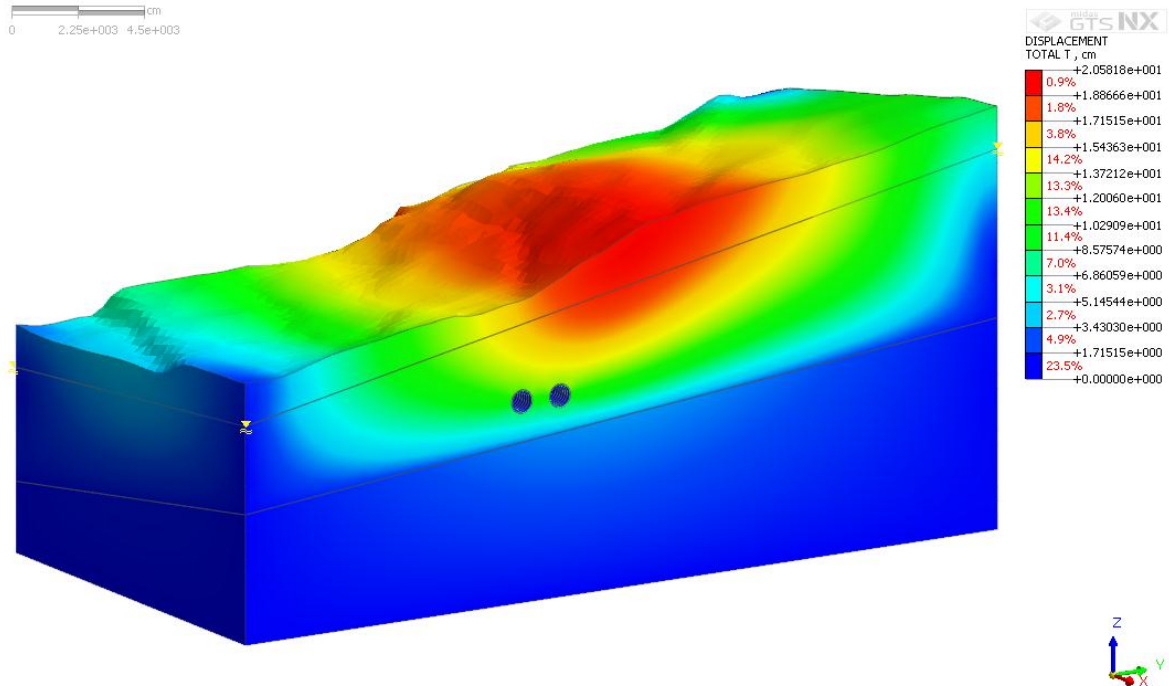


Figure 7.60. Meshed model for Km: 3+510 – 3+660.

Maximum and minimum displacement values can be provided from Table 7.11. Large deformations are examined in red regions for total (Figure 7.61), X (Figure 7.62), Y (Figure 7.63) displacement models. In contrast, maximum displacement locates in dark blue areas for Z displacement model (Figure 7.64).

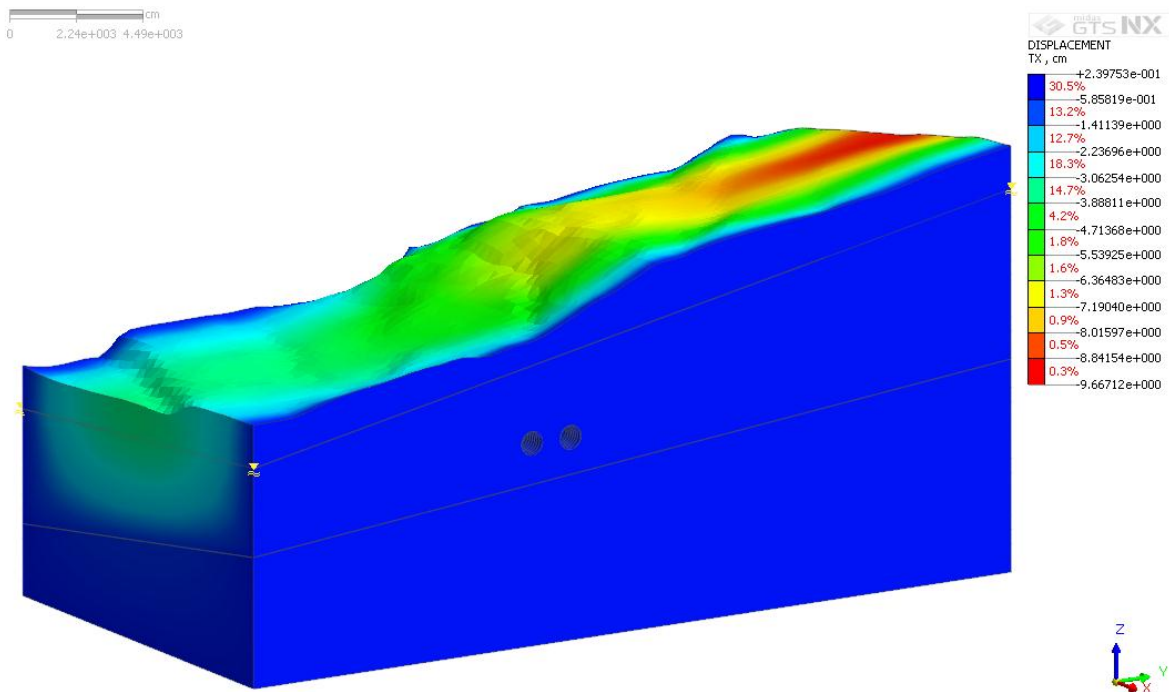
Table 7.11. Maximum and minimum displacement values for Km: 3+510 – 3+660.

<b><i>KM: 3+510 – 3+660</i></b>	<b><i>Displacement</i></b>	<b><i>Max (cm)</i></b>	<b><i>Min (cm)</i></b>
Figure 7.61	Total	20.6	0
Figure 7.62	X	9.7	0.24
Figure 7.63	Y	20.2	0.19
Figure 7.64	Z	8.3	0.19



[DATA] TBM, S57, INCR=1 (LOAD=1.000), [UNIT] kN, cm

Figure 7.61. Total displacement model for Km: 3+510 – 3+660.



[DATA] TBM, S57, INCR=1 (LOAD=1.000), [UNIT] kN, cm

Figure 7.62. Horizontal displacement model for Km: 3+510 – 3+660.



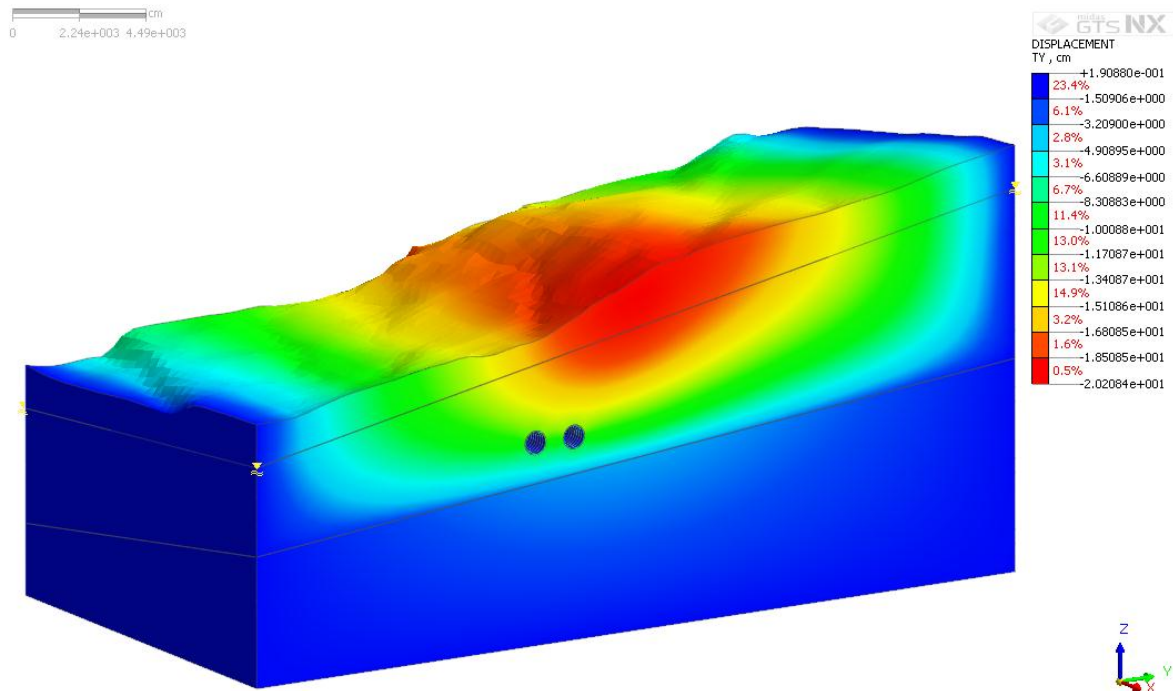


Figure 7.63. Displacement model along the Y-axis for Km: 3+510 – 3+660.

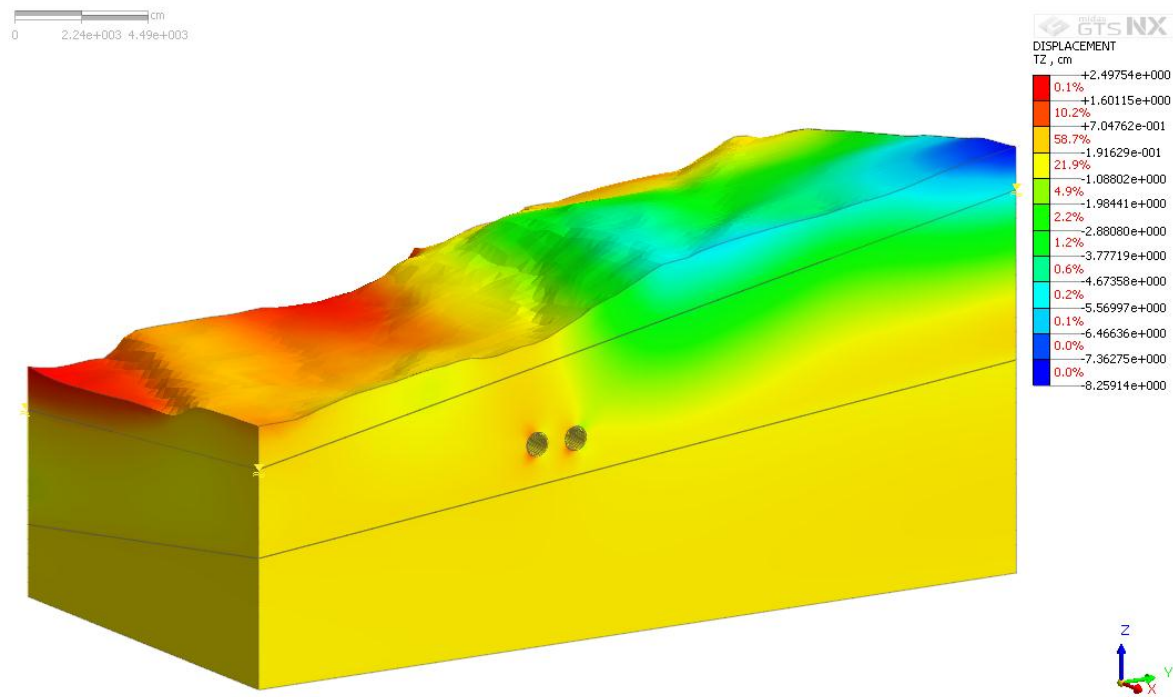


Figure 7.64. Vertical displacement model for Km: 3+510 – 3+660.

Maximum and minimum stress values for Km: 3+510 – 3+660 can be examined from Table 7.12. Figures 7.65, 7.66, 7.67, 7.68 and 7.69 clarify that maximum stresses are examined around tunnel.

Table 7.12. Maximum and minimum stress values for Km: 3+510 – 3+660.

<b><i>KM: 3+510 – 3+660</i></b>	<b><i>Stress</i></b>	<b><i>Max (kN/m<sup>2</sup>)</i></b>	<b><i>Min (kN/m<sup>2</sup>)</i></b>
Figure 7.65	Mean Total	3063	179
Figure 7.66	XX	5988	511
Figure 7.67	YY	8545	5.2
Figure 7.68	ZZ	8859	19.1
Figure 7.69	Mean Effective	2739	91.6

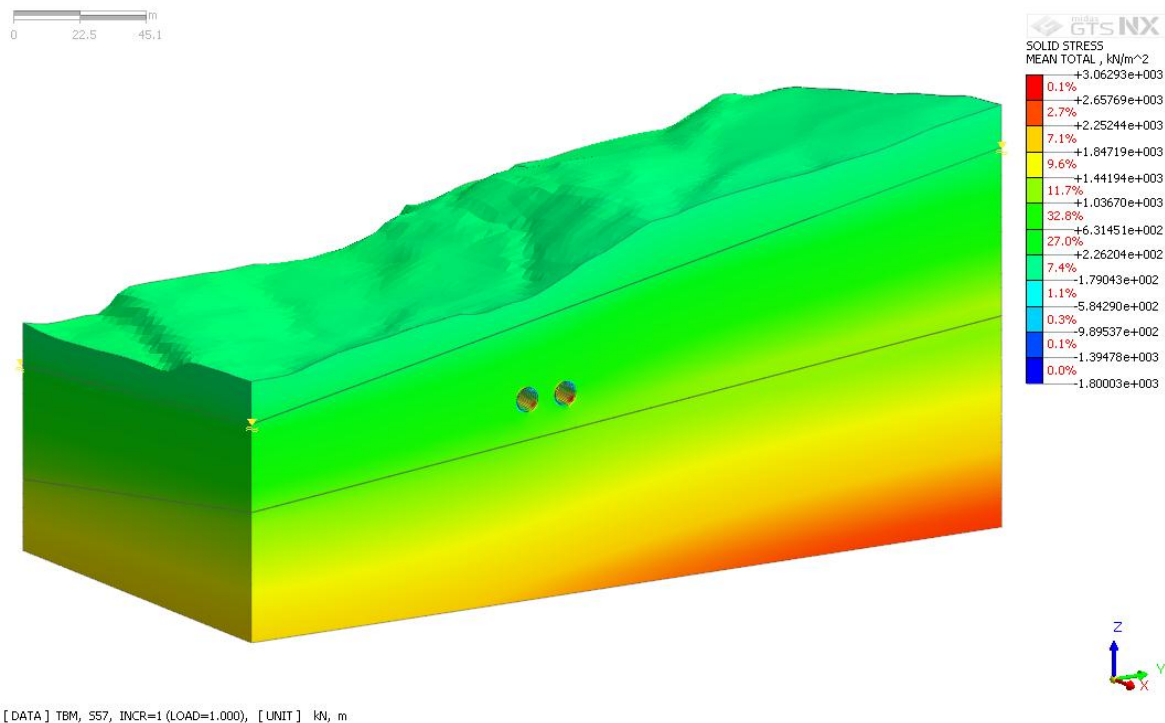
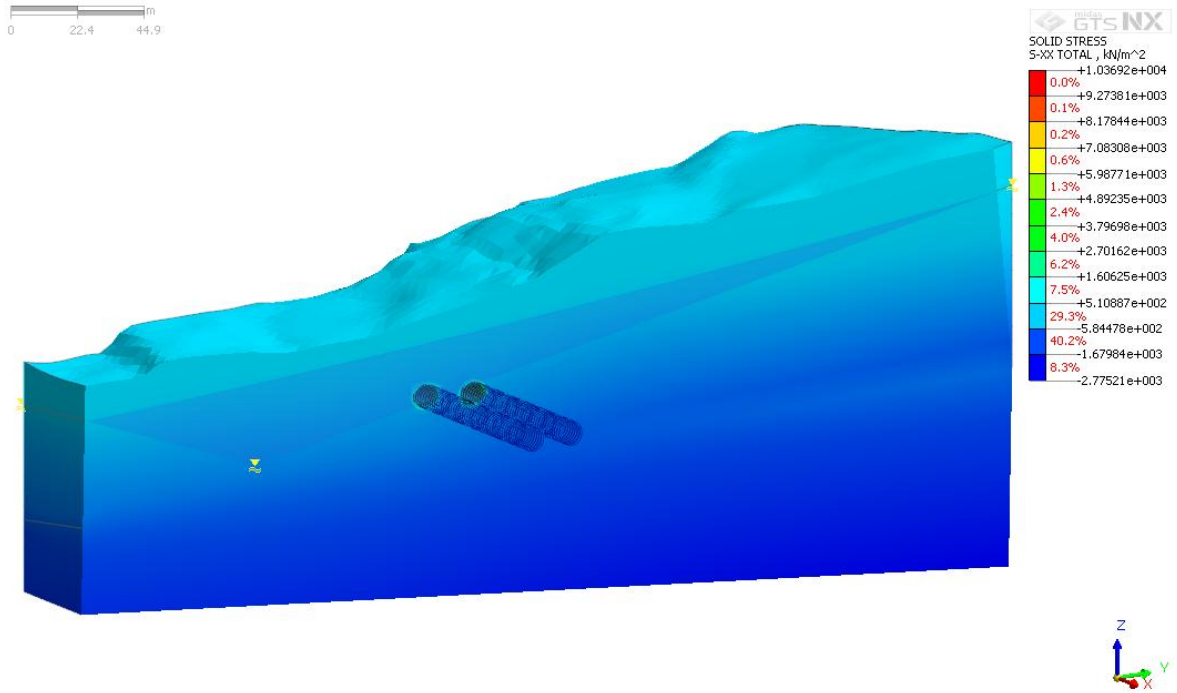
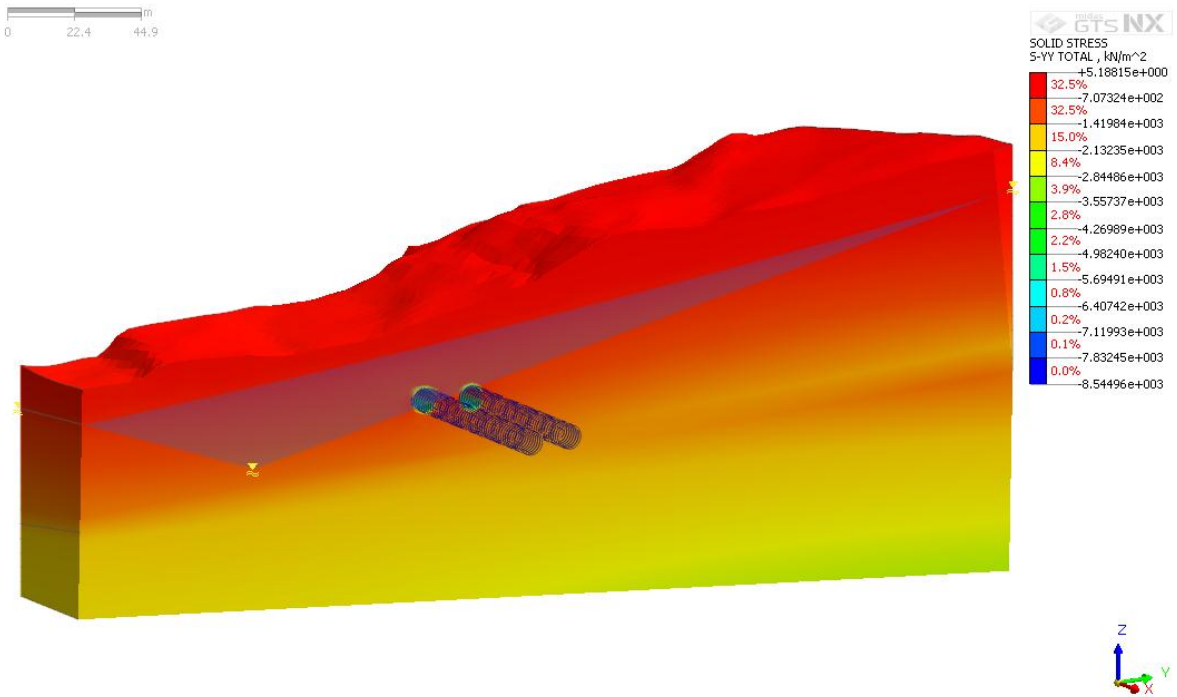


Figure 7.65. Total stress model for Km: 3+510 – 3+660.



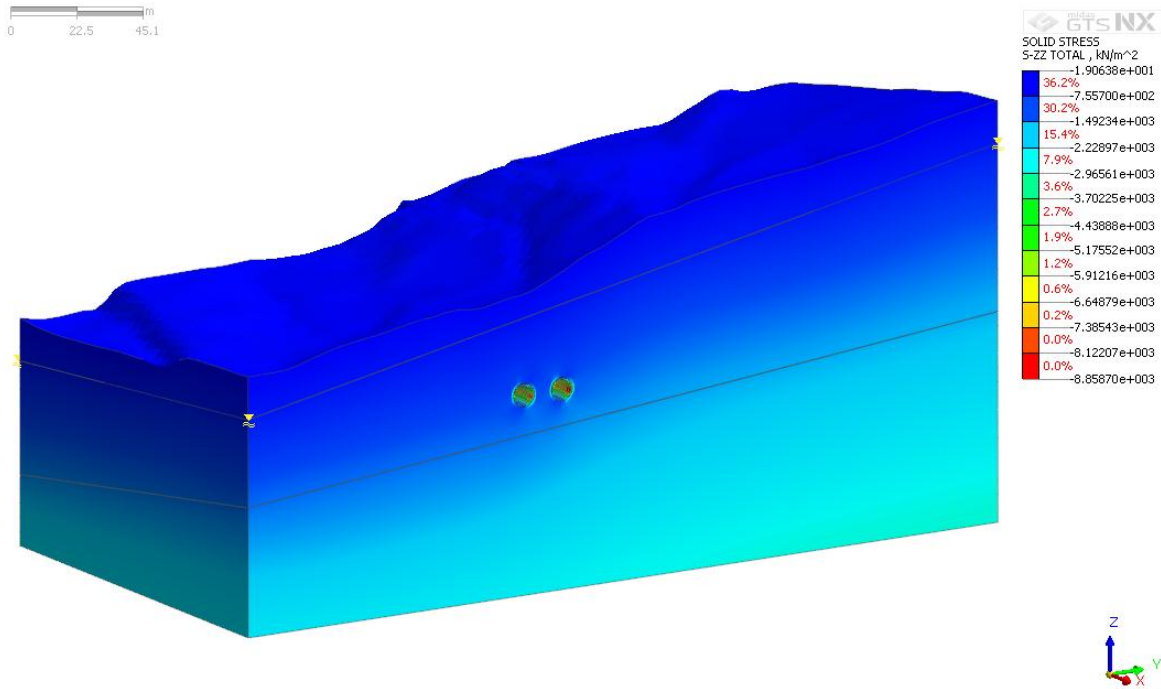
[DATA] TBM, S57, INCR=1 (LOAD=1.000), [UNIT] kN, m

Figure 7.66. XX stress model for Km: 3+510 – 3+660.



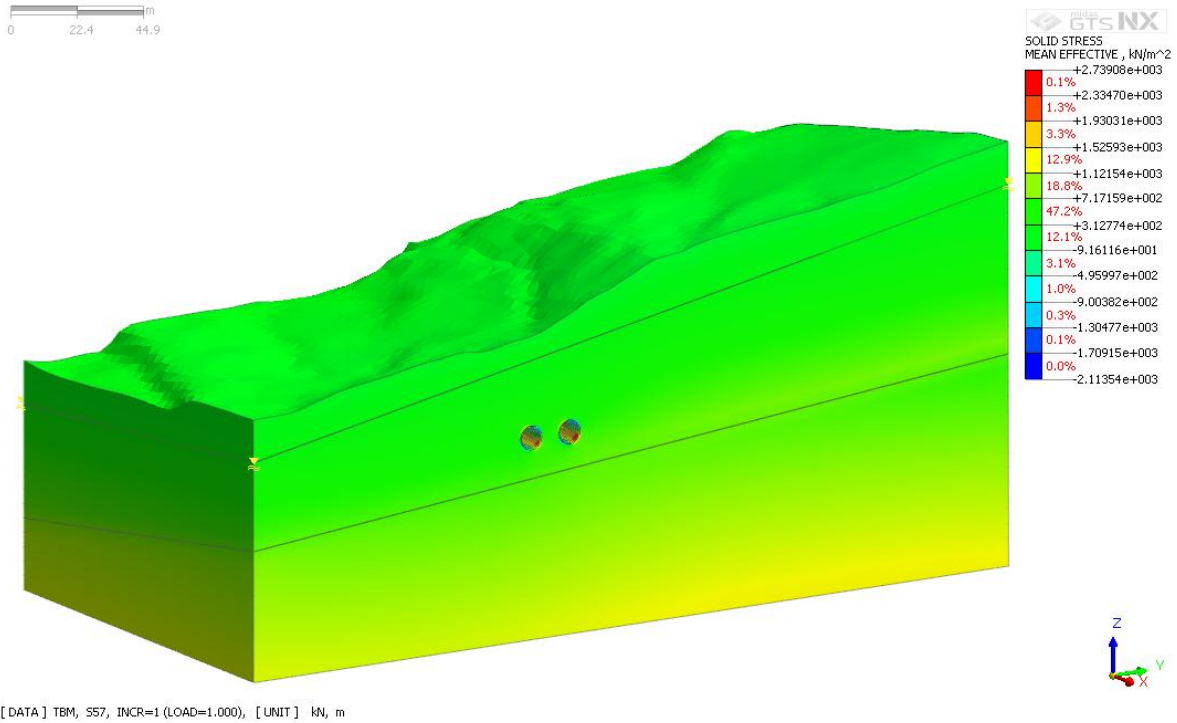
[DATA] TBM, S57, INCR=1 (LOAD=1.000), [UNIT] kN, m

Figure 7.67. YY stress model for Km: 3+510 – 3+660.



[DATA] TBM, S57, INCR=1 (LOAD=1.000), [UNIT] kN, m

Figure 7.68. ZZ stress model for Km: 3+510 – 3+660.



[DATA] TBM, S57, INCR=1 (LOAD=1.000), [UNIT] kN, m

Figure 7.69. Mean effective stress model for Km: 3+510 – 3+660.

Figure 7.70 manifests material status output for Km: 3+510 – 3+660. Failures on terrain and tunnel are demonstrated in Figure 7.70.

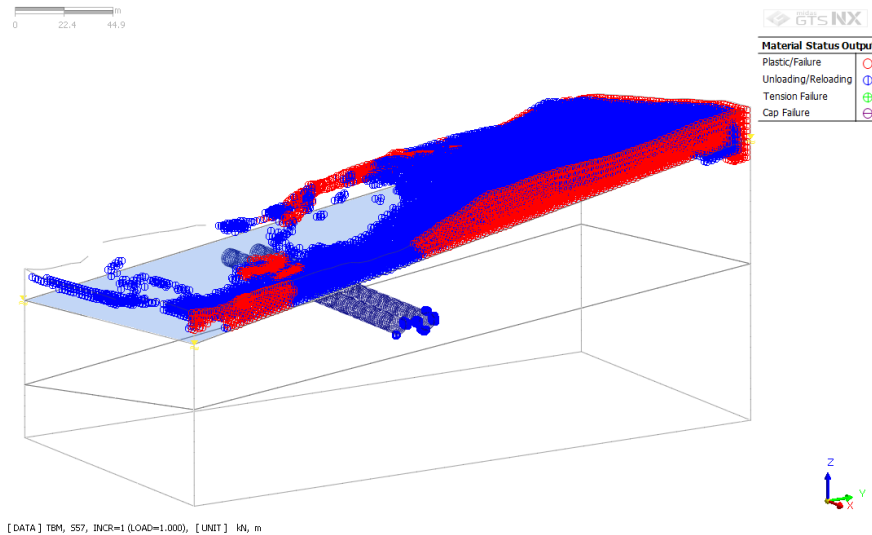


Figure 7.70. Material status model for Km: 3+510 – 3+660.

Table 7.13 explains maximum and minimum tunnel section displacement values for Km: 3+510 – 3+660. For Z tunnel section displacement model (Figure 7.74), light blue colors depict deformations on tunnel. In contrary to Z displacement model, dark blue color displacement range represents deformations for total (Figure 7.71), X (Figure 7.72), Y (Figure 7.73) tunnel section displacement models. In addition, maximum displacements values around tunnel can be examined from Table 7.13 for each model.

Table 7.13. Maximum and minimum tunnel section displacement values for Km: 3+510 – 3+660.

<b><i>KM: 3+510 – 3+660</i></b>	<b><i>Displacement</i></b>	<b><i>Max (cm)</i></b>	<b><i>Min (cm)</i></b>
Figure 7.71	Total	13.72	0
Figure 7.72	X	6.37	0.24
Figure 7.73	Y	8.31	0.19
Figure 7.74	Z	2.50	0.19

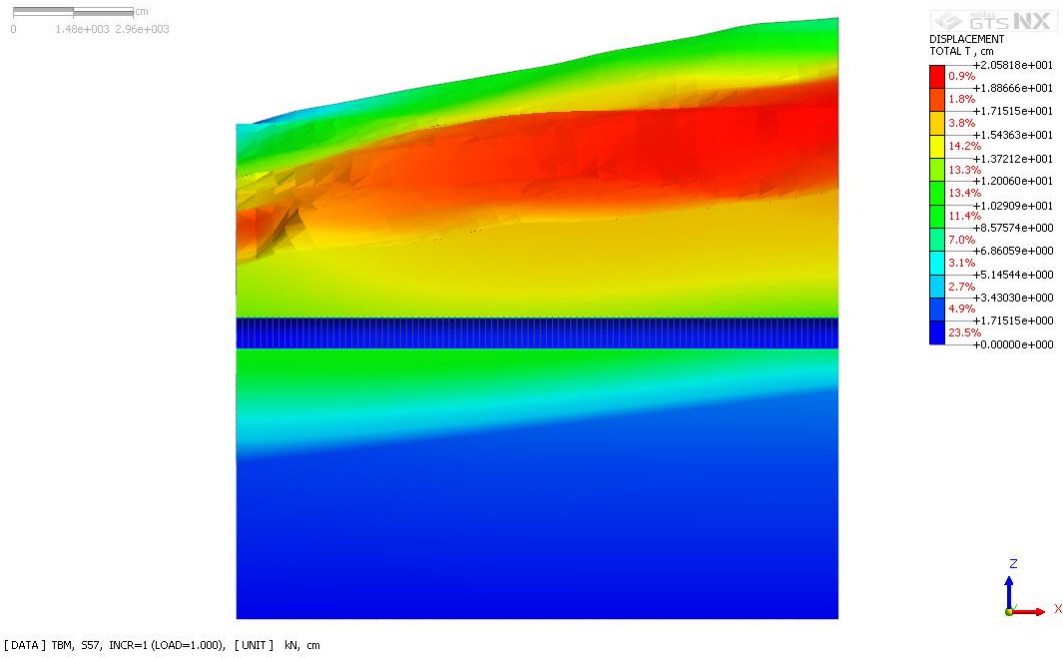


Figure 7.71. Tunnel section of total displacement model for Km: 3+510 – 3+660.

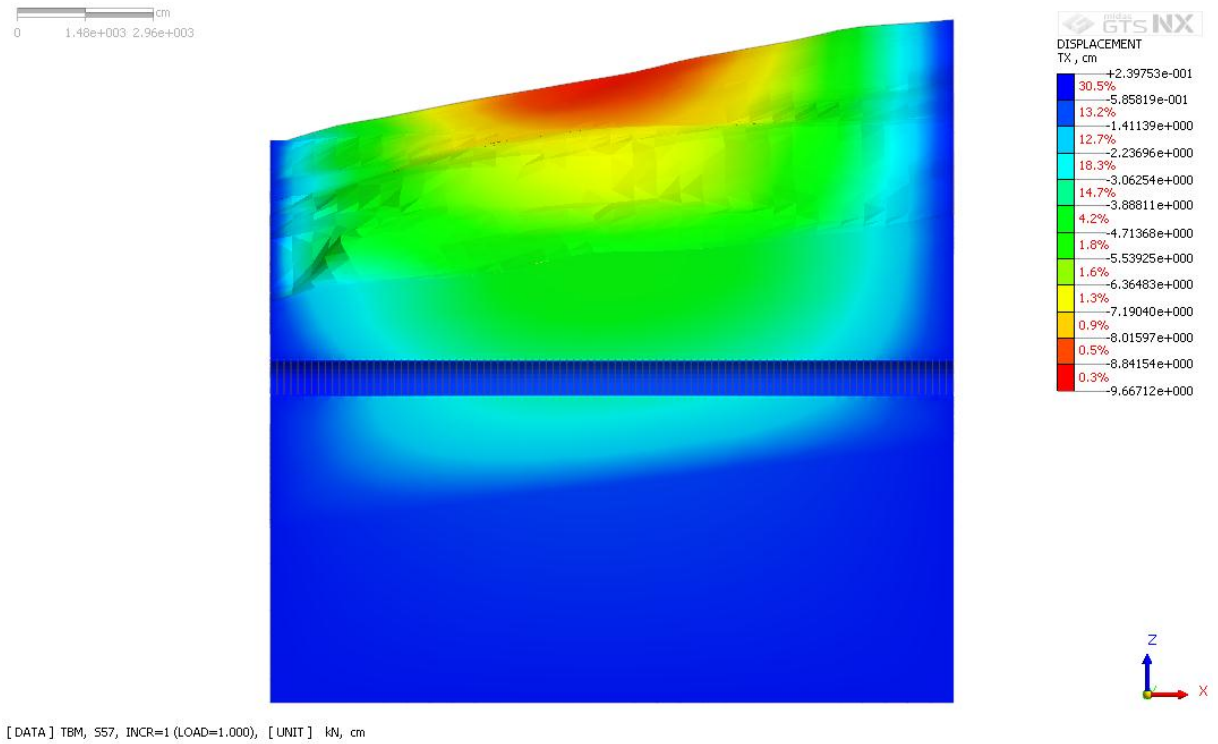


Figure 7.72. Tunnel section of X displacement model for Km: 3+510 – 3+660.

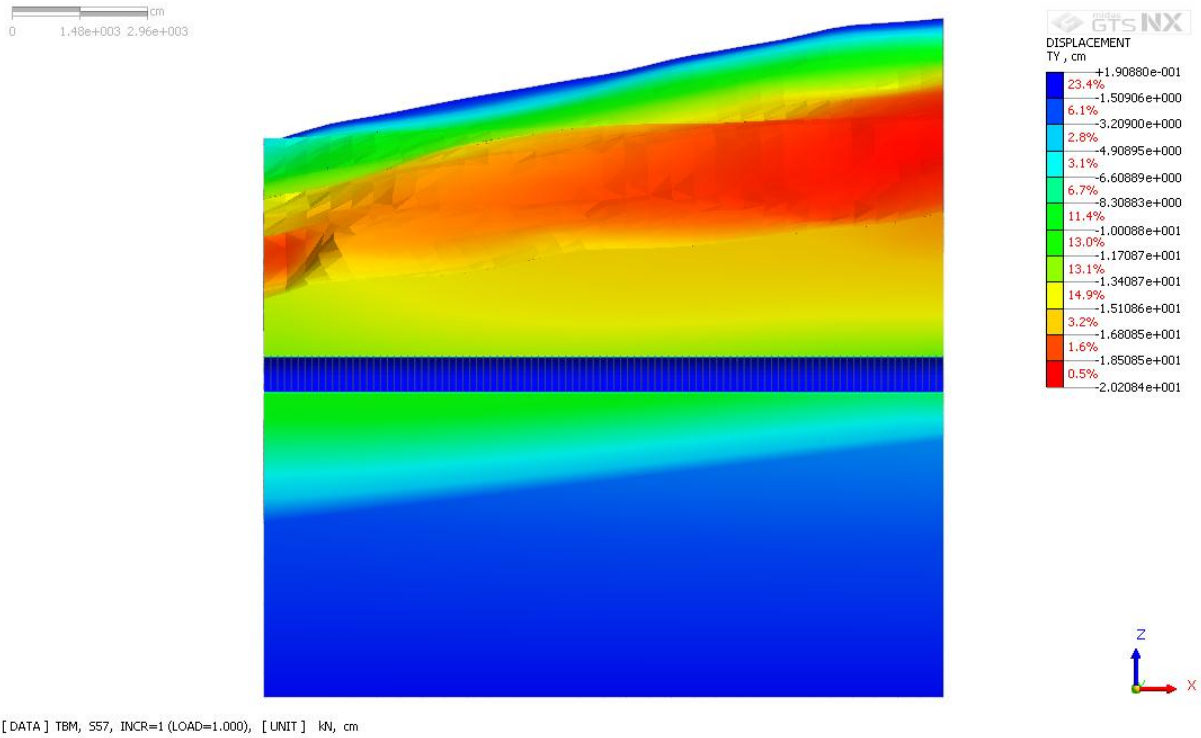


Figure 7.73. Tunnel section of Y displacement model for Km: 3+510 – 3+660.

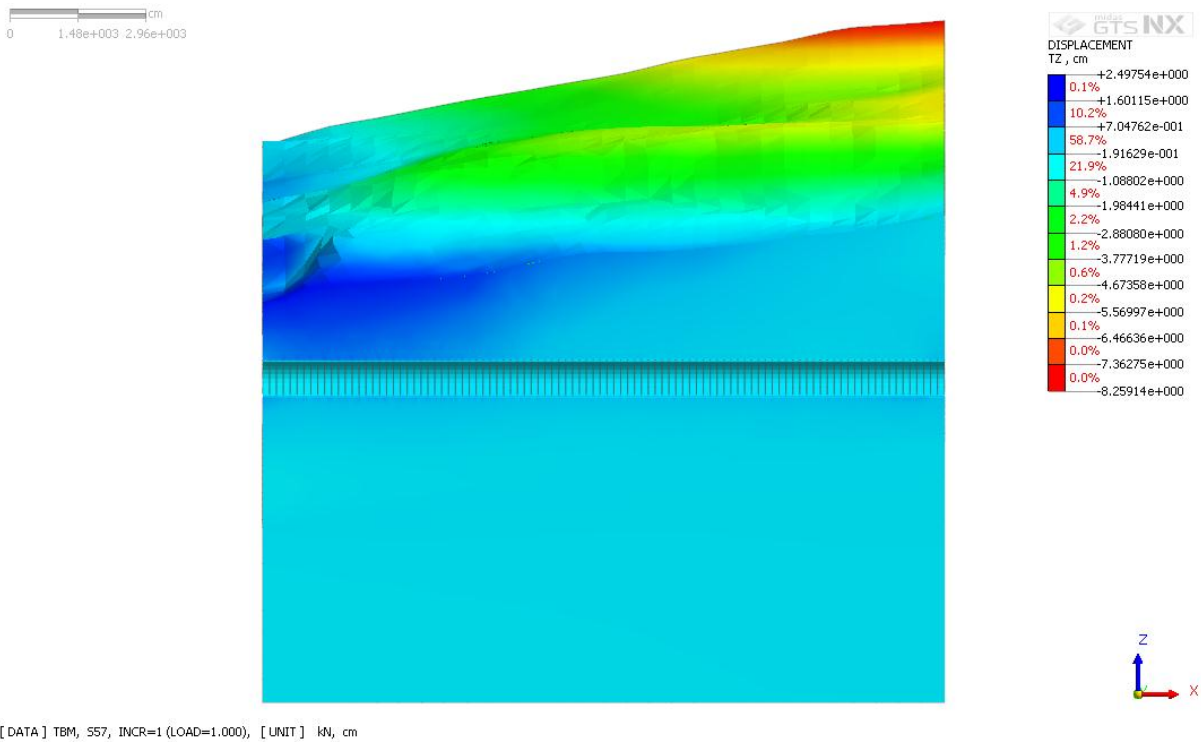


Figure 7.74. Tunnel section of Z displacement model for Km: 3+510 – 3+660.

Figure 7.75 presents the failures on tunnel section for Km: 3+510 – 3+660.

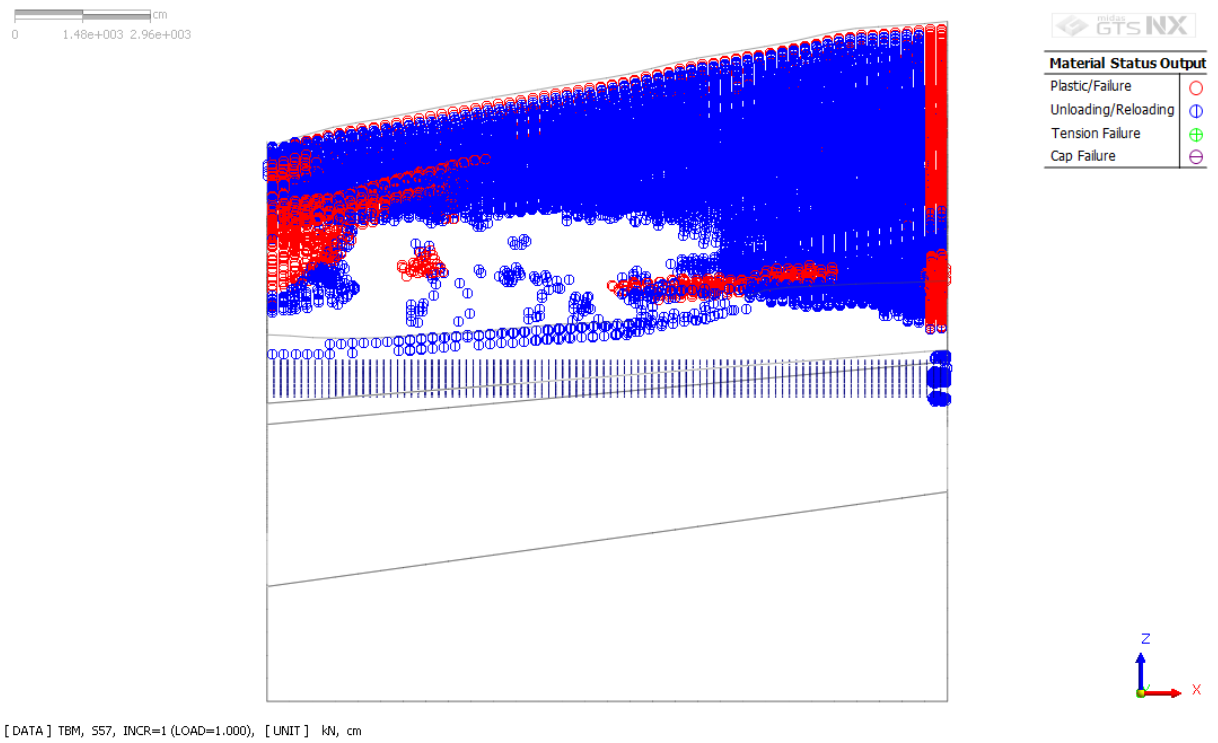


Figure 7.75. Tunnel section of material status model for Km: 3+510 – 3+660.



## 8. DISCUSSION

Analyses results and their interpretations are given in this chapter. Purpose of these analyses was to predict possible deformation on the rock mass and debris. Considering 3D finite element model, critical locations were probed to interpret rock response in terms of deformation. This study highlights that numerical analyses are necessary in order to remain on the safe side during the construction of tunnel. All parameters are properly established in order to account for rock responses during TBM tunneling process. Monitored analyses results clearly explain that TBM has negative effect on rock in accordance with displacement and failure models results. Failure models also give opportunity to comprehend aspects of TBM-landslide; hence, TBM - landslide relationship might require the cancellation of the TBM where debris may trigger landslide. Identification of the factors that generate landslide in the area is important to determine the appropriate tunnel construction method and to prevent potential hazard. According to static load results, TBM constructions displacement values were within the scope of thesis, which had impacts on Bahçe portal area. Thus, it can be suggested that TBM construction may be cancelled for TBM safety in the scope of the Bahçe-Nurdağ Project in order to minimize the possible hazards which might arise from landslide. Moreover, this study is vital research to improve the understanding of the landslide-tunnelling interactions for static load situation by performing rigorous 3D FEM analyses. To sum up, interpretations of displacement result models are required for secure tunnel construction. Results elaborately reveal that prepared deformation models were capable of accounting for complex relations in this study. The most crucial situation in the TBM tunnel-landslide relationship that might be necessary to determine the region of inactivation of the TBM-tunneling having possible landslide hazard which caused by debris in order to avoid TBM-squeezing problem.

## 9. CONCLUSION

Site investigation studies consisting of description of study area with respect to topography, climate and vegetation, geology, hydrogeology, landslide, seismicity and engineering geology have been completed within the scope of the study. Landslide-tunnel numerical model has been established in order to better understand TBM-landslide relationship. In this study, TBM tunnelling- landslide interaction analysis was carried out by considering the simplified FEM results with the MIDAS GTS NX software. This study demonstrated that numerical modelling is a productive tool for interpreting the problems in tunnel design. It is important to ensure whether the ground conditions of whole tunnel route are appropriate for TBM construction or not. Construction of Bahçe-Nurdağ Tunnel's Bahçe portal part can be described as difficult conditions with respect to engineering geology. Therefore, when deformation results are evaluated TBM tunnelling excavation method, TBM does not provide safety results. Although TBM is fast method, it may cause a problem of landslide in between 3+810 Km and 4+110 Km by interpreting of the deformation results. Result also probe that between the Km: 3+510 and 3+710 is more complex than interval of Km: 3+810 and 4+110 with respect to geology; thus, construction of the tunnel in these sections (3+510-4+110) can be cancelled with TBM. It is supposed that this study contributes to an enhanced knowledge of TBM-landslide relationships in complex region. Nevertheless, it can be recommended that impacts of  $K_0$  may be examined in the preparation of numerical modelling stage by appraising the fault zones along the tunnel route for future study.

In conclusion, 3D finite element models are developed to not only ensure the effects of TBM tunnelling on landslide but also decide tunnel construction method in order to complete tunnel safely by considering all factors. Therefore, TBM tunnelling excavation should be stopped for the last 600 meters in the project of Bahçe-Nurdağ Tunnel due to possible landslide problem detected from the FEM analysis results.

## 10. REFERENCES

- Abdallah, M., Marzouk, M., Planning of Tunneling Projects Using Computer Simulation and Fuzzy Decision Making, *Journal of Civil Engineering and Management*, 19 (2013) 4.
- Abdel-Meguid, M., Rowe, R.K., Lo, K.Y., 3D Effects of Surface Construction over Existing Subway Tunnels, *The International Journal of Geomechanics*, 2 (2002) 4.
- AFAD, Disaster Management and Natural Disaster Statistics in Turkey, [https://www.afad.gov.tr/upload/Node/35429/xfiles/Turkiye\\_de\\_Afetler.pdf](https://www.afad.gov.tr/upload/Node/35429/xfiles/Turkiye_de_Afetler.pdf), (Accessed: **28 December, 2018**).
- AFAD, AFAD 2018 Türkiye Deprem Haritası, <https://deprem.afad.gov.tr/deprem-tehlike-haritasi?lang=en>, (Accessed: **19 January, 2019**).
- Allahverdi, N., Nasri, V., Three dimensional numerical analysis for soft ground tunneling, *Seventh International Conference on Case Histories in Geotechnical Engineering*, 29 April- 4 May, Chicago, **2013**.
- Ambrassey, N.N., Temporary Seismic Quiescence, SE Turkey, *Geophysical Journal*, 96 (1989).
- Arpat, E., Saroğlu, F., Doğu Anadolu Fayı ile İlgili Bazı Gözlemler, *MTA Dergisi*, 78 (1972).
- Arpat, E., Saroğlu, F., Türkiye'deki Bazı Önemli Genç Tektonik Olaylar, *Türkiye Jeoloji Kurumu Bülteni*, 18 (1975) 1.
- Arshadnejad, S., Determination of “mi” in the Hoek–Brown Failure Criterion of Rock, *Mining Science*, 25 (2018).
- Barla, G., Pelizza, S., Tbm Tunnelling in difficult ground conditions, *ISRM International Symposium*, 19-24 November, Melbourne, Australia, **2000**.
- Barton, N., Rock mass characterisation and seismic measurements to assist in the design and execution of TBM projects, *Taiwan Rock Engineering Symposium*, 12-13 December, **1996**, p.1-16.
- Berilgen, M., Doran, B., Yıldırım, S., Bulut, A., İkiz metro tünelleri üzerinde yer alan bir yapıda zemin yapı etkileşimi analizi, *Zemin Mekaniği ve Temel Mühendisliği 1. Özel Konulu Sempozyum*, 8 Kasım, İstanbul, Türkiye, **2007**.
- Bieniawski, Z.T., *Engineering Rock Mass Classifications*, Wiley, Newyork, Chapter 4, **1989**.
- Blumenetal, M., Seydişehir-Beyşehir Hınerlandındaki Toros Dağları'nın Jeolojisi, *Maden Teknik ve Arama Genel Müdürlüğü Yayını*, Ankara, **1947**.

- Brabant, J.D., Duhme, R., Hard rock TBM tunneling – Technical developments and recent experience, Advances in Structural Engineering and Mechanics World Congress, 28 August- 1 September, Seoul, Korea, **2017**.
- Bulut, F., Bohnhoff, M., Eken, T., Janssen, C., Kilic, T., Dresen, G., The East Anatolian Fault Zone: Seismotectonic Setting and Spatiotemporal Characteristics of Seismicity Based on Precise Earthquake Locations, Journal of Geophysical Research, 117 (**2012**).
- Cho, W.S., Song, K.I., Kim, K.Y., Mechanical behavior of ground due to EPB shield TBM tunnel excavation passing through fractured zone. Geotechnical Aspects of Underground Construction in Soft Ground, Yoo, C., S-W., Park, Kim, B., H. Ban (Eds), Korean Geotechnical Society, Seoul, Korea, 577-580, **2014**.
- Cruden, D.M., A Simple Definition of a Landslide, Bulletin of the International Association Engineering Geology, 43 (**1991**).
- Dean, W., T., Monod, O., The Lower Palaeozoic Stratigraphy and Faunas of the Taurus Mountains near Beyşehir, Turkey: 1. Straigraphy (London), Ibid, 19 (**1970**).
- Delmonaco, G., Leoni, G., Margottini, C., Puglisi, C., Spizzichino, D., Large Scale Debris-Flow Hazard Assessment: a Geotechnical Approach and GIS modelling, Natural Hazards and Earth System Sciences, 3 (**2003**).
- Doğruoğlu, M.T., Tbm Metodu ile Açılan İkiz Tünellerde Meydana Gelebilecek Deformasyonların Sonlu Elemanlar Metodu ve Numerik Hesaplarla Tahmini, Yüksek Lisans Tezi, Yıldız Teknik Üniversitesi Fen Bilimleri Enstitüsü İnşaat Anabilim Dalı Geoteknik Programı, İstanbul, **2009**.
- Doruk, P., Analysis of Laboratory Strength Data Using the Original and Modified Hoek Brown Failure Criteria, Master of Science Thesis, Univerty of Toronto, **1991**.
- Dragojević, S.M., Analysis of Ground Settlement Caused by Tunnel Construction, GRAĐEVINAR, 64 (**2012**) 7.
- Duman, T.Y., Çan, T., Emre, Ö., 1/1.500.000 Türkiye Heyelan Envanteri Haritası, Maden Tetkik ve Arama Genel Müdürlüğü Özel Yayınlar Serisi, No.27, Ankara, Türkiye, **2011**.
- Fugro Sial Yerbilimleri Müşavirlik ve Mühendislik Ltd, Bahçe Nurdağ Geçiş Tüneli (KM: 03+653.12 – KM: 13+450): Jeolojik – Jeoteknik Proje Raporu, **2014**.
- General Directorate of Turkish State Railways, Bahçe Nurdağ Tüneli (KM: 3+653 - 13+450) KM: Jeolojik – Jeoteknik Proje Raporu, **2014**.
- General Directorate of Turkish State Railways, Bahçe Nurdağ Tüneli (KM: 3+510 - 13+452) KM: 3+510 ile KM: 4+110 kesimi NATM Projesi Jeolojik Profili, **2018**.

- Girmscheid, G., Schexnayder, C., Drill and Blast Tunneling Practices, Practice Periodical on Structural Design and Construction, 7 (2002) 3.
- Gnilsen R., Underground Structures Design and Instrumentation, Sinha R.S (Ed.), Elsevier, Amsterdam, 84-128, 1989.
- Gökçeoğlu, C., TCDD Bakım Dairesi Başkanlığı Bahçe – Nurdağ (Fevzipaşa) Varyantı Projesi Hakkında Ek Rapor, Ankara, 2018.
- Gutenberg, B., Richter, C.F., Seismicity of the Earth, 2. Edition, Princeton Press, 1954.
- Haghi, A.H., Asef, M.R., Taheri, A., Mohkam, M., 2013, Evaluation of the Heading Confinement Pressure Effect on Ground Settlement for EPBTBM Using Full 3D Numerical Analysis, Int J Min & Geo-Eng (IJMGE), 47 (2013) 1.
- Heama, N., Jongpradist, P., Lueprasert, P., Suwansawat, S., Investigation on Tunnel Responses due to Adjacent Loaded Pile by 3d Finite Element Analysis, International Journal of GEOMATE, 12 (2017) 31.
- Herece, H., Akay, E., Karlıova-Çelikhan Arasında Doğu Anadolu Fayı, Bildiriler: Jeoloji, Jeofizik Mühendisleri Odası, Türkiye Petrol Jeologları Derneği and Petrol Mühendisleri Odası (Eds.), 9th Petroleum Congress and Exhibition of Turkey, Ankara, 17-21 February 1992, Ankara, 1992, p.361-372.
- Herrenknecht Tunnelling System, EPB Shield,  
<https://www.herrenknecht.com/en/products/productdetail/epb-shield/> (Accessed: 21 January 2019).
- Hoek, E., Brown, E.T., Practical Estimates of Rock Mass Strength, International Journal of Rock Mechanics and Mining Sciences, 34 (1997) 8.
- Hoek, E., Rock Mass Properties for Underground Mines, Engineering Fundamentals and International Case Studies, 2001.
- Hoek, E., Carranza-Torres CT, Corkum B., Hoek-Brown failure criterion - 2002 edition, Proceedings of the fifth North American Rock Mechanics Symposium, Toronto, Canada, 2002, p. 267–73.
- Hoek, E., Diederichs, M.S., Empirical Estimation of Rock Mass Modulus, International Journal of Rock Mechanics & Mining Sciences, 43(2006).
- Hu, M.J., Wang, R., Chen, Z.X., Wang, Z.B., Initiation Process Simulation of Debris Deposit Based on Particle Flow Code, Rock and Soil Mechanics, 31 (2010) 1.
- Iverson, R., M., The Physics of Debris Flows, Reviews of Geophysics, Vol.35, Willey, 245-296, 1997.

- İmamoglu, M.S., Çetin, E., Güneydogu Anadolu Bölgesi ve Yakın Yöresinin Depremselliği, D.Ü. Ziya Gökalp Eğitim Fakültesi Dergisi 9, **2007**.
- Jing, L., Hudson, J.A., Numerical Methods in Rock Mechanics, International Journal of Rock Mechanics & Mining Sciences, 39 (**2002**).
- Kanungo, D.P., Arora, M.K., Sarkar, S. and Gupta, R.P. , 'A Comparative Study of Conventional, ANN black box, Fuzzy and Combined Neural and Fuzzy Weighting Procedures for Landslide Susceptibility Zonation in Darjeeling Himalayas', Engineering Geology, 85 (**2006**) 3.
- Kanungo, D.P., Pain, A., Sarkar, S., Sharma, S., Jain, S.K., Ahmad, Z., Field Investigation and Finite Element Modelling of Progressive Debris Slide in the Indian Himalayas, WIT Transactions on Engineering Science, 73 (**2012**).
- Lahner, L., Geologische Untersuchungen an der Ostflanke des mittleren Amanos, Geotekt Forschungen, 42 (**1972**).
- Lee, S.C., Ismail, M.A.M., Ng, S.M., The Evaluation of Tunnel Behaviours under High Rock Stress Using Numerical Analysis Method, EJGE, 17 (**2012**).
- Liu, C., Zhang, L., Bai, B., Chen, J., Wang, J., Nonlinear Analysis of Stress and Strain for a Clay Core Rock-Fill Dam with FEM, Procedia Engineering, 31 (**2012**).
- Marinos, P., Hoek, E., Estimating the Geotechnical Properties of Heterogeneous Rock Masses such as Flysch, Bulletin of the Engineering Geology & the Environment (IAEG), 60 (**2001**).
- McKenzie, D., Active Tectonics of the Mediterranean Region. Geophysical Journal of the Royal Astronomical Society, 30 (**1972**).
- Meng, Z., Xian, X., Analysis of the Mechanical Property of Mudstone/Shale in Paralic Coal Measures and its Influence Factors, Journal of Coal Science & Engineering, 19 (**2013**) 1.
- MIDAS GTS NX, Tunnels, <http://www.midasgtsnx.com/solutions/tunnels.asp>, (Accessed: **11 February, 2019**)
- Nalbant, S.S., McCloskey, J., Steacy, S., Barka, A. A., Stress Accumulation and Increased Seismic Risk in Eastern Turkey, Earth and Planetary Science Letters, 195 (**2002**).
- Ninic, J., Freitag, S., Meschke, G., A Hybrid Finite Element and Surrogate Modelling Approach for Simulation and Monitoring Supported TBM Steering, Tunnelling and Underground Space Technology, **2016**.
- Ochmanski, M., Bzowka, J., Numerical Model of SCL Tunnels in Complex Subsoil Conditions. Architecture Civil Engineering Environment, 3 (**2012**).

- Ota, K., Kuruoka, S., Takeshi T., Numerical Analysis to Examine the Effect of Landslides on Tunnel, International Conference on Case Histories in Geotechnical Engineering. Seventh International Conference on Case Histories in Geotechnical Engineering, 29 April- 4 May, Chicago, **2013**.
- Palmstrom, A., Measurements of and Correlations between Block Size and Rock Quality Designation (RQD), Tunnels and Underground Space Technology, 20 (**2005**).
- Paltrinieri, E., Analysis of TBM Tunneling Performance in Faulted and Highly Fractured Rocks, Doctoral Thesis, École Polytechnique Fédérale De Lausanne, **2015**.
- Phadke, V., Titirmare, N., Construction of Tunnels, by New Austrian Tunnelling Method (NATM) and by Tunnel Boring Machine (TBM), International Journal of Civil Engineering (IJCE), 6 (**2017**) 6.
- Potts D.M., Zdravkovic L., Finite Element Analysis in Geotechnical Engineering-Theory, Thomas Telford, London, **2001**.
- Progeo Proje Mühendislik Müşavirlik San. ve Tic.Ltd.Şti, Bahçe Nurdağ Tüneli (KM: 3+510 - 13+452) KM: 3+510 ile KM: 4+110 Kesimi NATM Projesi Jeolojik Profili, **2018**.
- Republic of Turkey Ministry of Environment and Urbanization-Directory of Osmaniye Province, Osmaniye İli 2016 Yılı Çevre Durum Raporu, **2017**.
- Rocscience, RocLabManual, <https://www.rocscience.com/downloads/roclab/RocLabManual.pdf>, (Accessed: **23 February 2019**).
- Robbins, Tunnel Boring Machines, <https://www.therobbinscompany.com/products/tunnel-boring-machines/> (Accessed: **16 January 2019**).
- Salam, S.A., Ata, A., Shaalan, O., Hammad, N., Modeling of Tbm Tunnel Construction for the Greater Cairo Metro Line 3, International Journal of Engineering and Innovative Technology (IJEIT), 4 (**2015**) 10.
- Salimi, A.R., Esmaeili, M., Salehi, B., Analysis of a tbm tunneling effect on surface subsidence: A case study from Tehran, Iran, World Academy of Science, Engineering and Technology International Journal of Environmental, Chemical, Ecological, Geological and Geophysical Engineering, 7 (**2013**) 6.
- Şaroğlu, F., Emre, Ö., Boray, A. Türkiye'nin Diri Fayları ve Depremsellikleri, MTA Derleme No: 8174, 394, **1987**.
- Şaroğlu, F., Emre, Ö., Kusçu, I., Türkiye Diri Fay Haritası, MTA Yayını, Ankara, **1992a**.
- Şaroğlu, F., Emre, Ö., Kusçu, I., East Anatolian Fault Zone of Turkey, Annal. Tect., 6 (**1992b**).
- Schmidt, G.C., Proposed Rock Unit Nomenclature Petroleum District V, SE-Turkey (Autochthonous terrain) (Mobil Exploration Mediterranean Inc.): Petrol İşleri Genel Müdürlüğü Teknik Arşiv, No.3955/1, Ankara, **1964**.

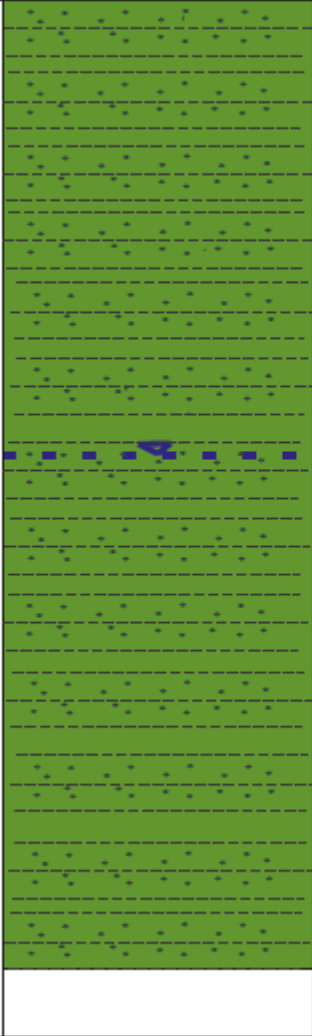
- Schubert, W., Steindorfer, A., Advanced Monitoring Data Evaluation For Tunneling Poor Rock, 8th International Congress on Rock Mechanics, 25-30 September, Tokyo, Japan, Balkema, A.A.(ed.), 1420-1424, **1995**.
- Seymen, İ., Aydın, A. Bingöl Deprem Fayı ve Bunun Kuzey Anadolu Fayı ile ilişkisi, MTA Dergisi, 79 (**1972**).
- Sönmez, H., Ulusay, R., A Discussion on the Hoek-Brown Failure Criterion and Suggested Modifications to the Criterion Verified by Slope Stability Case Studies, *Yerbilimleri (Earthsciences)*, 26 (**2002**).
- Spencer, M., Stolfa, A., Bentz, E., Cross, S., Blueckert, C., Forder, J., Wannick, H., Guggisberg, B., Gallagher, R., Tunnel boring machines, IMIA Working Group Paper, IMIA Conference, 28-30 September, Istanbul, Turkey, **2009**.
- SRTM, SRTM DEM Digital Elevation Database, <http://srtm.csi.cgiar.org/>, (Accessed: **17 December 2018**).
- Sun, W., Shi, M., Zhang, C., Zhao, J., Song, X., Dynamic Load prediction of Tunnel Boring Machine (TBM) Based on Heterogeneous in Situ Data, *Automation in Construction*, 92 (**2018**).
- Thuro, K., Eberhardt, E., Gasparini, M., Adversetunnelling conditions arising from slope, instabilities-A case history, In *UEF International Conference on Landslides – Causes, Impacts and Countermeasures*, 17-21 June, Davos, Switzerland, **2001**.
- Turkish State Meteorological Service, Köppen İklim Sınıflandırmasına Göre Türkiye İklimi, Araştırma Dairesi Başkanlığı Klimatoloji Şube Müdürlüğü, **2016**.
- Turkish State Meteorological Service, <https://www.mgm.gov.tr/veridegerlendirme/il-ve-ilceler-istatistik.aspx?m=OSMANIYE>, (Accessed: **15 November 2018**).
- Turkish State Meteorological Service, <https://www.mgm.gov.tr/veridegerlendirme/il-ve-ilceler-istatistik.aspx?m=GAZIANTEP>, (Accessed: **15 November 2018**).
- UDIM, Boğaziçi University Kandilli Observatory and Earthquake Research Institute, National Earthquake Monitoring Center, <http://www.koeri.boun.edu.tr/sismo/mudim/katalog.asp> (Accessed: **1 April 2018**)
- Ulusay, R., Aydan, Ö., Tünel Açma Makinalarıyla Yapılan Kazı İşlemlerinin Olumlu ve Olumsuz Yönlerinin Değerlendirilmesi: Takisato Tüneli (Japonya) Örneği, *Jeoloji Mühendisliği Dergisi*, 51 (**1997**).
- Ulusay, R., Tuncay, E., Sönmez, H., and Gökçeoğlu, C., An Attenuation Relationship Based on Turkish Strong Motion Data and Iso-Acceleration Map of Turkey, *Engineering Geology*, Science Direct, Elsevier, 74 (**2004**).



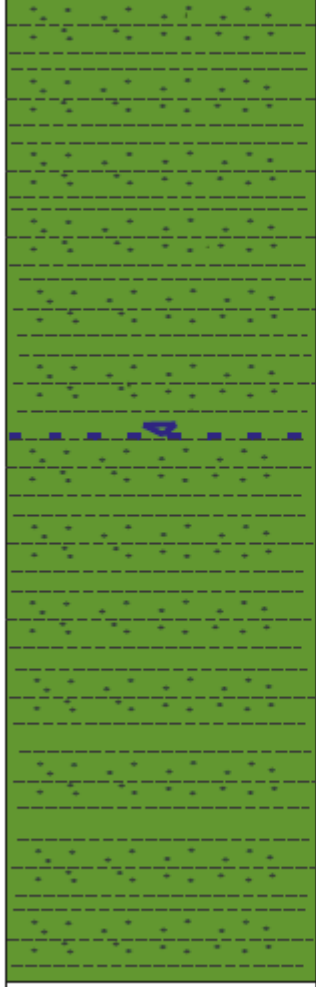
- United States Geological Survey, The Landslide Handbook—A Guide to Understanding Landslides, [http://pubs.usgs.gov/circ/1325/pdf/C1325\\_508.pdf](http://pubs.usgs.gov/circ/1325/pdf/C1325_508.pdf) (Accessed: **14 March 2019**).
- Usta, D., Türkiye Jeoloji Haritaları Serisi Gaziantep-N37 Paftası, Maden Tetkik Arama Genel Müdürlüğü (MTA), Jeoloji Etütleri Dairesi, No.266, Ankara, **2018**.
- Vassallo, R., Mishraa, M., Santarsiero, G., Masia, A., Interaction of a Railway Tunnel with a Deep Slow Landslide in Clay Shales, *Procedia Earth and Planetary Science*, 16 (**2016**).
- Vineetha K, Boominathan A, Banerjee, S., Tbm ground interaction modeling, *Proceedings of the 19th International Conference on Soil Mechanics and Geotechnical Engineering*, 17-22 September, Seoul, Korea, **2017**.
- Yalçın, N., Orta Amanoslar'ın Jeolojisi ve Petrol Olanakları, İstanbul Üniversitesi Yerbilimleri Fakültesi Jeoloji Mühendisliği Bölümü, TPAO Arama Grubu, No.1393, **1979**.
- Yang, B., Utiliti, S., Jones, B.D., Numerical analysis of TBM tunneling in sand using a state parameter model, *International Conference on Geomechanics, Geo-energy and Geo-resources IC3G*, 28- 29 September, Melbourne, Australia, **2016**.
- Yanıktepe, B., Özalp, C., Kaşka, Ö., Köroğlu, T., An assessment of wind power potential in Osmaniye, Turkey, *6<sup>th</sup> International Advanced Technologies Symposium (IATS'11)*, 16-18 May, Elazığ, Turkey, **2011**.
- Yılmaz, Y., Demirkol, Gürpınar, O., Yalçın, N., Yetiş, C., Yiğitbaş, E., Günay, Y., Sarıtaş, B., Amanos Dağlarının Jeolojisi, TPAO Rapor No.1920, Ankara, **1984**.

## APPENDICES

### Appendix 1- Boreholes Information

BAHÇE-NURDAĞ TUNNEL				
DEPTH (m)	LITHOLOGY	DESCRIPTIONS	EXPLANATIONS	
0		Metasandstone Metamudstone	<b>SK-1 INFORMATION</b>	
			Block / Country : Turkey	
			City : Osmaniye	
			X: 553486.445	
			Y: 4118276.627	
			Z: 674.144	
35				
75				
80				

Borehole information of SK-1 (Reproduced after TCDD, 2018).

BAHÇE-NURDAĞ TUNNEL				
DEPTH (m)	LITHOLOGY	DESCRIPTIONS	EXPLANATIONS	
0		Metasandstone Metamudstone	<b>SK-2 INFORMATION</b>	
			Block / Country : Turkey	
			City : Osmaniye	
			X: 553582.824	
			Y: 4118278.827	
			Z: 673.999	
34				
76				
80				

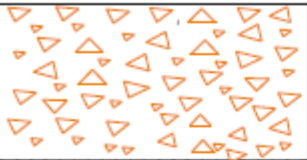
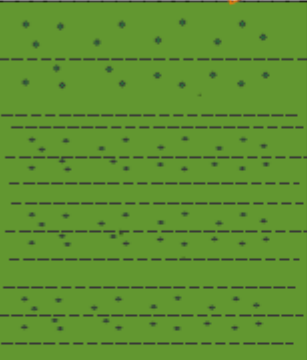
Borehole information of SK-2 (Reproduced after TCDD, 2018).

BAHÇE-NURDAĞ TUNNEL			
DEPTH (m)	LITHOLOGY	DESCRIPTIONS	EXPLANATIONS
0		Debris	<b>SK-7A INFORMATION</b> Block / Country : Turkey City : Osmaniye X: 553448.802 Y: 4118083.800 Z: 627.407
17.40			Metasandstone Metamudstone
41			
80			

Borehole information of SK-7A (Reproduced after TCDD, 2014).

BAHÇE-NURDAĞ TUNNEL			
DEPTH (m)	LITHOLOGY	DESCRIPTIONS	EXPLANATIONS
0			<b>SK-8 INFORMATION</b> Block / Country : Turkey City : Osmaniye X: 553414.789 Y: 4118139.799 Z: 629.850
4.50		Debris	
13.50		Metasandstone Metamudstone	
40			
80			

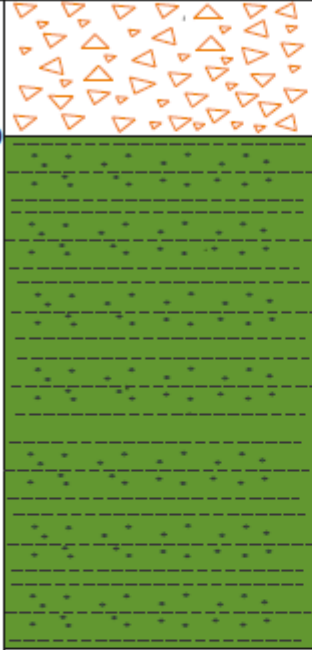
Borehole information of SK-8 (Reproduced after TCDD, 2014).

BAHÇE-NURDAĞ TUNNEL			
DEPTH (m)	LITHOLOGY	DESCRIPTIONS	EXPLANATIONS
0		Debris	<b>SK-8Y INFORMATION</b> Block / Country : Turkey City : Osmaniye X: 553302.3337 Y: 4118294.786 Z: 634.8622
12			
40			
80			

Borehole information of SK-8Y (Reproduced after TCDD, 2014).

BAHÇE-NURDAĞ TUNNEL			
DEPTH (m)	LITHOLOGY	DESCRIPTIONS	EXPLANATIONS
0		Debris	<b>SK-9 INFORMATION</b> Block / Country : Turkey City : Osmaniye X: 553544.349 Y: 4118154.948 Z: 639
3.35			
		Metasandstone	
		Metamudstone	
50			
80			

Borehole information of SK-9 (Reproduced after TCDD, 2014).

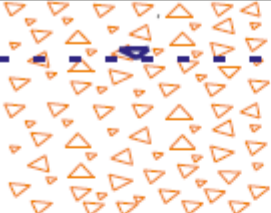
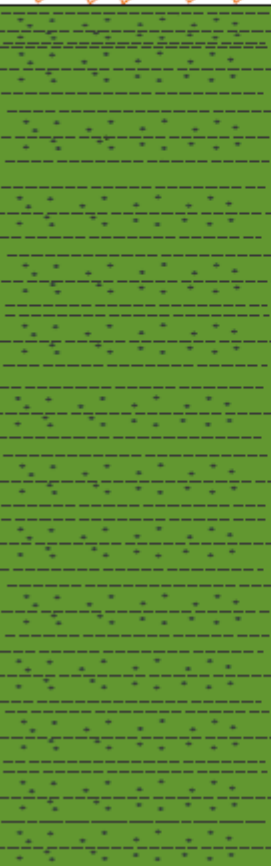
BAHÇE-NURDAĞ TUNNEL									
DEPTH (m)	LITHOLOGY	DESCRIPTIONS	EXPLANATIONS						
0		Debris	<table border="1"> <thead> <tr> <th>SK-9Y INFORMATION</th> </tr> </thead> <tbody> <tr> <td>Block / Country : Turkey</td> </tr> <tr> <td>City : Osmaniye</td> </tr> <tr> <td>X: 553382.91</td> </tr> <tr> <td>Y: 4118295.532</td> </tr> <tr> <td>Z: 644.3197</td> </tr> </tbody> </table>	SK-9Y INFORMATION	Block / Country : Turkey	City : Osmaniye	X: 553382.91	Y: 4118295.532	Z: 644.3197
SK-9Y INFORMATION									
Block / Country : Turkey									
City : Osmaniye									
X: 553382.91									
Y: 4118295.532									
Z: 644.3197									
10.50									
50									
80									

Borehole information of SK-9Y (Reproduced after TCDD, 2014).



BAHÇE-NURDAĞ TUNNEL			
DEPTH (m)	LITHOLOGY	DESCRIPTIONS	EXPLANATIONS
0			<b>SK-10 INFORMATION</b> Block / Country : Turkey City : Osmaniye X: 553701.371 Y: 4118151.093 Z: 642.300
3		Debris	
15.50		Metasandstone Metamudstone	
50			
80			

Borehole information of SK-10 (Reproduced after TCDD, 2014).

BAHÇE-NURDAĞ TUNNEL									
DEPTH (m)	LITHOLOGY	DESCRIPTIONS	EXPLANATIONS						
0		Debris	<table border="1"> <thead> <tr> <th colspan="1">SK-11 INFORMATION</th> </tr> </thead> <tbody> <tr> <td>Block / Country : Turkey</td> </tr> <tr> <td>City : Osmaniye</td> </tr> <tr> <td>X: 554035.719</td> </tr> <tr> <td>Y: 4118164.758</td> </tr> <tr> <td>Z: 685</td> </tr> </tbody> </table>	SK-11 INFORMATION	Block / Country : Turkey	City : Osmaniye	X: 554035.719	Y: 4118164.758	Z: 685
SK-11 INFORMATION									
Block / Country : Turkey									
City : Osmaniye									
X: 554035.719									
Y: 4118164.758									
Z: 685									
5									
18.90		Metasandstone Metamudstone							
92.50									

Borehole information of SK-11 (Reproduced after TCDD, 2014).

## Appendix 2- Test Standard

<b><i>SK-7A</i></b>	Uniaxial Compressive Strength Tests	ISRM 2006 (1981)
<b><i>SK-8</i></b>	Static Elasticity Modulus Tests	ISRM 2006 (1981)
<b><i>SK-9</i></b>	Indirect (Brazilian) Tensile Strength Tests	ISRM 2006 (1981)
<b><i>SK-10</i></b>	Point Load Strength Test	ASTM D-5731-02
<b><i>SK-11</i></b>		
<b><i>SK-8Y</i></b>	Uniaxial Compressive Strength Tests	Ulusay, R., Hudson, J.A., (eds.), “The Complete ISRM Suggested Methods for Rock Characterization, Testing and Monitoring: 1974-2006”, Ankara, 2007.
<b><i>SK-9Y</i></b>	Point Load Strength Test	Ulusay, R., Hudson, J.A., (eds.), “The Complete ISRM Suggested Methods for Rock Characterization, Testing and Monitoring: 1974-2006”, Ankara, 2007.

## Appendix 3- Permission Form



T.C.  
DEVLET DEMİRYOLLARI İŞLETMESİ GENEL MÜDÜRLÜĞÜ  
DEMİRYOLU BAKIM DAİRESİ BAŞKANLIĞI  
YOL ALTYAPI BAKIM ŞUBE MÜDÜRLÜĞÜ

161<sup>yi</sup>

Sayı : 64444451-755.01-E.0199281  
Konu : TÜNEL

17.05.2018

Sayın Müge Pınar KOMU

İlgi : Müge Pınar KOMU'nun 11.05.2018 tarihli başvurusu.

İlgi yazı ile istemiş olduğumuz, Yüksek lisans tezinizde kullanılmak üzere, Bahçe-Nurdağ sahasına ilişkin sondaj verisi ve ihtiyaç olacak tünellere ilişkin teknik dokümanların kullanım izni tarafımıza verilmiştir.

Bilgilerinizi rica ederiz.

e-imzadır

Ali ÖZTÜRK  
Daire Başkan Yardımcısı

e-imzadır

Fahrettin YILDIRIM  
Daire Başkanı

Not: 5070 sayılı elektronik imza kanununun 5.maddesi gereği bu belge elektronik imza ile imzalanmıştır.

YOL ALT YAPI ŞUBE MÜDÜRLÜĞÜ

Bilgi için: Nihan AKDEMİR  
Mühendis  
Telefon No:(312) 309 05 15-4321



HACETTEPE UNIVERSITY  
GRADUATE SCHOOL OF SCIENCE AND ENGINEERING  
THESIS/DISSERTATION ORIGINALITY REPORT

HACETTEPE UNIVERSITY  
GRADUATE SCHOOL OF SCIENCE AND ENGINEERING  
TO THE DEPARTMENT OF OF GEOLOGICAL ENGINEERING

Date: 02/07/2019

Thesis Title / Topic: Investigation of Tunnel Boring Machine – Landslide Relation in a Tunnel Excavating in a Complex Geological Condition: Bahçe – Nurdağ Tunnel

According to the originality report obtained by my thesis advisor by using the *Turnitin* plagiarism detection software and by applying the filtering options stated below on 02/07/2019 for the total of 105 pages including the a) Title Page, b) Introduction, c) Main Chapters, d) Conclusion sections of my thesis entitled as above, the similarity index of my thesis is 7 %.

Filtering options applied:

1. Bibliography/Works Cited excluded
2. Quotes ~~excluded~~ / included
3. Match size up to 5 words excluded

I declare that I have carefully read Hacettepe University Graduate School of Science and Engineering Guidelines for Obtaining and Using Thesis Originality Reports; that according to the maximum similarity index values specified in the Guidelines, my thesis does not include any form of plagiarism; that in any future detection of possible infringement of the regulations I accept all legal responsibility; and that all the information I have provided is correct to the best of my knowledge.

I respectfully submit this for approval.

Name Surname: Müge Pınar KÖMÜ  
Student No: N16228171  
Department: Geological Engineering  
Program: Geological Engineering –Masters with Thesis  
Status:  Masters  Ph.D.  Integrated Ph.D.

Date and Signature  
02.07.2019  
Müge Pınar Kömü

**ADVISOR APPROVAL**

APPROVED.  
  
Prof. Dr. Candan GÖKÇEOĞLU

(Title, Name Surname, Signature)

## CURRICULUM VITAE

Name-Surname : Müge Pınar KÖMÜ  
Place of Birth : ANKARA  
Date of Birth : 23.04.1992  
Marital Status : Single  
Address : Yaprıcak Mah. Evliya Çelebi Cad. CK-13 Blok  
No: 68/3 İç Kapı No: 31 ETİMESGUT / ANKARA  
Phone : 0536 701 98 65  
E-mail : mugekomu@gmail.com  
Languages : Turkish (Native) - English (Advance) - German (Elementary)

Education  
Undergraduate : Middle East Technical University Department of Geological Engineering

